Characterization of the prokaryotic HemW and eukaryotic RSAD1 heme chaperones

Von der Fakultät für Lebenswissenschaften

der Technischen Universität Carolo-Wilhelmina zu Braunschweig

zur Erlangung des Grades

einer Doktorin der Naturwissenschaften

(Dr. rer. nat.)

genehmigte

D i s s e r t a t i o n

von Vera Haskamp

aus Vechta

1. Referent: Professor Dr. Dieter Jahn

2. Referentin: Professorin Dr. Gunhild Layer

eingereicht am: 28.09.2016

mündliche Prüfung (Disputation) am: 12.12.2016

Druckjahr 2016

Vorveröffentlichungen der Arbeit

Teilergebnisse aus dieser Arbeit wurden mit Genehmigung der Fakultät für Lebenswissenschaften, vertreten durch den Mentor der Arbeit, in folgenden Beiträgen vorab veröffentlicht:

Publikationen

Haskamp, V., Karrie, S., Mingers, T., Alberge, F., Magalon, A., Müller, K., Bill, E., Lubitz, W., Kleeberg, K., Schweyen, P., Bröring, M., Sassen, W., Köster, R., Jahn, M. & Jahn, D. The radical SAM proteins HemW and RSAD1 are Heme Chaperones, The EMBO Journal (submitted).

Tagungsbeiträge

Haskamp, V., Huhn, S., Jahn, M. & Jahn, D.: Characterisation of the potential heme chaperone HemW (Poster), Tetrapyrrole Discussion Group Meeting (TPDG), Cambridge, England (2012).

Haskamp, V., Huhn, S., Jahn, M. & Jahn, D.: Characterization of the potential heme chaperone HemW (Poster), Vereinigung für Allgemeine und Angewandte Mikrobiologie (VAAM) -Jahrestagung, Tübingen, Germany (2012).

Haskamp, V., Huhn, S., Jahn, M. & Jahn, D.: Characterization of the potential heme chaperone HemW (Poster), Gordons Research Conference (GRC), Newport, USA (2012).

Haskamp, V.: Characterisation of the potential heme chaperone HemW (oral presentation), Tetrapyrrole Discussion Group Meeting (TPDG), Canterbury, England (2013).

Haskamp, V., Jahn, M. & Jahn, D.: Biochemical characterisation of the heme chaperone HemW (Poster), Tetrapyrrole Discussion Group Meeting (TPDG), Canterbury, England (2013).

Haskamp, V., Jahn, M. & Jahn, D.: Characterization of the potential heme chaperone HemW (Poster), Vereinigung für Allgemeine und Angewandte Mikrobiologie (VAAM)-Jahrestagung, Bremen, Germany (2013)

Table of Contents

II Abbreviations

A	Ampere
ALA	5-aminolevulinic acid
amp	ampicillin
APS	ammonium peroxodisulfate
ATP	adenosine triphosphate
BCIP	5-Bromo-4-chloro-3-indolyl phosphate
b_D	distal heme
b_P	proximal heme
bp	base pair
C	Celsius (°C)
COPROGEN	coproporphyrinogen III
CPDH	coproporphyrinogen III dehydrogenase
CPO	coproporphyrinogen III oxidase
cv	column volume
Da	Dalton
DIG	digoxigenin
DNA	deoxyribonucleic acid
dNTP	deoxyribonucleotide triphosphate
DTT	1,4-dithio-DL-threitol
EDTA	ethylenediaminetetraacetic acid
e.g.	*exempli gratia* (for instance)
et al.	*et alia* (and others)
F	forward
FA	formamide

F-S	Iron-sulfur cluster
g	→ *centrifugation*: earth gravity
	→ *weight*: gram
G	giga
GluTR	glutamyl-tRNA reductase
GST	glutathione S-transferase
h	hour
H_2O_{dest}	*aqua destillata*
HemF	oxygen-dependent coproporphyrinogen III oxidase
HemH	ferrochelatase
HemN	oxygen-independent coproporphyrinogen III dehydrogenase
hpf	hours post fertilization
HPLC	high performance liquid chromatography
Hz	hertz
IPTG	Isopropyl-ß-D-1-thiogalactopyranoside
K	Kelvin
k	kilo
kDa	kilo Dalton
l	liter
λ	wavelength
LB	Lysogenic broth
m	milli
M	molar (mol/l)
µ	micro
min	minute
MOPS	3-Morpholinopropane-1-sulfonic acid

MQ	menaquinone
MQH_2	menaquinol
M_r	relative molecular mass
n	nano
NADH	nicotinamide adenine dinucleotide, reduced form
NarGHI	quinol-nitrate oxidoreductase
NBT	nitro blue tetrazolium
N/O	nitrogen/oxygen
OD	optical density at wavelength λ in nm
Pa	Pascal
PBG	porphobilinogen
PBGD	porphobilinogen deaminase
PBGS	porphobilinogen synthase
PBS	phosphate-buffered saline
PBST	phosphate-buffered saline-tween20
PCR	polymerase chain reaction
PFA	paraformaldehyde
PLP	pyridoxal-5'-phosphate
PPIX	protoporphyrin IX
PPO	protoporphyrinogen IX oxidase
PROTOGEN	protoporphyrinogen IX
psi	pounds per square inch
R	reverse
rpm	rotations per minute
RT	room temperature
s	second

SAM	S-adenosyl-L-methionine
SDS	sodium dodecyl sulfate
SDS-PAGE	sodium dodecyl sulfate polyacrylamide gel electrophoresis
TAE	Tris-acetate/EDTA
TEMED	tetramethylethylenediamine
TFA	trifluoroacetic acid
T_M	annealing temperature
Tris	tris-(hydroxymethyl)-aminomethane
(t)RNA	(transfer) ribonucleic acid
U	unit
UV	ultraviolet
V	volt
vol.	volume
v/v	volume per volume
w/v	weight per volume
∞	infinite

1 Introduction

1.1 Tetrapyrroles

Tetrapyrroles are key molecules of life. They are the most abundant pigments found in nature. The structure of tetrapyrroles consists of a macrocycle of four pyrrole rings linked by four methine bridges (Figure 1). The only exceptions are the corrinoids, e.g. cobalamin. This class of tetrapyrrols lacks one carbon between the first and fourth pyrrole ring. In all linear tetrapyrrols, e.g. bilirubin the four pyrrole rings are connected by only three methine bridges as a result of the cleavage of cyclic tetrapyrroles. The pyrrole rings of the macrocycle are denoted A–D around the circle in clockwise direction. Carbon and nitrogen atoms are numbered 1-20 and 21-24 respectively. The α-position describes the carbon atoms adjacent to nitrogen atoms and the β-position the remaining carbon atoms without direct bond to nitrogen, while the methine bridge carbons are in meso-position.

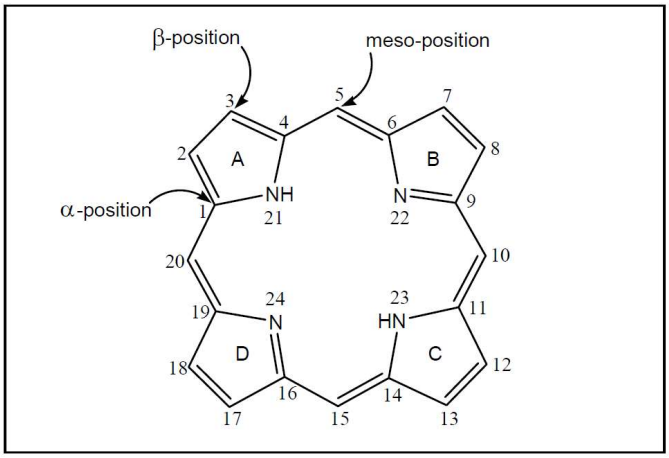

Figure 1: Basic structure of cyclic tetrapyrroles. The basic structure consist of four pyrrole rings (A-D). The carbon and nitrogen atoms are numbered 1-20 and 21-24. The α- position describes the carbon atom adjacent to nitrogen atoms in contrast to β- position representing carbon atoms without direct bond to nitrogen. Carbon atoms within the methine bridges are in meso-position.

Already in 1862 Hoppe-Seyler prepared porphyrins successfully from blood. Fifty years later in 1912 the tetrapyrrolic structure of heme was revealed by Küster, confirmed by the synthesis of hemin in 1929 by Hans Fischer (Vasudevan *et al.,* 2013). Hans Fischer received the Nobel prize in 1930 for synthesis of hemin and noting similarities to chlorophyll (Oakes, 2007). For his studies on chlorophyll Richard Willstätter was

awarded the Nobel prize in 1915. All cyclic tetrapyrroles share a system of fully conjugated double bonds and are able to chelate metal ions like Fe^{2+}, Mg^{2+}, Ni^{2+} or Co^{2+} (Heinemann *et al.,* 2008). The expanded π-electron system is responsible for the chromaticity. In case of the blood, heme gives the red color and in leaves, the green chlorophyll is present.

1.2 Heme biosynthesis

The biosynthesis of heme starts in all organisms with the formation of 5-aminolevulinic acid (ALA). This precursor provides all essential carbon and nitrogen atoms for the formation of tetrapyrroles. There are two ways of synthesis of ALA known. First, ALA is formed via the condensation of succinyl-CoA and glycine. This "Shemin pathway" was discovered by Shemin and Russell in 1953 (Shemin & Russell, 1953) and is present in animals, fungi and the α-group of proteobacteria (Kadish *et al.,* 2011). The one-step condensation of the two substrates is catalyzed by 5-aminolevulinic acid synthase (ALAS, EC 2.3.1.37). First ALAS activity was shown 1958 by Neuberger and colleagues (Gibson *et al.,* 1958) and in parallel by Shemin and colleagues (Kikuchi *et al.,* 1958). ALAS uses pyridoxal phosphate (PLP) as cofactor and the reaction gives rise to ALA, carbon dioxide and free coenzyme A (Kikuchi *et al.,* 1958). The crystal structure of the enzyme was solved in 2005 and recently a detailed enzyme mechanism was proposed (Astner *et al.,* 2005; Stojanovski *et al.,* 2014).

The second pathway called "C5-pathway" due to the ALA formation starts from the C5-skeleton of glutamate. This pathway is present in plants, archaea and most bacteria (Beale & Castelfranco, 1974). In contrast to the "Shemin pathway" two enzymes are involved in the formation of ALA. The first step is the reduction of glutamyl-tRNA to glutamate-1-semialdehyde (GSA) catalyzed by the NADPH-dependent glutamyl-tRNA reductase (GluTR, EC 1.2.1.70; Chen *et al.,* 1990). The instable GSA is transaminated in the next step by the PLP-dependent glutamate- 1-semialdehyde- 2,1-aminomutase (GSAM, EC 5.4.3.8) to ALA (Jahn *et al.,* 1991). Due to the instability of GSA a direct channeling from GluTR to GSAM was reviewed. The solved crystal structure of both enzymes suggested the formation of a tight channeling complex (Moser *et al.,* 2001; Schulze *et al.,* 2006). In 2005, Moser and colleagues confirmed the interaction by e.g. co-immuno-precipitation experiments (Lüer *et al.,* 2005).

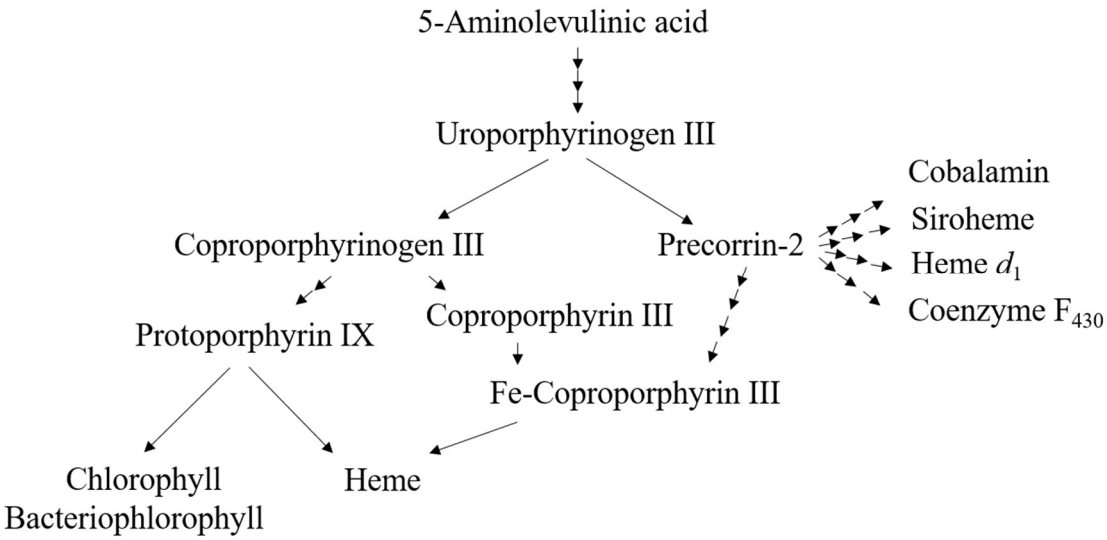

Figure 2: Overview of the divergent tetrapyrrole biosynthetic pathways. All tetrapyrroles derive from the common precursor 5-aminolevulinic acid. The major branching point of tetrapyrrole biosynthesis is uroporphyrinogen III. Coproporphyrinogen III is used to synthesize hemes and chlorophylls, whereas precorrin-2 gives rise to cobalamin, siroheme, heme d_1, and coenzyme F_{430}. In archaea and some bacteria, precorrin-2 is also the precursor for heme. A further pathway from coproporphyrinogen III over coproporphyrin III to Fe-coproporphyrin III was described in 2015 by Dailey *et al.* Modified according to Buchenau *et al.,* 2006; Dailey *et al.,* 2015; Lobo *et al.,* 2015.

Uroporphyrinogen III is the first cyclic intermediate and branching point of the tetrapyrrole biosynthesis between two distinct groups, the porphinoids (siroheme, coenzyme F430, vitamin B_{12}, siroheme) and hemes and chlorophylls (Figure 2). Uroporphyrinogen III is formed from eight molecules of ALA. For this three enzymatic steps are required. First, two molecules of ALA are condensed to form porphobilinogen (PBG) by the porphobilinogen synthase (PBGS, EC 4.2.1.24). In the next step, the enzyme porphobilinogen deaminase (PBGD, EC 2.5.1.61) catalyzes the linkage of four molecules PBG to obtain pre- uroporphyrinogen. The final formation of the intermediate uroporphyrinogen III is carried out via the uroporphyrinogen III synthase (UROS, EC 4.2.1.75). To receive this cyclic tetrapyrrole the inversion of the D ring of pre- uroporphyrinogen is essential (Heinemann *et al.,* 2008; Kaufholz *et al.,* 2013; Jahn & Jahn, 2012).

To form the next intermediate coproporphyrinogen III (COPROGEN), the four acetate chains of uroporphyrinogen III are decarboxylated to form methyl groups by uroporphyrinogen III decarboxylase (UROD, EC 4.1.1.37). The decarboxylation begins

with the acetate side chain of ring D followed by A, B and finally C (Jackson *et al.,* 1980). Next, the oxidative decarboxylation of the propionate side chains of rings A and B to vinyl groups is carried out by coproporphyrinogen III oxidase (CPO, EC 1.3.3.3; Dailey, 1990). In nature, there are two CPO known. On the one hand, the oxygen-dependent CPO HemF is found in mammals and some bacteria, whereas in most bacteria the oxygen-independent coproporphyrinogen III dehydrogenase HemN inherits the reaction of coproporphyrinogen III to protoporphyrinogen IX (PROTOGEN). The crystal structure of HemN and its corresponding mechanism were solved and identified the enzyme as radical SAM-enzyme (Wang & Frey, 2007; Sofia *et al.,* 2001; Layer *et al.,* 2003).

The colorless protoporphyrinogen IX is converted in a six-electron oxidation to the red colored protoporphyrin IX (PPIX) by the protoporphyrinogen IX oxidase (PPO, EC 1.3.3.4; Dailey, 1990). Thus, this oxidation results in a planar system of completely conjugated double bonds and represents the branching point between the chlorophylls and heme. Comparable to CPO, there exist an oxygen-dependent PPO (HemY) and an oxygen-independent PPO (HemG) (Koch *et al.,* 2004; Möbius *et al.,* 2010).

The last step of the heme biosynthesis is the insertion of ferrous iron into protoporphyrin IX. This reaction is catalyzed by the ferrochelatase (FC, EC 4.99.1.1; (Layer *et al.,* 2010). In a potential reaction mechanism the porphyrin ring is distorted to allow the insertion of the metal iron (Al-Karadaghi *et al.,* 2006). In eukaryotes, the ferrochelatase is a membrane-associated homodimer, while in bacteria it is monomeric (Wu *et al.,* 2001; Wang *et al.,* 2001).

In 2015, an alternative pathway was observed in Actinobacteria and Firmicutes (Dailey *et al.,* 2015). Here, coproporphyrinogen III is oxidized to coproporphyrin III by HemY. Afterwards, HemH inserted the iron to form Fe-coproporphyrin III. In the next step, the Fe-coproporphyrin III is carboyxlated by HemQ to form heme (Dailey *et al.,* 2015).

1.3 Heme transport

Heme is hydrophobic and above all cytotoxic. The toxicity of heme ranges from lipid peroxidation in presence of H_2O_2 (Ursini *et al.,* 1981) to oxidative degradation of proteins in presence of reducing agents (Aft & Mueller, 1984). Furthermore, heme is able to change membrane permeability which leads to changes in lipid organization and cell

damage (Schmitt *et al.,* 1993). These characteristics also explain the low level of free heme in the cell and the high amount of protein-bound heme. However, in prokaryotes and eukaryotes, heme-utilizing proteins are located in different compartments and organelles. Therefore, heme has to be transported to these target locations (Thöny-Meyer, 2009). The transfer via heme chaperones seems indispensable. Up to now, the knowledge of intracellular heme transport in prokaryotes and eukaryotes is limited (Thöny-Meyer, 2009).

The last step of heme biosynthesis is the insertion of iron into protoporphyrin IX by ferrochelatase, located in mitochondria, chloroplasts or in bacteria in the cytosol. Arising from the ferrochelatase, heme is transported to proteins for insertion or degradation or to membranes. The incorporation of heme as a cofactor into the target heme proteins is poorly understood. In bacteria, heme delivery to heme proteins is hypothesized to take place directly by ferrochelatase or indirectly via heme chaperones (Thöny-Meyer, 2009). However, an alternative way for the delivery of heme to heme proteins is achieved using a heme uptake transporter system. For example, heme auxotrophes like *Streptococcus agalactiae* require heme from the environment (Lechardeur *et al.,* 2010) and pathogens use similar systems for heme acquisition as iron source (Stojiljkovic & Hantke, 1992). Since heme is too large for diffusion through porins, specialized receptors are essential. Similar to the transport of larger molecules in bacteria, heme is transported into the cell by the TonB complex consisting of three proteins, TonB, ExbB, ExbD, localized in the cytoplasmic membrane (Wandersman & Delepelaire, 2004). Furthermore, some Gram negative bacteria, e.g. *Pseudomonas aeruginosa*, uses soluble secreted hemophores for scavenging heme from the environment and delivering it to outer membrane receptors. For example, HasA from *P. aeruginosa* is a hemophore which delivers heme to the receptor HasR (Létoffé *et al.,* 1998; Létoffé *et al.,* 1999).

The shuttle of heme between the outer and the inner membrane is mediated by the periplasmic heme-binding protein (PBP), e.g. PhuT in *Pseudomonas aeruginosa* or ShuT in *Shigella dysenteriae* (Ho *et al.,* 2007). These proteins belong together with one or two hydrophobic integral membrane-spanning proteins and one or two hydrophilic proteins with ATPase activity to the periplasmic binding protein-dependent transport (PBT) system (Stojiljkovic & Hantke, 1994; Ho *et al.,* 2007).

In 2004, a potential heme chaperone for heme utilization, HutZ from *Vibrio cholerae* was published (Wyckoff *et al.,* 2004). Biochemical experiments indicated a heme transfer

from HutZ to the *Neisseria* heme oxygenase HmuO. However, HutZ was discussed to be a heme oxygenase. This proposal was based on the functional complementation of *hmuO* mutants (Wyckoff *et al.,* 2004) and the high sequence similarity with the heme oxygenase HugZ from *Helicobacter pylori* (Liu *et al.,* 2012). Finally, the function of HutZ as a heme degrading protein was shown by Uchida and colleagues (Uchida *et al.,* 2012).

Until today, the cytoplasmic heme-binding protein PhuS from *P. aeruginosa* is the only candidate for a bacterial heme chaperone, although the catalyzed incorporation of heme into proteins was not shown. PhuS belongs to the *Pseudomonas* heme utilization (*phu*) system. Wilks and colleagues identified in 2006 PhuS as an intracellular heme-trafficking protein (Lansky *et al.,* 2006). They showed the release of heme from PhuS and the parallel incorporation of heme into the heme oxygenase *pa*-HO of *P. aeruginosa*. In detail, heme binding of PhuS induced a conformational rearrangement required for the interaction with the heme oxygenase (O'Neill *et al.,* 2012). Further experiments suggested a regulation of heme uptake based on the interaction of heme oxygenase and PhuS (O'Neill & Wilks, 2013).

In eukaryotes, heme biosynthesis and its regulation are well characterized. In contrast, the mechanism for heme transport remains poorly understood (Yuan *et al.,* 2013). In the heme auxotroph model organism *Caenorhabditis elegans* the first potential heme importers CeHRG- 1 and CeHRG- 4 were identified. Experiments with orthologues in zebrafish and human supported these findings (Yuan *et al.,* 2013). For example, CeHRG- 1 rescued all phenotypes observed due to the knockdown of the *hrg-1* gene in zebrafish. Furthermore, electrophysiological measurements revealed a heme-dependent change in current after the injection of cRNA from the human homolog hHRG-1 in *Xenopus laevis* oocytes, indicating a heme-dependent transport across the plasma membrane (Rajagopal *et al.,* 2008). Another protein, the heme carrier protein 1 (HCP1) isolated from mouse duodenum, was implicated in heme absorption in the intestine (Shayeghi *et al.,* 2005). HCP1 is a membrane protein and expression of the HCP1 cRNA in *Xenopus* revealed a 2-3 fold increase of heme uptake. An alignment from various species including zebrafish showed that the protein is highly conserved (Shayeghi *et al.,* 2005). Moreover, first experiments indicated a further heme importer, FLVCR2 (Duffy *et al.,* 2010). Duffy and colleagues revealed an enhanced heme uptake in mammalian cells expressing the human FLCVR2 gene. To prevent heme accumulation in the cell, the heme exporter FLVCR1 and ATP-binding cassette transporter G2 (ABCG2) are essential.

Human ABCG2 binds directly via a porphyrin-binding domain to heme and possibly transfers it to the heme carrier albumin (Desuzinges-Mandon *et al.,* 2010). The overexpression of another isoform of FLVCR, FLVCR1b, resulted in an increase of cytosolic heme, whereas the knockdown implicated heme accumulation in mitochondria (Yuan *et al.,* 2013).

Two further mitochondrial heme transporters were identified, the ABC transporter ABCB6 and ABCB10. ABCB6 is located in the outer membrane and ABCB10 in the inner mitochondrial membrane. ABCB10 interacts with mitoferrin1, a mitochondrial inner membrane iron transporter, and ferrochelatase (Hung *et al.,* 2013; Yuan *et al.,* 2013). Relating to cytosolic heme transfer several heme-binding proteins were found. One candidate for a heme chaperone and not only a heme-binding protein is glyceraldehyde-3-phosphate dehydrogenase (GAPDH). In 2010 Chakravarti and colleagues proposed that GAPDH delivers heme to the inducible nitric oxide synthase (iNOS) (Chakravarti *et al.,* 2010), but further investigations are necessary to establish the general role of GAPDH as heme chaperone (Yuan *et al.,* 2013).

1.4 HemW

In 2012, a protein was identified in *Lactococcus lactis* with a role in heme trafficking (Abicht *et al.,* 2012). Annotated as *hemN*, a coproporphyrinogen III dehydrogenase (CPDH) involved in heme biosynthesis, the protein showed no CPDH activity neither *in vitro* nor *in vivo*. Abicht and colleagues renamed the protein due to their findings HemW. Furthermore, they showed the release of heme from the HemW-heme complex after incubation with *L. lactis* membrane vesicles. This indicated a putative role for HemW in channeling heme.

L. lactis HemW has a high amino acid homology to CPDH. In contrast to *E. coli* CPDH, *L. lactis* HemW is missing 47 N-terminal amino acids and the fourth cysteine residue of the conserved CX_3CX_2CXC motif (Abicht *et al.,* 2012). An amino acid sequence alignment of both proteins revealed an identity of 50 %. However, there are essential differences in the sequence (Figure 3). First, *E. coli* HemN possesses the extra N-terminal residue. These residues were proposed to be crucial for substrate binding (Layer *et al.,* 2003). In HemN the first three cysteine residues of the CX_3CX_2CXC motif are involved in iron-sulfur ([Fe-S]) cluster coordination (Layer *et al.,* 2003), and the fourth cysteine

was found essential for the enzymatic function (Layer *et al.,* 2002). Instead of the fourth cysteine, HemW contains a phenylalanine. On the other hand, the sequence of HemW reveals two binding sites for S-adenosyl-L-methionine (SAM) similar to HemN. SAM plays an important role in the catalysis of the oxygen-independent conversion of coproporphyrinogen-III to protoporphyrinogen-IX.

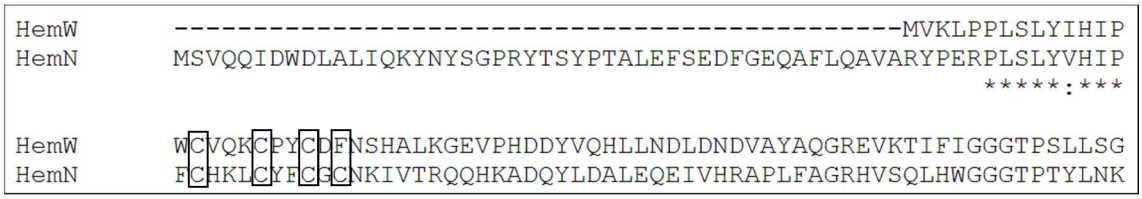

Figure 3: Alignment of N-terminus of *E. coli* HemN and HemW. Boxed is the conserved CX_3CX_2CXC motif in HemN and CX_3CX_2CXF motif in HemW. The alignment was generated with the program Clustal Omega by EMBL-EBI (Huhn, 2012; Sievers *et al.,* 2011).

In contrast to *L. lactis*, *E. coli* exhibits a complete heme biosynthesis. Therefore, *E. coli* possesses the CPO HemF, the CPDH HemN, and additionally a HemW-like protein annotated as YggW. According to the renaming of *L. lactis* HemW, *E. coli* YggW was named HemW (Huhn, 2012). Similar to *L. lactis* HemW, *E. coli* HemW exhibits a reduced N-terminus and the conserved cysteine motif lacks the fourth cysteine. First studies revealed a covalent binding of heme to HemW and a high specificity for binding heme and no analogues, for example protoporphyrin IX. Furthermore, HemW is able to dimerize in presence of heme. In addition, electron paramagnetic resonance spectroscopy indicated the presence of a [4Fe-4S] cluster (Huhn, 2012).

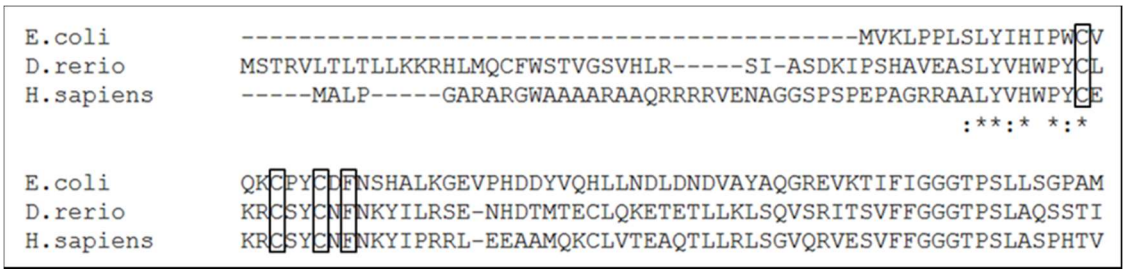

Figure 4: Alignment of the N-terminus of HemW from *E. coli, Danio rerio* and *Homo sapiens*. Boxed is the conserved CX_3CX_2CXF motif. The alignment was generated with the program Clustal Omega by EMBL-EBI (Sievers *et al.,* 2011).

An amino acid sequence alignment of HemW of various organisms, e.g. Gram positive and Gram negative bacteria, vertebrates and plants displays a high sequence identity. Figure 4 shows exemplarily the alignment of the amino acid sequences of *E. coli*, *Danio rerio* and *Homo sapiens.* All three exhibit the conserved CX_3CX_2CXF motif, as shown for HemW-like proteins (Abicht *et al.,* 2012). The presence of HemW in a wide range of organisms confirmed again its biological importance.

In 2002, Thompson and coworkers generated a ferric uptake regulator (*fur*) knockout strain of *Shewanella oneidensis* (Thompson *et al.,* 2002). Among others, microarray analysis revealed an up-regulation of *yggW*. The ferric uptake regulator controls the siderophore-mediated iron assimilation (Bagg & Neilands, 1987). The Fur protein acts in presence of iron as a transcriptional repressor for several genes. Iron serves as cofactor and mediates the dimerization and within binding to specific sequence elements in the promotor regions (Bagg & Neilands, 1987). Disruption of the *fur* locus resulted in constitutive expression of e.g. *hemR* and *hxuC* genes (Thompson *et al.,* 2002). In *Leptospira*, HemR is a regulator, activating the transcription of the heme biosynthesis proteins (Morero *et al.,* 2014). HxuC, a predicted TonB-dependent outer membrane protein in *Haemophilus influenzae* utilizes heme:hemopexin, low levels free heme and hemoglobin for obtaining its required heme (Cope *et al.,* 2001; Cope *et al.,* 1995; Hanson *et al.,* 1992). The up-regulation of *hemW* in the *fur* knock out mutant is in agreement with an increased heme biosynthesis and heme uptake. Furthermore, a transposon mutant of *yggW* in *Moraxella catarrhalis* was generated by de Vries and colleagues (de Vries *et al.,* 2013). This mutant showed a growth defect under iron-limiting conditions, which was restored by genetic complementation (de Vries *et al.,* 2013). Microarray analysis revealed a large number of differentially expressed genes. Among others, gene expression of proteins of the energy metabolism were down-regulated. In contrast, expression of nitrate reductase genes was increased (de Vries *et al.,* 2013). In parallel, expression of genes for the nitrite reductase was found decreased. With a decreased *narK2* expression, the gene for a putative nitrate/nitrite transporter, the effect was counteracted. These findings indicated a non-functional aerobic respiration in Δ*yggW*. This assumption is supported by a lower expression of genes coding for cytochrome *c* biogenesis proteins and the NADH-quinone oxidoreductase subunit H (de Vries *et al.,* 2013).

1.5 Iron-sulfur cluster and radical SAM-enzymes

Cofactors are essential for the function of many proteins. Fe-S clusters are probably some of the oldest cofactors in evolution and some of the most ubiquitous and functional versatile prosthetic groups (Beinert, 2000). Described are [2Fe-2S], [3Fe-4S], [4Fe-4S], [8Fe-7S] and [8Fe-8S] clusters in different oxidation states. Three systems for iron-sulfur biosynthesis in bacteria, namely NIF (nitrogen fixation), ISC (iron-sulfur cluster) and SUF (sulfur mobilization) systems exist. Homologous components of the ISC system are present in mitochondria. Moreover, the SUF system is found in chloroplasts (Roche *et al.,* 2013; Lill *et al.,* 2006). First of all the NIF system for maturation of nitrogenase was discovered in *Azotobacter vinelandii* (Jacobson *et al.,* 1989). In contrast, the ISC and SUF system are responsible for maturation of all iron-sulfur cluster in the cell (Roche *et al.,* 2013).

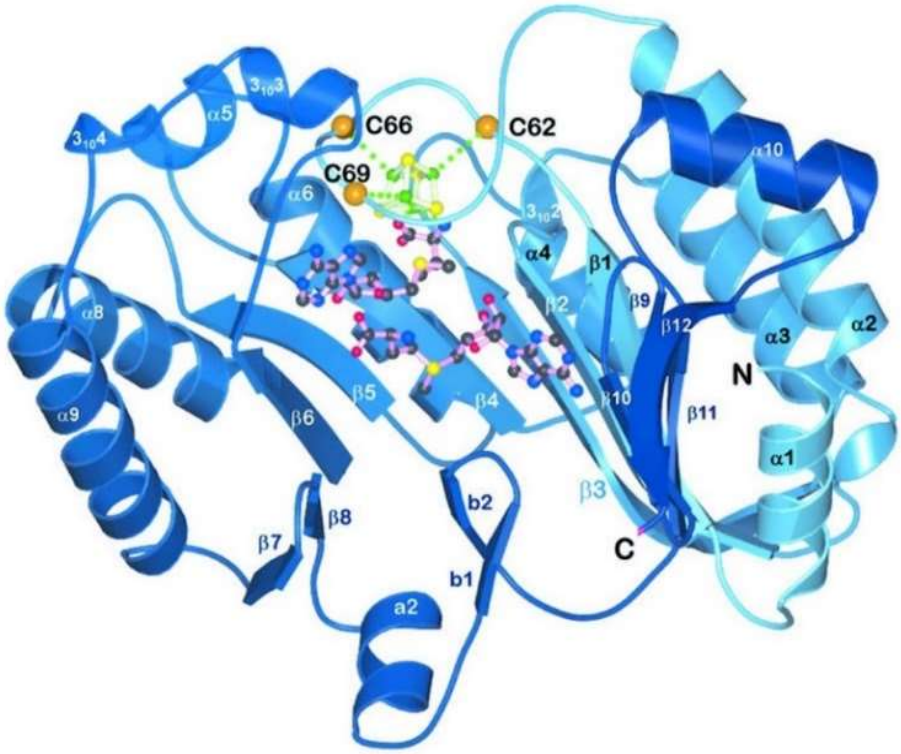

Figure 5: Structure of *E. coli* HemN. Indicated are the three cysteines involved in iron-sulfur cluster coordination. Furthermore, the two SAM molecules are illustrated (Layer *et al.,* 2003).

Functions of Fe-S cluster are e.g. electron transfer, substrate binding and activation, regulation of gene expression or structural (Johnson *et al.,* 2005). In the case of MutY, a *E. coli* DNA repair enzyme, the $[4Fe\text{-}4S]^{2+}$ is critical for folding and therefore for the

recognition of substrate DNA (Porello *et al.,* 1998). [4Fe-4S] clusters are also present in radical SAM enzymes. Enzymes of the radical SAM superfamily catalyze for example methylations or ring formations in cofactor, vitamin or antibiotic biosynthesis (Sofia *et al.,* 2001; Booker & Grove, 2010). The reactions are initiated by cleavage of S-adenosyl-L-methionine (SAM) to methionine and a 5′-desoxyadenosyl radical (5′-dA·), using an electron provided by a reduced $[4Fe\text{-}4S]^{1+}$ cluster (Frey & Booker, 2001). The cluster is coordinated through three conserved cysteine residues in a characteristic CX_3CX_2CXC motif (Sofia *et al.,* 2001). Therefore, the fourth iron of the cluster represents an available coordination site for SAM (Walsby *et al.,* 2002). The first crystal structure of a radical SAM enzyme, HemN from *E. coli*, was published in 2003 (Layer *et al.,* 2003) (Figure 5).

1.6 Quinol-nitrate oxidoreductase from *E. coli*

Under anaerobic conditions and in presence of nitrate *E. coli* utilizes a respiratory chain for energy generation with the quinol-nitrate oxidoreductase, NarGHI (Guigliarelli *et al.,* 1992) as terminal oxidase. NarGHI is a heterotrimeric protein, forming a ´butterfly`-shaped dimer and is composed of a catalytic molybdenum cofactor subunit (NarG), an iron-sulfur cluster-containing electron transfer subunit (NarH) and a heme-containing membrane anchor subunit (NarI) (Bertero *et al.,* 2003).

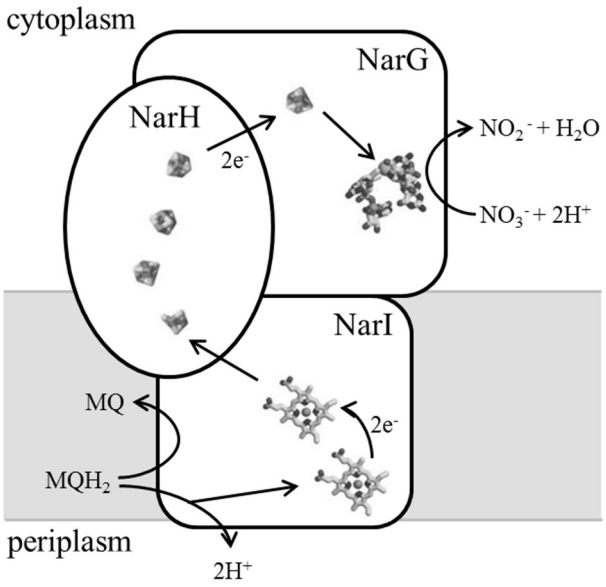

Figure 6: Proposed mechanism for the electron transfer of NarGHI. The electron transfer occurs via menaquione, hemes, iron-sulfur clusters and the molybdenum cofactor. NarGHI reduces nitrate to nitrite in the last step. MQ: menaquinone; MQH_2: menaquinol. Modified according to Rothery *et al.,* 2001; Bertero *et al.,* 2003.

NarG exhibits one molybdenum cofactor and one [4Fe-4S] cluster, NarH one [3Fe-4S] cluster and three [4Fe-4S] clusters and NarI two *b*-type hemes responsible for the menaquinol (MQH_2) oxidation and proton translocation (Figure 6; (González *et al.,* 2006). Furthermore, the two low-spin hemes mediate the electron transfer from the quinol binding and oxidation site to the Fe-S clusters in NarH. The electrons are passed to the Fe-S cluster and the molybdenum cofactor of NarG and reduce nitrate to nitrite (Berks *et al.,* 1995). In conclusion, the redox-active prosthetic groups mediate an electron transfer chain from the periplasmic to cytoplasmic site resulting in nitrate reduction.

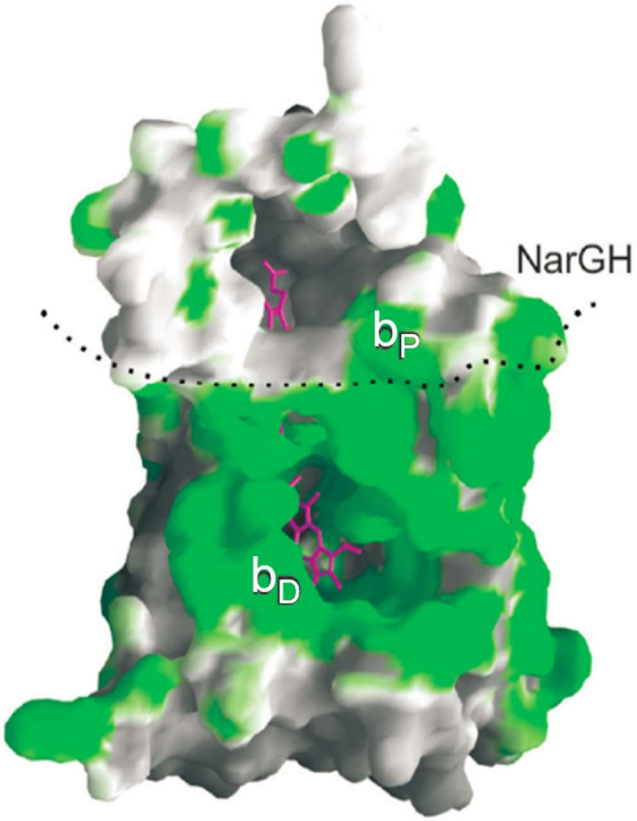

Figure 7: Surface representation of the structure of NarI. Polar and hydrophobic areas are in gray and green, respectively. The region above the dotted line is involved in interactions with NarGH (Bertero *et al.,* 2003). b_P: heme b proximal, b_D: heme b distal

The subunit NarI contains five transmembrane helices. The irons of the two low-spin hemes are each coordinated by two histidine residues. Heme b_P (proximal) is located near to the interaction area to NarG and forms hydrogen bonding and electrostatic interaction with various amino acids (Figure 7). In the more hydrophobic area of NarI the second heme b_D (distal) is located. It is arranged near to the quinol binding and oxidation site.

The hydrophobic environment should protect the hemes from interactions with solvent and probably a fast exchange of quinol-quinone molecules between NarI and the membrane (Bertero *et al.,* 2003).

1.7 The model organism zebrafish

The teleost fish *Danio rerio*, commonly known as zebrafish, has become a favorite model organism for studying vertebrate development. This model organism has several advantages compared to others. For example, a benefit are the transparent zebrafish embryos for direct visualization of tissue formation and organogenesis (Berman *et al.,* 2003). Furthermore, zebrafish forms large broods and the embryos form organs with earliest stage of development within 24 hours after fertilization.

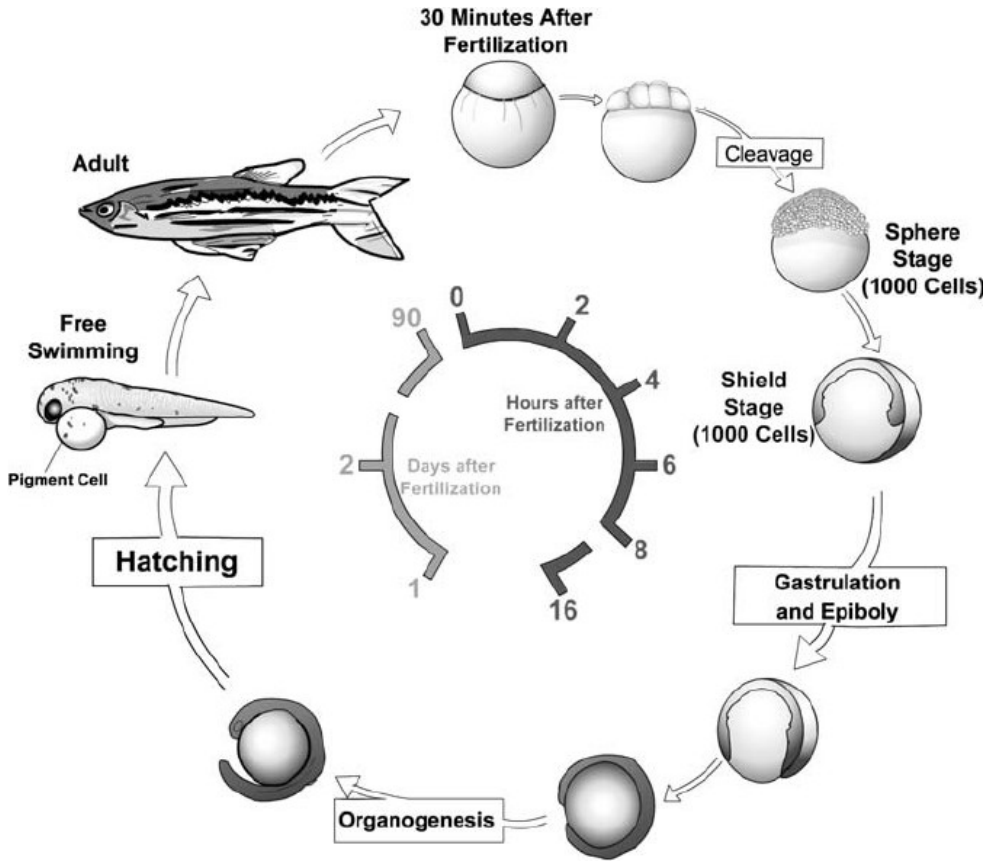

Figure 8: Stages of development in *D. rerio*. (D'Costa & Shepherd, 2009)

The first stage of the development of zebrafish is the zygote period with the first zygotic cell (Figure 8). In the following cleavage period and blastula period a 1000-cell stage

after 3 hours is formed. After 6 hours an embryonic shield from the animal pole is visible. Also in the gastrula period an epiboly from the animal to vegetal pole occurs. In the segmentation and pharyngula period different somite stages and the organogenesis takes place. After the last period, the hatching period, the embryo has a length of 3.5 mm and is free swimming. The final zebrafish embryo development takes about 20 days into adulthood (Gilbert *et al.,* 2006).

Zebrafish is well suited for studying blood diseases. For example zebrafish forms analogous blood cell types to mammals and other higher vertebrates (Berman *et al.,* 2003). Furthermore, in zebrafish the heme biosynthesis enzymes ALAS1, ALAS2, PBGS, PBGD, UROS, UROD, CPO, PPO and FC are present and the heme biosynthesis occurs like in mammals (Yanga *et al.,* 2015). A homologue of the heme chaperone HemW from *E. coli* is annotated in zebrafish as radical S-adenosyl methionine domain-containing protein 1 (RSAD1), a probable oxygen-independent coproporphyrinogen III oxidase. There consist a short and a long version, RSAD1-001 and RSAD1-002 (http://zfin.org/ZDB-GENE-030131-2508), located on chromosome 3. Alignments with *E. coli* HemW revealed an amino acid identity of 26.07 % for RSAD1-001 and 19.57 % amino acid identity for RSAD1-002. An involvement in heme trafficking of these proteins is not known until now.

1.8 Objectives of the work

At the start of this work, initial experimental evidence for the existence of a bacterial heme chaperone called HemW was obtained. Firstly, HemW from *L. lactis* was described as an iron-sulfur cluster containing protein with high affinity to heme (Abicht *et al.,* 2012). Secondly, Simone Karrie showed specific heme binding for *E. coli* HemW and the evidence for an iron-sulfur cluster was obtained (Huhn, 2012).

The aim of this study was to identify an enzymatic function for *E. coli* HemW and elucidate the corresponding enzyme mechanism. The function of the radical SAM-type iron-sulfur cluster of HemW should be investigated with EPR and Mössbauer spectroscopy. Corresponding coordinated cysteine residues should be exchanged to study the function of the cluster. Heme binding amino acids were to be identified via a mutagenesis approach. The function as heme chaperone should be tested via the heme transfer from heme-loaded *E. coli* HemW to heme-free nitrate reductase with subsequent functional assaying.

Finally, the function and location of the eukaryotic HemW analog RSAD1 should be tested using a zebrafish model.

2 Material and Methods

2.1 Instruments and Chemicals

Several instruments and chemicals from different manufacturers were used in this work. Following, the instruments and chemicals are listed.

2.1.1. Instruments

Article description and manufacturer of the used instruments are listed in Table 1.

Table 1: Instruments

Instrument	Model	Manufacturer
Agarose gel electrophoresis	Agagel Mini Agagel Standard G45/1	Biometra GmbH, Germany
Agarose gel documentation	MD-20/HD-20	WEALTEC Corporation, USA
Anaerobic chamber	Type B flexible vinyl chamber	Coy Laboratory Products, USA
	MACS MG-1000	Don Whitley Scientific Limited, UK
Autoclave	LVSA 50/70	Zirbus technology GmbH, Germany
Blotting equipment	Trans-Blot® Turbo™ Transfer System	Bio-Rad Laboratories, Germany
CCD camera	CoolSNAP *HQ*^{2}	Photometrics, USA
Cell disruption	FastPrep24	MP Biomedicals Germany GmbH, Germany

	French Pressure Cell Press	Thermo Fisher Scientific, USA
Centrifuges	Centrifuge 5804	Eppendorf AG, Germany
	Minispin	
	Avanti® J-26 XP	Beckmann Coulter GmbH, Germany
	Avanti® J-E	
	Avanti® J-30I	
	Optima L-90K Ultracentrifuge	
	Biofuge primoR	Hereaus, Germany
	Qik Spin QS 7000	Edwards Instruments, USA
	Savant™ Speed Vac SPD 110B	Thermo Fisher Scientific, USA
Chromatography	Äkta™ Purifier UV-900	GE Healthcare Europe GmbH, Germany
Cryo vessel	DryShipper QWick 14/24	MVE BioMedical, USA
Digital microscope	VH-Z20R	Keyence Corporation, Japan
Electrophoresis power supply	PowerPac 300	Bio-Rad Laboratories, Germany
	Standard Power Pack P25	Biometra GmbH, Germany
	BL030623	
High performance liquid chromatography	HPLC 2000 series	JASCO Labor- und Datentechnik GmbH, Germany
Liquid Scintillation Analyzer	Tri-Carb 2900TR	PerkinElmer LAS GmbH, Germany

Magnetic stirrer	IKAMAG® Reo	IKA®-Werke GmbH & Co.KG, Germany
	IKACOMBIMAG® Reo	
	MR3001	Heidolph Instruments GmbH & Co.KG, Germany
Microscope	TCS SP8 confocal laser scanning microscope	Leica Microsystems, Germany
pH determination	pH meter C 6840 B	Schott AG, Germany
Photometer	Ultrospec 2000	Biochrom, Germany
Pipettes	Eppendorf Research	Eppendorf AG, Germany
Protein concentration cells	Amicon Stirred Cell Model 8010	Merck Millipore, USA
Scales	572	Kern&Sohn GmbH, Germany
	BP 61S	Sartorius AG, Germany
	SBA 52	Scaltec Instruments GmbH, Germany
SDS-PAGE documentation	Dark Hood DH-50	biostep GmbH, Germany
SDS-PAGE system	Mini-Protean II 2-D Cell	Bio-Rad Laboratories, Germany
Shaker	TR-125	Infors AG, Switzerland
	3020	GFL GmbH, Germany
Spectrophotometer	NanoDrop® ND-1000	Peqlab Biotechnologie GmbH, Germany
Thermocycler	Tpersonal	Biometra GmbH, Germany
	96 universal peqSTAR	Peqlab Biotechnologie GmbH, Germany

	C1000™ Thermal Cycler	Bio-Rad Laboratories, Germany
	CFX96™ Real-Time System	
Thermomixer	Thermomixer compact	Eppendorf AG, Germany
	Thermomixer comfort	
	ThermoStat Plus	
UV-visible Spectrophotometer	V-550	JASCO Labor- und Datentechnik GmbH, Germany
	V-650	
Vortex	Vortex Genie 2	Scientific Industries, USA
Water purification	Milli-Q®-Synthesis	Merck Millipore, USA

2.1.2. Chemicals, Kits and Materials

For convenience, the manufacturer and article description of used chemicals, kits and materials are listed in Table 2.

Table 2: Chemicals, kits and materials

	Product	Source
Antibody	Anti-DIG	Roche Deutschland Holding GmbH, Germany
Blotting material	Blotting paper	Munktell&Filtrak GmbH, Germany
	Hybond ECL blotting membrane	GE Healthcare Europe GmbH, Germany
	Amersham ECL Prime Western Blotting Detection Reagent	

Chemicals	Bradford reagent	Sigma-Aldrich Chemie GmbH, Germany
	Hemin	Fluka, Germany
	NADH	Sigma-Aldrich Chemie GmbH, Germany
Chromatography Columns	Econo-Pac®	Bio-Rad, Hercules, USA
	Hypercarb™	Thermo Fisher Scientific, USA
	Superdex™ 200 10/300 GL	GE Healthcare Europe GmbH, Germany
Crystal Screens	NeXtal Tubes Cryos Suite	Qiagen, Germany
	NeXtal Tubes JCSG Core Suite I-IV	
	Morpheus®	Molecular Dimensions, UK
	Index Screen	Hampton Research, USA
Cuvettes	114-QS, 10 mm	Hellma GmbH & Co. KG, Germany
	105.202-QS, 10 mm	
	Cuvettes 10x4 mm	Sarstedt, Nümbrecht, Germany
Enzymes	Phusion DNA Polymerase	New England BioLabs, Germany
	T4 DNA Ligase	
	Taq DNA Polymerase	
	Restriction Enzymes	
	SuperScript® II Reverse Transcriptase	Thermo Fisher Scientific, USA
	PreScission™ Protease	GE Healthcare Europe GmbH, Germany
	RNA Polymerases	Roche Deutschland Holding GmbH, Germany

Kits	Q5® Site-Directed Mutagenesis Kit	New England BioLabs, Germany
	QuikChange II Site-Directed Mutagenesis Kit	Agilent Technologies, USA
	Gel Filtration Markers Kit for Protein Molecular Weights 12.000-200.000 Da	Sigma-Aldrich Chemie GmbH, Germany
	QIAquick Gel Extraction Kit	Qiagen, Germany
	QIAquick PCR Purification Kit	
	QIAprep® Spin Miniprep Kit	
	RNeasy Mini Kit	
Molecular weight standards	GeneRuler™ DNA LadderMix	Thermo Fisher Scientific, USA
	PageRuler™ Prestained Protein Ladder	
	Pierce™ Unstained protein molecular weight marker	
PCR materials	Oligonucleotides	Thermo Fisher Scientific, USA
	Deoxynucleotide Solution Mix	New England BioLabs, Germany
Other materials	Amicon®Ultra-0.5 ml, 10K	Merck Millipore, USA
	Protino® Glutathione Agarose 4B	Machery-Nagel, Germany
	Instant*Blue*™	Expedeon, UK
	Lysing Matrix B Bulk	MP Biomedicals, Germany GmbH, Germany

	Syringe filter (0.2 µm pore size)	Sarstedt, Nümbrecht, Germany
	Syringe filter (0.45 µm pore size)	
	Filtropur BT50 0.2	
	Ultracel®30 kDa Ultrafiltration Discs	Merck Millipore, USA
	illustra NAP-5 Columns	GE Healthcare Europe GmbH, Germany

Further chemicals and reagents were purchased from following companies: Amersham Biosciences, Applichem, Fluka, GE Healthcare, Merk, Roth, Sigma and MP Biomedicals.

2.2 Strains and Plasmids

In Table 3 and Table 4 are the used bacterial strains, cell lines and plasmids listed.

Table 3: Used *E. coli* strains and animal cell line.

Strain	Genotype	Reference
***Escherichia coli* BL21(DE3)**	F⁻ *dcm ompT hsdS*(r_B^- m_B^-) *gal* λ(DE3)	Agilent Technologies, USA
***Escherichia coli* DH10B**	F⁻ *mcr*A Δ(*mrr-hsd*RMS-*mcr*BC)Φ80*lacZ*ΔM15Δ*lac*X74 *rec*A1 *end*A1 *ara*Δ139Δ(*ara*, *leu*)7697 *gal*U *gal*K λ- *rps*L (Str^R) *nup*G	Invitrogen, Carlsbad, USA
***Escherichia coli* MC4100**	F- *araD139*Δ(*argF-lac*)*U169*, *rspL150*, *relA1*, *flbB5301*, *fruA25*, *deoC1*, *ptsF25*, *rbsR22*	Casadaban, 1976

***Escherichia coli* SHSP18**	F^- *lacY1*, *glnX44*(AS), *hemA8*, *trpA43*, *rpsL134*(strR), *malT1*(λ^R), *metB1, supE44, strA134*	Săsărman *et al.,* 1968
COS7	ECACC Cat# 87021302, RRID: CVCL_0224, DSMZ No. ACC-60; Isolated from *Cercopithecus aethiops*,; established by transfection with a mutated SV40 virus; 6 bp deletion in the replication origin	Gluzman, 1981

Table 4: List of used plasmids.

Plasmid	Description	Reference
pGEX-6P-1	Expression vector carrying N-terminal sequence for GST from *Schistosoma japonicum* and recognition sequence for PreScission™ Protease, *lac* promoter, *amp*^{r}	GE Healthcare Europe GmbH, Germany
pVA700	Expression vector carrying pJF119EH (*nar GHJI*) *amp*^{r}	Guigliarelli *et al.,* 1996
pGEX-hemW$_{E.c.}$	pGEX-6P-1 derivative, encodes N-terminal fusion of GST with HemW from *E. coli*	Grage, 2005; Huhn, 2012
pGEX-hemW-H140A	pGEX-hemW$_{E.c.}$ derivative with exchange of triplet CAT to GCG, protein carries alanine instead of histidine in position 140	This work
pGEX-hemW-H190A	pGEX-hemW$_{E.c.}$ derivative with exchange of triplet CAT to GCG, protein carries alanine instead of histidine in position 190	This work
pGEX-hemW-H250A	pGEX-hemW$_{E.c.}$ derivative with exchange of triplet CAC to GCG, protein carries alanine instead of histidine in position 250	This work

pGEX-hemW-H250R	pGEX-hemW$_{E.c.}$ derivative with exchange of triplet CAC to CGC, protein carries arginine instead of histidine in position 250	This work
pGEX-hemW-H268R	pGEX-hemW$_{E.c.}$ derivative with exchange of triplet CAC to CGC, protein carries arginine instead of histidine in position 268	This work
pGEX-hemW-W255L	pGEX-hemW$_{E.c.}$ derivative with exchange of triplet TGG to CTG, protein carries leucine instead of tryptophane in position 255	This work
pGEX-hemW-C16S	pGEX-hemW$_{E.c.}$ derivative with exchange of triplet TGC to AGC, protein carries serine instead of cysteine in position 16	This work
pGex-hemW-C16S-C20S-C23S	pGEX-hemW$_{E.c.}$ derivative with each exchange of triplet TGC to AGC, protein carries serine instead of cysteine in position 16, 20, 23	Toni Mingers, unpublished work
pCS2+	Mammalian expression vector with CMV, T7 and SP6 promoter, *amp*^{r}	Rupp *et al.,* 1994
pCS2+-FynVenus-GIpA	Expression vector to generate fusion proteins for cell transfection	Prof. Reinhard Köster
pCS2+-Venus-rsad1-GIpA	pCS2+ derivate, encodes N-terminal fusion of Venus with *D. rerio rsad1*	This work
pCS2+-RFP-GIpA	Expression vector to generate fusion proteins for cell transfection	Prof. Reinhard Köster
pCS2+-RFP-rsad1-GIpA	pCS2+ derivate, encodes N-terminal fusion of RFP with *D. rerio rsad1*	This work
pCS2+-mTFP-GIpA	Expression vector to generate fusion proteins for cell transfection	Prof. Reinhard Köster

pCS2+-mTFP-rsad1-GIpA	pCS2+ derivate, encodes N-terminal fusion of TFP with *D. rerio rsad1*	This work
pBluescript SK-	Cloning vector, *amp*^{r}	Stratagene, USA
pBlue-rsad1$_{D.r.}$	pBluescript SK- derivative for RNA transcription of *D. rerio rsad*	This work

2.3 Growth Media and Media Additives

2.3.1 Growth Media

For the cultivation of *E. coli* cells the nutritionally rich medium lysogeny broth (LB) (Bertani, 1951) was used.

LB medium:

trypton	10	g/l
NaCl	10	g/l
Yeast extract	5	g/l

For solid medium 15 g/l agar was added before sterilization.

2.3.2 Media Additives

Media additives were prepared as stock solutions and sterile filtrated. Additives were added after sterilization. In Table 5 the used media additives are listed.

Table 5: Media additives

Medium additive	Stock solutions	end concentration	storage
ampicillin (amp)	100 mg/ml in H_2O_{dest}	100 µg/ml	-20 °C
Isopropyl-1-thio-β-D-galactoside (IPTG)	1 molar in H_2O_{dest}	500 µM	-20°C

2.4 Microbial Techniques

2.4.1 Sterilization

All media and solutions were vapor sterilized for 20 min at 120 °C and 1 bar overpressure. Heat-sensitive substances were sterilized by filtration (pore width 0.2 µm).

2.4.2 Cultivation of Bacteria

For recombinant protein production, pre-cultures of *E. coli* BL21 (DE) containing the corresponding plasmids were grown at 200 rpm and 37 °C overnight in 50 ml LB medium containing the required additive. A 500 ml main culture was inoculated with pre-culture to a final dilution of 1:100 and incubated at 200 rpm and 37 °C. At an optical density (OD) of 0.6 at a wavelength of 578 nm, IPTG (Isopropyl β-D-1-thiogalactopyranoside) was added for initiation of protein production. Further growth occurred at 200 rpm and 17 °C.

Cultivation on agar-plates occurred as plating cell suspension with beads. Furthermore, cells were streaked with an inoculation loop from liquid culture or a single colony. Incubation occurred at 37 °C.

The cultivation of bacteria occurred under aerobic conditions.

2.4.3 Determination of Cell Density

For determination of the cell density of bacterial solutions OD was measured at wavelength 578 nm with a photometer. Dilutions were prepared for cell densities with $OD_{578} \geq 1$. OD_{578} of 1 equated 1 x 10^9 *E. coli* cells per ml.

2.4.4 Storage of Bacteria

Bacteria on agar-plates were stored for approximately 4 weeks at 4 °C. For long term storage, glycerol stocks were prepared. For this purpose, 800 µl of bacterial culture was mixed with 500 µl of sterile 80 % (v/v) glycerol. Glycerol stocks were immediately frozen and stored at -80 °C.

2.5 Molecular Biology Techniques

2.5.1 Preparation of Plasmid DNA

Plasmid DNA was isolated with the help of the QIAprep® Spin Miniprep Kit from Qiagen (Hilden, Germany) according to manufacturer's instructions. Plasmid DNA was stored in H_2O_{dest} at -20 °C.

2.5.2 Preparation of RNA from Zebrafish Embryos

RNA was isolated from around 24 hpf old zebrafish embryos with the help of the RNeasy Kit (Qiagen, Hilden, Germany). For disruption a pestle was used followed by homogenization using a QIAshredder homogenizer (Qiagen, Hilden, Germany). Afterwards, a DNase digestion of the RNA eluate was performed. Therefore, 50 µl RNA eluate was mixed with 6 µl 10x transcription buffer (Roche, Basel, Switzerland), 2 µl RNasin (Promega, Madison, USA) and 2 µl DNaseI (Roche, Basel, Switzerland) and incubated at 37 °C for 30 min. A RNA cleanup by the RNeasy Kit (Qiagen, Hilden, Germany) followed, according to manufacturer's instructions. The quality of the isolated RNA was determined by agarose gel electrophoresis (see 2.5.7).

2.5.3 cDNA Synthesis from *Danio rerio* RNA

For cDNA synthesis, 5 µl total RNA was incubated with 1 µl random hexamer primers (Promega, Madison, USA) at 70 °C for 5 min. Afterwards, 10 µl 5x SuperScript® II Reverse Transcriptase buffer (Invitrogen, Carlsbad, USA), 1 µl RNasin (Promega, Madison, USA), 5 µl dNTPs (2mM each), 5 µl DTT (0.1 mM) and 23 µl H_2O was added and incubated at 25 °C for 5 min. 1 µl SuperScript® II Reverse Transcriptase (Invitrogen, Carlsbad, USA) was added and the following incubation steps were:

25 °C	10 min
42 °C	60 min
70 °C	10 min
10 °C	∞

The resulting cDNA was kept at - 20°C for long-term storage.

2.5.4 Preparation of DIG-labeled Riboprobes

For preparation of riboprobes, the construct with *rsad1* was linearized and checked via agarose gel electrophoresis. The RNA was generated and labeled with digoxigenin (DIG) using *in vitro* transcription with T7 polymerase (Roche, Mannheim, Germany) for the antisense probe and T3 polymerase (Roche, Mannheim, Germany) for the sense probe. The sense probe was used as a control. The approach is listed below:

linearized plasmid DNA	10	µl
RiboLock (Thermo Fisher Scientific, Waltham, USA)	1	µl
10x transcription buffer (Roche, Mannheim, Germany)	2	µl
RNA Polymerase (20 U/µl)	1	µl
10x DIG labeling (Roche, Mannheim, Germany)	2	µl
H_2O (RNA-free)	3	µl

The mixture was incubated for 1 h at 37 °C before an additional 1 µl RNA Polymerase was added. After an additional hour 1.5 µl DNase (2 U/µl)) was added, followed by incubation at 37 °C for 20 min. The RNA was purified using the RNeasy Mini Kit according to manufacturer's instructions (Qiagen, Hilden, Germany). The quality of RNA was checked by agarose gel electrophoresis.

Incorporation of digoxigenin in antisense and sense probe was tested by dot blot with serial dilutions and detection via anti-DIG antibody. Riboprobes were stored in hybridization buffer (2.8.1.1) at -20 °C.

2.5.5 Determination of DNA Concentration

The concentration and purity of DNA were determined by a spectrophotometer. The ratio of OD_{260}/OD_{280} of 1.8-2.0 indicated a pure DNA solution.

2.5.6 Production and Transformation of Rubidium Chloride Competent *E. coli* Cells

For the *E. coli* main culture 250 ml LB medium were inoculated with the respective pre-culture to a final dilution of 1:100 and incubated at 200 rpm and 37 °C. At an OD_{578} of 0.6 the cells were harvested by centrifugation at 4500 x g at 4 °C for 5 min. The sediment was resuspended in 0.4 volumes ice-cold TFB1, referring to the original volume, and incubated on ice for 5 min. After a second centrifugation step at 4500 x g at 4 °C for 5 min the resuspension of the cell pellet was performed with 0.04 volumes ice-cold TFB2 and incubated for 15 - 60 min on ice. Fifty µl aliquots were stored at -80 °C.

For transformation, competent cells were thawed on ice for 30 min. About 200 ng plasmid DNA were added and incubated for 10 min on ice. After a heat shock at 42 °C for 45 sec the cells were cooled on ice for 5 min. In the next step, 250 µl LB medium were added and the cells were incubated at 37 °C for 15 - 60 min. Different amounts of cell suspension was plated on LB agar plates with the respective antibiotics and incubated at 37 °C overnight.

TFB1:

KOAc	30	mM
$CaCl_2$	10	mM
$MnCl_2$	50	mM
RbCl	100	mM
glycerol	15	% (v/v)
in H_2O_{dest}, pH 5.8		

TFB2:

MOPS	10	mM
$CaCl_2$	75	mM
RbCl	10	mM
glycerol	15	% (v/v)
in H_2O_{dest}, pH 6.5		

2.5.7 Agarose Gel Electrophoresis

DNA and RNA molecules were separated according to their mass proportions by gel electrophoresis in gels consisting of 1 % (w/v) agarose in TAE buffer. The negative charged molecules migrate toward the anode by voltage application of around 100 V. Before DNA loading, the DNA samples were mixed with loading dye to facilitate loading. GeneRuler™ DNA Ladder Mix (Thermo Fisher Scientific, Waltham, USA) was used as size standard.

Before RNA loading, the RNA samples were mixed with loading dye from the SP6 Transcription Kit (Thermo Fisher Scientific, Waltham, USA) and incubated at 99 °C for 10 min.

For detection of DNA and RNA the gel was stained after electrophoresis with ethidium bromide for approximately 15 min and visualized at a wavelength of 312 nm via UV light.

TAE buffer:

Tris-acetate	40	mM
EDTA	1	mM
in H_2O_{dest}, pH 8		

6x DNA loading dye:

bromophenol blue	0.45	mM
xylene cyanol	0.45	mM
glycerol	34.0	% (v/v)
in H_2O_{dest}		

ethidium bromide solution:

ethidium bromide	1	% (v/v)
in H_2O_{dest}		

2.5.8 Site-Directed Mutagenesis of DNA

For the exchange of single amino acid residues in a protein, site-specific mutant variant of the corresponding gene sequence can be generated. In this work the QuikChange Site-directed Mutagenesis Kit (Qiagen, Hilden, Germany) and the Q5® Site-Directed Mutagenesis Kit (New England Biolabs, Frankfurt am Main, Germany) served for the development of several HemW$_{E.c.}$ variants.

For site-directed mutagenesis using the QuikChange Site- directed Mutagenesis Kit a dsDNA plasmid carrying the gene of interest and two synthetic oligonucleotide primers which contain the desired mutation (

Table 6) are necessary. The PCR reactions with the QuikChange Site-Directed Mutagenesis Kit were carried out according to manufacturer's instructions. After isolation of mutated plasmid DNA, the DNA was transformed into *E. coli* strain DH10B. Sequencing performed by GATC Biotech AG (Konstanz, Germany) of the plasmid DNA verified the mutation.

The Q5® Site-Directed Mutagenesis Kit needs a dsDNA plasmid similar to the other kit, however, it uses different primers than the QuikChange Kit. In detail, only the forward primer includes the desired mutation. The primers were designed with the online tool NEBaseChanger™ v1.2.4 and are listed in Table 6.

Table 6: Oligonucleotide primers used for site-directed mutagenesis of HemW$_{E.c.}$. "F" refers to forward primer and "R" refers to reverse primer. The underlined sequences indicate the changed nucleic acid triplet.

Mutant designation in HemW$_{E.c}$	Sequence of oligonucleotide primer (5´→3´)
pGEX-hemW-H140A	F: CTTGGGCGTATTGCGGGCCCGCAAGAA R: TTCTTGCGGGCCCGCAATACGCCCAAG
pGEX-hemW-H190A	F: CTGAATCCGCCGGCGCTTTCCTGGTAT R: ATACCAGGAAAGCGCCGGCGGATTCAG
pGEX-hemW-H250A	F: TATCAGTGCCAGGCGAATCTCAACTAC R: GTAGTTGAGATTCGCCTGGCACTGATA

pGEX-hemW-H250R	F: TCAGTGCCAGCGCAATCTCAACT R: TAACCGGGTTTGGCGTAAG
pGEX-hemW-H268R	F: CTGCGGCGCACGCGGCAAAGTGA R: CCAATACCGATGTAGTCACCAAAGCGC
pGEX-hemW-W255L	F: TCTCAACTACCTGCGCTTTGGTG R: TTGTGCTGGCACTGATAAC
pGEX-hemW-C16S	F: CACATCCCGTGGAGCGTGCAGAAATGC R: GCATTTCTGCACGCTCCACGGGATGTG
pGEX-hemW-H250R-W255L (generated from pGEX-hemW-H250R)	F: TCTCAACTACCTGCGCTTTGGTGAC R: TTGCGCTGGCACTGATAA

2.5.9 Amplification of DNA Fragments

2.5.9.1 Design and synthesis of oligonucleotide primers

Primers for the amplification of *D. rerio rsad1* gene were designed with recognition sites of restriction endonucleases necessary for insertion at both ends of the genes. In Table 7 the oligonucleotide primers are listed. The recognition sites of restriction endonucleases are underlined. All primers were purchased from Eurofins Genomics (Ebersberg, Germany).

Table 7: Oligonucleotide primers used for amplification of DNA fragments. "F" refers to forward primer and "R" refers to reverse primer. Underlined are the restriction sites used for cloning.

Primer	Sequence of oligonucleotide primer (5′→3′)	additional information
RSAD1-F	TATGAATTCCACCATGTCGACACGAG TTTTAACTTTAAC	pBS/pCS2+ forward, *EcoRI* restriction site

RSAD1-R-pBS	ATTCTCGAGTTATTGTGTCCTTTTGATTCCCCTGCTGTG	pBS reverse, *XhoI* restriction site
RSAD1-R-pCS2+	ATACTCGAGCCTTGTGTCCTTTTGATTCCCCTGCTGTGG	pCS2+ reverse, *XhoI* restriction site

2.5.9.2 Polymerase Chain Reaction (PCR)

The polymerase chain reaction (PCR) was used to amplify the gene *rsad1* from *D. rerio* cDNA. The utilized DNA Polymerase was the Phusion® High-Fidelity DNA Polymerase (New England Biolabs, Frankfurt am Main, Germany). The standard composition of the reaction is listed below.

PCR composition:

Template cDNA	20 - 200	ng
5x Phusion™ HF buffer	10	µl
forward primer	100	pmol
reverse primer	100	pmol
dNTP mix	280	µM
Phusion™ DNA polymerase	1	U
H_2O_{dest}	ad 50	µl

In the first step, the template cDNA was denaturized for 5 min at 98 °C. Afterwards, 40 cycles of denaturation, primer annealing and extension occurred. The last step is a final extension at 72 °C for 10 min. Annealing temperature depends on length and GC content and was calculated as follows:

$$T_m\ [°C] = 69.3 + 0.41\ (\%\ G+C) - 650/n$$

In this formula the percental G+C content and the number of nucleotides (n) of the primers are included. The duration of the elongation step depends on the length of the amplicon.

For the used Phusion® High-Fidelity DNA Polymerase an extension time of 15 sec per 1 kb amplicon can be used. Following, the PCR protocol is listed.

PCR program:

98 °C	5 min	
98 °C	1 min	
68-72 °C	1 min	40x
72 °C	60 - 120 sec	
72 °C	10 min	
8 °C	∞	

2.5.9.3 Purification of PCR products

Amplified DNA by PCR was controlled via agarose gel electrophoresis. If only one PCR product was present, the PCR products were purified via QIAquick PCR Purification Kit (Qiagen, Hilden, Germany) according to manufacturer's instructions. Otherwise, the DNA fragment of interest was excised from the gel and purified with the QIAquick Gel Extraction Kit (Qiagen, Hilden, Germany) resulting in an isolated DNA fragment.

2.5.10 Enzymatic Modification of PCR Products

2.5.10.1 DNA Cleavage

For DNA cleavage restriction endonucleases were used. A specific palindromic DNA sequence is necessary for recognition by the enzymes. Hydrolysis of two phosphodiester bonds inside this sequence results in either blunt or sticky ends. All used restriction endonucleases were purchased from New England Biolabs (Frankfurt am Main, Germany). The cleavage was performed according to manufacturer's instructions for either at 37 °C for 2 h or at 17 °C overnight. Successful cleavage was controlled via agarose gel electrophoresis.

2.5.10.2 Ligation

DNA double-strand breaks are repaired by the DNA ligase. In this context, the 3' hydroxyl end of one nucleotide is covalently connected with the 5' phosphate end of another nucleotide. To prevent a recirculation of cleaved vectors the 5' phosphate group was removed by the alkaline phosphatase treatment (New England Biolabs, Frankfurt am Main, Germany). The procedure was performed according to manufacturer's instructions.

For ligation of DNA and vector, T4 DNA ligase (New England Biolabs, Frankfurt am Main, Germany) was used. The ratio of insert DNA to vector DNA was around 5:1. The reaction mixtures were incubated either at room temperature for 1 h or at 17 °C overnight.

2.5.11 DNA Sequencing and Data Analysis

For determination of DNA sequences, purified DNA was send to GATC Biotech AG (Konstanz, Germany). The sequence files were analyzed using the Applied Biosystems Sequence Scanner Software v1.0 (Thermo Fisher Scientific, Waltham, USA).

2.6 Biochemical Methods for Protein Analysis

2.6.1 Recombinant Production and Purification of *Escherichia coli* HemW

2.6.1.1 Cell Growth for Protein Production

The procedure for HemW protein production was described previously by Simone Karrie (Huhn, 2012) in her PhD thesis. In detail, cultures of *E. coli* BL21(DE3) carrying the plasmid pGEX-*hemW* or pGEX-*hemW* variants were grown at 200 rpm and 37 °C. For this purpose, 500 ml sterile LB medium containing 100 µg/ml ampicillin in 1 l baffled Erlenmeyer flasks were inoculated with 5 ml of an overnight culture of the production strain. The expression of *hemW* was induced at an OD 578 nm of 0.6 by addition of 500 µM IPTG. Further incubation overnight occurred at 180 rpm and 17 °C. The harvest of the cells was performed under anaerobic conditions. Therefore the cultures were transformed in centrifuge tubes and left open in an anaerobic chamber for 30 minutes. Afterwards, the cells were pelleted at 3500 x g and 4° C for 15 min. All following steps e.g. decanting the supernatant were carried out under anaerobic conditions.

2.6.1.2 Cell Disruption

All of the following steps were carried out under anaerobic conditions. The cell sediment (see 2.6.1.1) was resuspended in appropriate amounts of anaerobic protein buffer. The disruption of the cells was performed via a single passage through a French Press (Thermo Fisher Scientific, Waltham, USA) at 19,200 psi. (1324 bar). A centrifugation at 192.000 x g and 4 °C for 60 min separated the cell debris and insoluble proteins. The resulting supernatant was loaded onto a Protino® Glutathione Agarose column (Machery-Nagel, Düren, Germany) (2.6.1.3). The composition of the protein buffer is listed below.

Protein buffer:

NaCl	140	mM
KCl	2.7	mM
Na_2HPO_4	10	mM
KH_2PO_4	1.8	mM
DTT	5	mM
in H_2O_{dest}, pH 7.4		

2.6.1.3 Affinity Chromatography

The affinity chromatography was performed under anaerobic conditions. An Econo-Pac® Chromatography Column (Bio-Rad, Hercules, USA) was prepared with 5 ml Protino® Glutathione Agarose (Machery-Nagel, Düren, Germany) according to manufacturer's instructions. After 10 column volumes (cv) of H_2O_{dest} the glutathione agarose was equilibrated with 10 cv protein buffer (2.6.1.2). The cell-free extract (2.6.1.2) was mixed with the glutathione agarose and incubated for 2 h. The flow-through was collected and the column was washed with 12 cv protein buffer. All washing steps were collected. Afterwards, 7 ml buffer containing 800 U PreScission Protease (GE Healthcare, Freiburg, Germany) were mixed with the column resin and incubated overnight. In this step, the protein was clipped off the GST-tag. The separated protein was rinsed twice with 7 ml protein buffer and twice with 15 ml protein buffer and collected separately. To elute the GST-tag, the column was washed with 12 cv of elution buffer. The composition of the used buffer systems is listed below.

All collected fractions including flow-through, washing steps, protein fractions and elution fractions were analyzed via SDS-PAGE (2.6.12).

Elution buffer:

NaCl	140	mM
KCl	2.7	mM
Na_2HPO_4	10	mM
KH_2PO_4	1.8	mM
glutathione	10	mM
in H_2O_{dest}, pH 7.4		

2.6.2 Recombinant production of *E. coli* NarGHI

The production of *E. coli* membrane vesicles with the overproduced *E. coli* quinol oxidoreductase was performed by the group of Prof. Dr. Axel Magalon (Laboratoire de Chimie Bacterienne, CNRS, Marseille, France).

2.6.2.1 Cell Growth for Protein Production

The Δ*hemA* strain SHSP18 is disabled in synthesis of the heme cofactor due to a mutation in the *hemA* gene encoding the first enzyme of the glutamyl-tRNA reductase pathway (Săsărman *et al.,* 1968). The cells were transformed with the pVA700 plasmid allowing overexpression of the NarGHI complex (Guigliarelli *et al.,* 1996). Due to the lack of the heme cofactor, the transformants were isolated on LB-agar plates supplemented with 150 µM δ-aminolevulinic acid permitting the synthesis of heme, 0.8 % glucose and 100 µg/ml ampicillin for selection.

Wild type strain *E. coli* MC4100 was likewise transformed with the pVA700 plasmid for the overproduction of the NarGHI complex. The following steps are the same for the Δ*hemA* strain SHSP18 transformed with the pVA700 plasmid and the wild type strain *E. coli* MC4100 transformed with the pVA700 plasmid. LB medium supplemented with glucose, sodium formate, sodium selenite, sodium molybdate and phosphate buffer was inoculated from a single colony, closed hermetically and incubated overnight at 37 °C. The detailed medium composition is listed in chapter 2.6.2.2.

For production of NarGHI, 2 L of the same medium supplemented with 200 µM IPTG were inoculated with the overnight culture at an $OD_{600\ nm}$ of 0.05 incubated for 24 h at 37 °C. At an $OD_{600\ nm}$ of 1.7 cells were pelleted by centrifugation at 5000 x g for 10 min and kept at -20 °C until further use.

2.6.2.2 Preparation of Membranes Vesicles

Cells were resuspended in 50 mM MOPS buffer with 1 mM $MgCl_2$, pH 7.2 and broken by two passages at the French press at 1100 psi (76 bar). Intact cells and debris were removed by a low speed centrifugation step at 14000 x g. Membrane fraction were obtained after ultracentrifugation at 400000 x g for 90 min. The membrane vesicles were resuspended in 50 mM MOPS buffer with 1 mM $MgCl_2$, pH 7.2 and kept at -80 °C until use.

Medium:

trypton	10	g/L
NaCl	10	g/L
yeast extract	5	g/L
glucose	0.8	%
sodium formate	12.5	mM
sodium selenate	2	µM
sodium molybdate	2.5	µM
ampicillin	100	µg/ml
phosphate buffer	100	mM, pH 6.8

2.6.3 Concentration of Protein Solutions

Large quantities of thin protein solutions were concentrated either in a 50 ml or in a 10 ml stirred ultrafiltration cell (Amicon Stirred Cell Model 8010; Merck Millipore, Billerica, USA) using a Ultracel®30 kDa Ultrafiltration Disc (Merck Millipore, Billerica, USA) at

2.5 bar. For smaller quantities 0.5 ml Amicon®Ultra, 10K concentrators (Merck Millipore, Billerica, USA) were used.

2.6.4 Determination of Protein Concentration

To determine the protein concentration, the Bradford Protein Assay Method (Bradford, 1976) from Sigma-Aldrich (Taufkirchen, Germany) was used. This protein assay is based on complexing of proteins with Brilliant Blue G. The protein sample is mixed with the reagent and incubated at room temperature for 20 min. The shift of the dye from 465 nm to 595 nm is proportional to the protein content. For calibration, Bradford assay were performed with different concentration of bovine serum albumine (BSA) and a calibration curve was established (Figure 9).

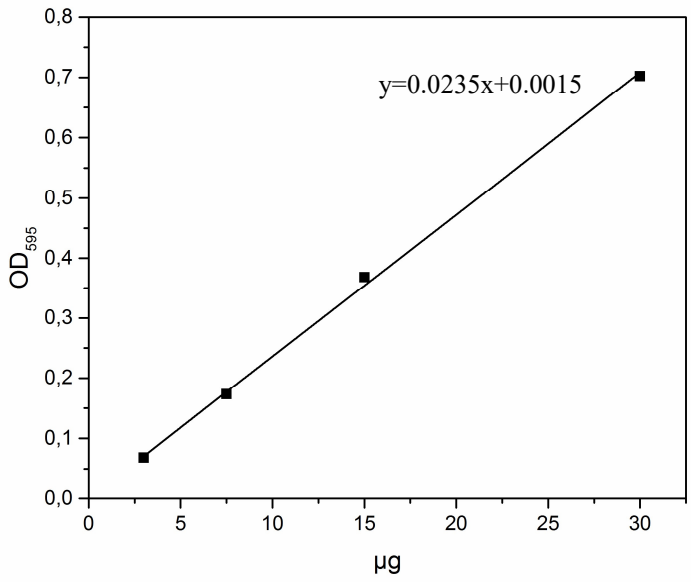

Figure 9: Calibration curve for determination of protein concentrations. Different amounts of BSA were incubated with Bradford reagent and incubated for 20 min. The used amount was plotted against the absorption at 595 nm. The calibration curve was prepared by Stefan Barthels (Technician, Institute of Microbiology, TU Braunschweig, Germany).

2.6.5 Reconstitution of the Iron-Sulfur cluster

The reconstitution of the iron-sulfur cluster of purified *E. coli* HemW and HemW variants were performed under anaerobic conditions at 17 °C. The protein was concentrated up to 100 - 200 µM and incubated with 10 mM DTT for 1 h. For the one expected [4Fe-4S] cluster of *E. coli* HemW 500 µM ammonium ferric citrate was added to the protein solution, mixed and incubated for 5 min. Afterwards, 500 µM lithium sulfide was added, inverted and incubated for 15 min. The reaction was stopped by a centrifugation step at

12.100 x g for 5 min. The buffer was exchanged via an illustra^{TM} NAP^{TM}-5 column (GE Healthcare, Freiburg, Germany) to remove residual ammonium ferric citrate and lithium sulfide. The buffer exchange was performed according to manufacturer's instructions. Successful reconstitution was checked via UV-Vis spectroscopy (2.6.10) and determination of iron and sulfur content (2.6.6; 2.6.7).

2.6.6 Determination of Protein Iron Content

The iron content of recombinant, purified HemW was determined colorimetrically (Fish, 1988). For this purpose, different amounts of protein solution were mixed with 45 µl of 1 M perchloric acid (PCA) and incubated for 15 min at RT. After centrifugation at 9000 x g for 5 min, 90 µl of the supernatant were mixed with 72 µl bathophenanthroline disulfate (1.7 mg/ml), 36 µl sodium ascorbate (38 mg/ml) and 27 µl 1:3 diluted saturated ammonium acetate solution and incubated for 30 min at RT. Samples were centrifuged at 9.300 x g for 5 min. Hundred µl of the resulting supernatant was photometrical tested at 535 nm and 680 nm wavelength using a quartz cuvette 105.202- QS (Hellma Analytics, Müllheim, Germany) and a V- 650 spectrophotometer (JASCO, Groß-Umstadt, Germany). On the basis of solutions containing different iron amounts (0, 0.5, 1, 2, 4, 8 nmol, Merck Millipore, Billerica, USA) a calibration curve was obtained (Figure 10).

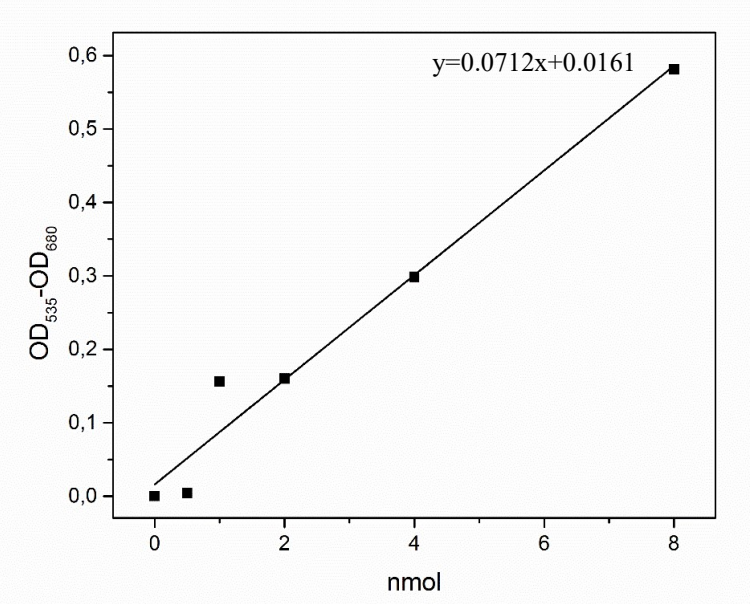

Figure 10: Iron calibration curve for determination of iron concentrations. The used amount of iron (0, 0.5, 1, 2, 4, 8 nmol) was plotted against the absorption at 535 nm minus the absorption at 680 nm.

2.6.7 Determination of Protein Sulfur Content

The sulfur content of recombinant, purified HemW was determined colorimetrically with bathophenanthroline (Beinert, 1983). Hundred µl protein solution was mixed vigorously with 300 µl 1 % $Zn(OAc)_2 \cdot 2\ H_2O$ and 15 µl 3 M NaOH, and incubated for 10 min at RT. Subsequently, 75 µl of 0.1 % Dimethyl-4-phenylenediamine (DMPD) and 16 µl 23 mM $FeCl_3$ were added and the solution was vigorously mixed and incubated at 4 °C for 3 h. A centrifugation step at 9.300 x g for 5 min stopped the reaction. The resulting supernatant was photometrical measured at 670 nm using a quartz cuvette 105.202- QS (Hellma Analytics, Müllheim, Germany) and a V- 650 spectrophotometer (JASCO, Groß-Umstadt, Germany). The sulfur content of the samples was determined via a calibration curve obtained from a series of dilutions of 20 mM lithium sulfide (Figure 11).

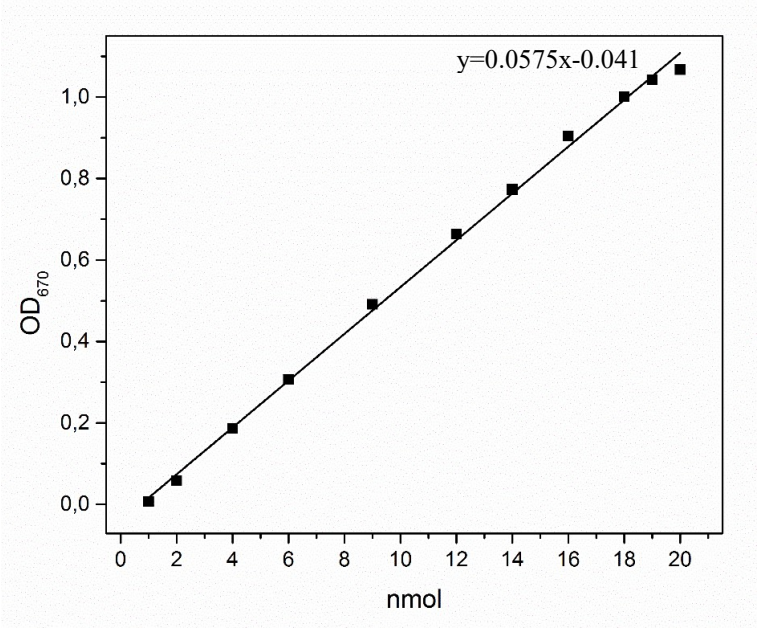

Figure 11: Sulfur calibration curve for determination of sulfur concentration. The used amount of sulfur was plotted against the absorption at 670 nm.

2.6.8 SAM-Binding Assay

The SAM-binding assay was performed as described previously (Storbeck *et al.,* 2009). All steps were performed anaerobically. HemW and hemin were incubated overnight in equimolar amounts. Afterwards, 100 µM HemW with bound hemin and reconstituted [4 Fe-4 S] cluster were incubated with 0.5 µCi of [methyl-^{14}C]-S-adenosyl-L-methionine

in a final volume of 250 µl at 25 °C for 1 h. The mixture was then passed over a illustra™ NAP™-5 column (GE Healthcare, Freiburg, Germany) and eluted with 3 ml protein buffer (2.6.1.2). The elution fractions of 200 µl were analyzed for radioactivity using a liquid scintillation counter (Perkin Elmar, Waltham, USA). The identical experiment was carried out with BSA, serving as control.

2.6.9 Assay for SAM Cleavage

For SAM cleavage, 25 µM HemW were incubated with 0.6 mM sodium dithionite and 0.6 mM S-adenosyl-L-methionine under anaerobic conditions at 17 °C overnight. The reaction was stopped by adding 5 % formic acid. As control, the experiment was performed with *E. coli* HemN. For HPLC analysis, the samples were centrifuged at 16.100 x g for 10 min. HPLC analysis was performed as described previously (Kühner, 2015). In detail, for detection of 5′-deoxyadenosine a Hypercarb™ column (Thermo Fisher Scientific, Waltham, USA) at a JASCO 2000 system (JASCO, Groß-Umstadt, Germany) was used. A 5 ml gradient of 0.1 % TFA in H_2O and 0.08 % TFA in acetonitrile with a flow rate of 0.2 ml/min was performed at room temperature. Detection of 5′-deoxyadenosine was at 254 nm.

2.6.10 UV-Vis light Absorption Spectroscopy

UV-Vis light absorption spectra were recorded under aerobic or anaerobic conditions using a V-550 and V-650 spectrophotometer (JASCO, Groß-Umstadt, Germany). Quartz cuvettes with different volumes and 10 mm light path were used (114- QS, 115-QS, 105.202-QS, Hellma Analytics, Müllheim, Germany).

2.6.11 Gel Permeation Chromatography

For performing an analytical gel permeation chromatography a 24 ml Superdex® 200 10/300 GL column (GE Healthcare, Freiburg, Germany) and an ÄKTApurifier system (GE Healthcare, Freiburg, Germany) were used. The column was calibrated using marker proteins (carbonic anhydrase (M_r= 29,000), bovine serum albumin (M_r= 66,200), yeast alcohol dehydrogenase (M_r= 150,000), and β-amylase (M_r= 200,000)). By means of the calibration curve (Figure 12) the native relative molecular mass of the analyzed proteins were determined. The column was equilibrated with 2 cv protein buffer. Before injection, the protein sample was centrifuged at 9.300 x g for 5 min or filtered through a 0.45 µm

pore size syringe filter (Sarstedt, Nümbrecht, Germany). Protein of a concentration of 3 mg/ml was chromatographed at a flow rate of 0.5 ml/min. The process was monitored by a UV detector at 280 nm, 410 nm and 420 nm. After gel permeation chromatography, collected fractions were analyzed by SDS-PAGE (2.6.12).

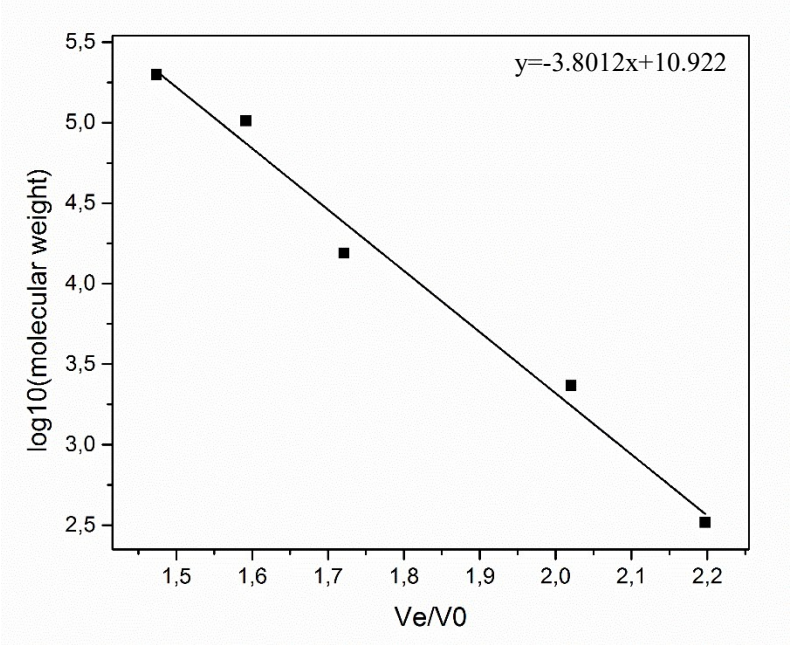

Figure 12: Superdex® 200 10/300 GL calibration curve. The decadic logarithm of the molecular weight of the marker proteins is plotted against their elution volume (V_e) divided with the 'dead volume' (V_0) of the column. Calibration curve was prepared by Maria Höninger (Student, Institute of Microbiology, TU Braunschweig, Germany).

2.6.12 Discontinuous SDS-PAGE

By SDS-polyacrylamide gel electrophoresis (SDS-PAGE) proteins are separated due to their molecular weight in a gel matrix subjected to an electric field (Conejero & Semancik, 1977).

Protein samples were mixed with 2x SDS loading buffer and heated for denaturation to 95 °C for 5 min. 8 µl of protein samples and 7 µl protein ladder (PageRuler™ Unstained Protein Ladder, PageRuler™ Prestained Protein Ladder, Thermo Fisher Scientific, Waltham, USA) were loaded onto the gel and the gel was run at 45 mA in electrophoresis buffer.

For visualization of the protein bands, the gel was stained with Instant*Blue*™ (Expedeon, Swavesey, UK) for 15 min and washed afterwards with water.

SDS-PAGE:

	running gel [12 % (v/v)]		stacking gel [6 % (v/v)]	
acrylamide stock solution	2.0	ml	500.0	µl
buffer for running gel	1.25	ml	-	
buffer for stacking gel	-		625.0	µl
$H_2O_{deion.}$	1.75	ml	1.375	ml
APS-Solution	5.0	µl	3.0	µl
TEMED	50.0	µl	30	µl

Acrylamide stock solution:

Rotiphorese® Gel 30 (37,5:1) (Roth, Karlsruhe, Germany)

APS solution:

Ammonium peroxodisulfate	10	%
in H_2O_{dest}		

Buffer for running gel:

Tris-HCl	1.5	M
SDS	0.4	% (w/v)
in H_2O_{dest}, pH 8.8		

Buffer for stacking gel:

Tris-HCl	0.5	M
SDS	0.4	% (w/v)
in H_2O_{dest}, pH 6.8		

Electrophoresis buffer:

Tris-HCl	14.5	mM
glycine	1.44	% (w/v)
SDS	1.0	% (w/v)
in H_2O_{dest}, pH 8.4		

SDS loading dye:

Tris-HCl, 1.5 M	100	mM
glycerol, 80 %	40	% (v/v)
β-mercaptoethanol	10	% (v/v)
SDS, 20 %	3.2	% (w/v)
bromphenol blue	0.2	% (w/v)
in H_2O_{dest}, pH 6.8		

2.6.13 Preparation of Hemin Solution

For all heme binding studies the commercial available hemin was used (Fluka, St. Gallen, Germany). Dissolving of hemin was performed according to Owens *et al.,* 2012. In detail, 4 mg hemin were dissolved in 400 µl 100 mM NaOH and thoroughly mixed. After 30 min 400 µl of 1 M Tris-HCl, pH 7.4 was added and centrifuged at 14.00 x g and 4 °C for 10 min. The concentration of the supernatant was determined by UV absorbance using an ε_{385} of 58.44 mM^{-1} cm^{-1}. For dilutions 50 mM Tris-HCl, pH 7.4 was used. Hemin was prepared immediately before use. If not otherwise declared, equimolar amounts of hemin were mixed with HemW and incubated overnight.

2.6.14 Heme Stain

For detection of bound heme in proteins a heme stain was performed (Feissner *et al.,* 2003). This technique utilizes the peroxidase activity of heme for the detection with a

chemiluminescent detection reagent (Amersham ECL Prime Western Blotting detection reagent, GE Healthcare, Freiburg, Germany).

Protein samples were mixed with SDS loading dye without β-mercaptoethanol (see below). In contrast to the standard protocol for SDS-PAGE (2.6.12), the samples were not heated. For this purpose, 8 µl protein solution (1 mg/ml) were loaded twice onto the gel and run at 45 mA. After electrophoresis, half of the gel was stained for proteins with Instant*Blue*™ (Expedeon, Swavesey, UK) and the second half was blotted onto a nitrocellulose membrane (Towbin *et al.,* 1979).

For the blotting, the nitrocellulose membrane (GE Healthcare, Freiburg, Germany) was activated with water. Afterwards the SDS gel and the membrane were incubated in transfer buffer for 10 min and the different components were assembled in following order in the semi dry blotting apparatus: cathode, blotting paper, SDS gel, PVDF membrane, blotting paper, anode (Figure 13). Proteins were blotted onto the membrane by applying 25 mA and 1 V for 12 min at the Trans-Blot® Turbo™ Transfer System (Bio-Rad, Hercules, USA). Following three washing steps for 5 min of the membrane with PBS buffer. After 5 min incubation time with Amersham ECL Prime Western Blotting Detection Reagent (GE Healthcare Europe GmbH, Germany) the heme signal was detected with a CCD camera (CoolSNAP *HQ*^{2}, Photometrics,Tucson, USA).

Figure 13: Schematics of a western blotting apparatus.

SDS loading dye for heme stain:

Tris-HCl, 1.5 M	100	mM
glycerol, 80 %	40	% (v/v)
SDS, 20 %	3.2	% (w/v)
bromophenol blue	0.2	% (w/v)
in H_2O_{dest}, pH 6.8		

Transfer buffer:

Tris-HCl, pH 8.5	21.3	mM
glycine	192	mM
methanol	10	% (v/v)

TBS buffer:

NaCl	150	mM
Tris-HCl	50	mM
in H_2O_{dest}, pH 7.5		

2.6.15 Acidified Butanone Extraction

Acidified butanone extraction was performed as described previously (Teale, 1959). In detail, 25 µM HemW or HemW variants were incubated with 15 µM hemin overnight in a final volume of 250 µl. The pH was adjusted to 1.5 - 2 with 10 % HCl before 250 µl ice-cold butanone were added. The reaction mix was carefully inverted and incubated on ice. Due to the formation of two phases, either non-covalent (hydrophobic phase) or covalent (hydrophilic phase) binding of heme is detectable.

2.6.16 Antibody Preparation

For interaction studies of HemW with potential interaction partners, e.g. NarGHI, antibodies are a helpful tool. Therefore, Sabine Buchmeier (Antibody Facility of the TU Braunschweig, Germany) isolated monoclonal antibodies based on the hybridoma technology. First, purified HemW was sterile filtrated and prepared for immunization of BALP/c mice according to an established protocol. The immunization, production of hybridoma cells and cloning were performed according to a standard protocol. Afterwards, the cell culture medium with secreted antibodies were tested in an enzyme linked immunosorbent assay (ELISA) and Western-Blot analysis. The antibodies were screened for denatured HemW and native HemW recognition. In addition, *E. coli* HemN served as negative control due to the high amino acid sequence homology. Several

specific antibodies were successfully generated, but the sensitivity remained to be determined.

2.6.17 Quinol Nitrate Oxidoreductase Assay

The activity of *E. coli* quinol nitrate oxidoreductase was spectrophotometrically measured according to Lanciano *et al.,* 2007. The changes in absorption of the ubiquinol analogue 2-methyl-1,4-naphtoquinol (menadiol), caused by oxidation, were detected at 260 nm. First, the menadione has to be reduced to menadiol by using zinc and HCl (Figure 14).

Reduction of menadione (Sigma Aldrich, St. Louis, USA)

Figure 14: Protocol for reduction of menadione. All steps were performed in a 2 ml amber glass vial with a screw top (Supelco, Bellefonte, Pennsylvania).

Due to the absorption limit of the spectrophotometer, an amount of 4 µg NarGHI isolated from the SHSP18 and MC4100 strains were used for the assays. The measurement was performed using the V-550 or V-650 UV-Vis Spectrophotometer, a double-beam spectrophotometer (JASCO, Groß-Umstadt, Germany) and the time course measurement program.

All following steps were performed under anaerobic conditions at 30 °C. First, 10 µl menadiol were added to 50 mM MOPS buffer pH 7 in a quartz cell in 1.4 ml total volume and mixed. Afterwards, 20 µl of membrane vesicles diluted with MOPS buffer and different additives were added and mixed. The background absorption was recorded and after 40 sec 10 µl 2 M potassium nitrate was added and the reaction started. The absorption at 260 nm was recorded altogether for 120 sec.

For heme transfer experiments, HemW and HemW variants were incubated overnight with equimolar amounts of hemin. Afterwards, different assays with HemW-hemin,

hemin solely, and membrane vesicles alone were filled up to 100 µl with MOPS buffer and incubated at 30 °C for 2 hours. Twenty µl were used for the assay respectively.

The determination of the absorption increase was performed using the JASCO software Kinetics Analysis Program (JASCO, Groß-Umstadt, Germany). Afterwards the quinol oxidase activity of the NarGHI complex was calculated and expressed in µmol/min/ml. One unit of quinol nitrate oxidoreductase activity is the amount of nitrate oxidoreductase catalyzing the production of 1 µmol of menadione min^{-1}.

2.7 Biophysical Techniques

2.7.1 Electron Paramagnetic Resonance (EPR) Spectroscopy

The sample preparation and filling of quartz sample tubes for electron paramagnetic resonance (EPR) spectroscopy were performed under strict anaerobic conditions.

HemW was produced and purified as described in 2.6.1. For each sample 200 µl of 0.5 mM protein was used. For reduction and oxidation of [4Fe-4S] cluster either 10 mM sodium dithionite or 1 mM potassium ferrocyanide were added. Furthermore, equimolar amounts of hemin were added to HemW and incubated overnight at 20 °C. The samples were filled in 4 mm quartz EPR sample tubes, immediately frozen in liquid nitrogen and stored until measurement in liquid nitrogen.

EPR measurements were performed in cooperation with Dr. Edward J. Reijerse (Max-Planck Institute for Chemical Energy Conversion, Mülheim an der Ruhr, Germany). The X-band spectra (9.4 GHz) were recorded with a Bruker Elexsys E500 spectrometer equipped with an Oxford Instruments ESR-910 helium flow cryostat. The samples were contained in quartz EPR sample tubes of 4 mm outer diameter. Following experimental conditions were adjusted: microwave frequency 9.4 GHz, microwave power 0.2 mW, T=5 K, 10 scans.

2.7.2 Mössbauer Spectroscopy

For Mössbauer spectroscopy a protein concentration of 350 µM was used. Sample preparation was performed under strict anaerobic conditions. The iron-sulfur cluster was reconstituted with ^{57}Fe-ammonium ferric citrate as described in 2.6.5. For the sample containing HemW with bound heme an equimolar molar ratio of heme to HemW was added and the mixture was incubated at 20 °C overnight. The solutions were transferred

to 350 µl Mössbauer cups and frozen in liquid nitrogen. ^{57}Fe-ammonium ferric citrate was kindly provided from Prof. Dr. Martin Bröring (Institute of Inorganic and Analytical Chemistry, TU Braunschweig, Germany).

Mössbauer measurements were performed in cooperation with Dr. Eckhard Bill (Max-Planck Institute for Chemical Energy Conversion, Mülheim an der Ruhr, Germany). Mössbauer analyses were recorded on a spectrometer with alternating constant acceleration of the γ-source. The minimum experimental line width was 0.24 mms^{-1} (full width at half-height). The sample temperature was maintained constant in an Oxford Instruments Variox cryostat, whereas the ^{57}Co/Rh source (1.8 GBq) was kept at room temperature. Isomer shifts are quoted relative to iron metal at 300 K.

2.7.3 Cyclic voltammetry

Cyclic voltammetry was performed as described previously (Kühner *et al.,* 2016). For measurements an Ametek Versastat 3 and a self-made anaerobic three-electrode electrochemical cell flushed with nitrogen were used. A silver/silver-chloride electrode was used as reference (3 mol/l KCl). For each experiment 10 cycles were recorded. The samples contained 120 µM HemW either with or without 120 µM hemin and 500 µM S-adenosylmethionine (Sigma-Aldrich, Taufkirchen, Germany). The samples were prepared, filled and measured under anaerobic conditions.

2.8 Cell Biological methods

All cell biological experiments were performed in cooperation with Dr. Simone Karrie and Dr. Wiebke Sassen (Division of Cellular and Molecular Neurobiology, Institute of Zoology, TU Braunschweig, Germany) in the group of Prof. Dr. Reinhard Köster.

2.8.1 Preparation of Zebrafish Embryos

Zebrafish were raised and maintained under a 14 hour light / 10 hour dark cycle at 28°C, according to standard protocols (Westerfield, 2000; Kimmel *et al.,* 1995). Wildtype brass were used.

Prior to fixation, the chorion was removed after incubation with 2 mg/ml pronase for 15 min. Embryos were washed twice with 0.003% 1-phenyl 2-thiourea (PTU, Sigma-Aldrich, Taufkirchen, Germany). Fixation occurred with 4 % PFA in PBS overnight and

stepwise dehydrated with increasing amounts of methanol. Embryos were stored in 100 % methanol at -20 °C.

2.8.1.1 Whole Mount *in-situ* Hybridization (WISH)

For WISH, the dehydrated embryos were treated with proteinase K (10 µg/ml in PBST) after rehydration with decreasing amounts of methanol (75, 50, 25, 0 % MeOH/PBST).

Developmental stage	Time of proteinase K digest
24 hpf	10 min
48 hpf	30 min
72 hpf	30 min
96 hpf	30 min

After fixation in 4 % PFA for 20 min, the embryos were washed with PBST and were pre-hybridized in hybridization buffer at 60 °C for 1 h. Depending on its quality, the RNA probe was diluted in hybridization buffer at the ratio of 1:25-1:50 and heated at 95°C for 10 min to disrupt secondary structures. After removal of the pre-hybridization buffer, the hot probe was directly transferred onto the embryos. The hybridization with the riboprobe in hybridization buffer was performed at 60 °C overnight. The samples were washed two times with 50% FA/ 2x SSC /0.1 % Tween 20, once with 2x SSC /0.1 % Tween 20, and two times with 0.2x SSC /0.1 % Tween 20 for 45 min each at 60 °C. For blocking and saturating unspecific binding sites for anti-DIG Fab-fragments, embryos were incubated in 10 % normal goat serum (NGS) for 1 h on a rotator at room temperature. Anti-DIG antibody conjugated to alkaline phosphatase (Roche, Basel, Switzerland) was diluted to 1:2000 in 10 %NGS and incubated at 4 °C overnight. Embryos were washed five times with PBST for 15 min on a horizontal shaker before equilibration in AP buffer two times for 5 min. The hybridized probe was detected by means of color reaction with 250 mg/ml NBT and 187.5 mg/ml BCIP (Roche, Basel, Switzerland) in AP buffer. The reaction was stopped by washing three times with PBST for 15 min. Samples were stored in 90 % glycerol at 4 °C.

PBS:

NaCl	137	mM
Na_2HPO_4	12	mM
KCl	2.7	mM
in H_2O_{dest}, pH 7.4		

PBST:

Tween 20	0.1	%
in PBS		

Hybridization buffer:

formamide	50	%
NaCl	0.6	M
sodium citrate	60	mM
torula yeast RNA	500	µg/ml
heparin	50	µg/ml
Tween 20	0.1	%

AP buffer:

Tris-HCl, pH 9.5	100	mM
NaCl	100	mM
$MgCl_2$	50	mM
Tween 20	0.1	%

2.8.2 Transfection of COS7 cells

COS7 is a fibroblast-like African green monkey kidney cell line (RRID: CVCL_0224). Cells were grown and maintained in Dulbecco's modified Eagle's medium (DMEM,

Gibco, Darmstadt, Germany) supplemented with 10 % fetal bovine serum (FBS), 100 U/ml penicillin, 100 µg/ml streptomycin and 2 mM L- glutamine at 37 °C in an atmosphere of 95 % air and 5 % CO_2. At near confluence cells were passaged in a ratio of 1:4 to 1:8. Therefore, medium was removed and cells were washed shortly in 5 ml PBS. Three ml trypsine were added and incubated at 37 °C for 3 min to detach the cells from the bottom of the plate. To stop the reaction 6 ml medium was added before centrifuging the cell-medium mixture at 700 x g for 3 min. After removal of the supernatant the cells were resuspended in 3 to 5 ml medium. For transfection, 150000 cells were seeded on imaging chambers (5 cm glass bottom dish). Subsequently, 1.5 µg of the pCS-HemW-Venus construct were co-transfected with 1.5 µg of pCS-mitotag-RFP construct using OptiMEM® (Gibco, Darmstadt, Germany) and polyethylenimine (PEI, Polysciences Inc., Warrington, USA). PEI interacts with the negatively charged DNA and forms complexes. The plasmid-DNA complexes are absorbed by endocytosis. The cells were incubated at 37 °C overnight in an atmosphere of 95 % air and 5 % CO_2. The pCS-mitoRFP construct carried the mitochondrial targeting sequence of subunit VIII of human cytochrome *c* oxidase cDNA fused to a red fluorescent protein gene. Cells were then examined using a Leica TCS SP8 confocal laser scanning microscope (Leica, Wetzlar, Germany). A 561 nm diode pumped solid state laser and a 458 nm, 476 nm 488 nm, 496 nm and 514 nm multiline argon laser (15 % basic setting) was used. Image processing was performed with GIMP software

3 Results and Discussion

Prior to this work only little was known about the function of HemW. The relevant *Escherichia coli* gene NP_417430.1 was annotated as bacterial coproporphyrinogen III dehydrogenase (HemN) but no HemN activity was observed for the purified recombinant protein previously (Huhn, 2012). First experiments of *Lactococcus lactis* HemW indicated an involvement of HemW in heme transfer by studying cytochrome maturation (Abicht *et al.,* 2012). Here, biochemical, biophysical and cell biological analyses were applied to elucidate the biological function of the *E. coli* HemW protein and its eukaryotic counterpart RSAD1.

3.1 Biochemical Studies of *Escherichia coli* HemW

3.1.1 Recombinant Production and Purification of *E. coli* HemW

The recombinant production and purification of *E. coli* HemW was performed using a glutathione S-transferase tag (GST) system. HemW fused to a GST-tag was produced by *E. coli* BL21 (DE3) cells. After cell disruption via French Press, the cell debris were removed by ultracentrifugation. The cell-free extracts were loaded onto a column with glutathione agarose (Machery-Nagel, Düren, Germany). After washing steps, Prescission^{TM} Protease (GE Healthcare, Freiburg, Germany) was added for cleavage of the GST-tag. The purified HemW was released from the column while GST- tag and the Prescission^{TM} Protease (GE Healthcare, Freiburg, Germany) were retained. Figure 15 provides the documentation of the purification procedure. SDS-PAGE analysis of the purified HemW (Figure 15, lanes 4-7) revealed an apparently homogenous protein with a relative molecular mass of ~ 45.000±5000, which is in good agreement with the calculated molecular mass of 42,6 kDa. Approximately 12.5 mg HemW were obtained from 1 L culture. The protein was stable for several weeks when stored at 4 °C. All steps were carried out under anaerobic conditions due to the oxygen-sensitive iron-sulfur cluster of HemW. A first indication for the presence of an iron-sulfur cluster was the light brownish color of the purified protein. Due to the high expression and successful stable purification, several further biochemical analyses were accessible.

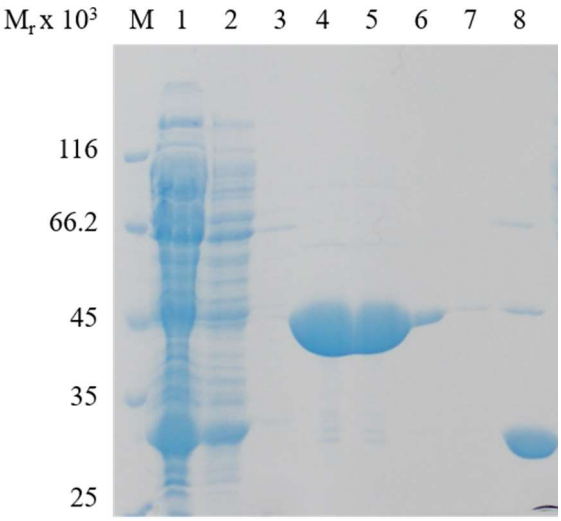

Figure 15: SDS-PAGE analysis of the purification steps of recombinant *E. coli* HemW produced in *E. coli*. Subsequent to electrophoresis, the 12% SDS gel was stained with Instant*Blue*™ (Expedeon Inc., San Diego, USA). Lane 1: total cellular extract after overnight induction of gene expression with 500 µM IPTG; lanes 2-3: washing steps; lanes 4-7: purified protein; lane 8: GST tag after cleavage. A marker with proteins of known relative molecular weights indicated the corresponding relative molecular mass (Pierce™ Unstained protein molecular weight marker; Thermo Fisher Scientific, Massachusetts, USA).

3.1.2 Characterization of the Radical SAM Cofactors: [4Fe-4S] cluster

The amino acid sequence motif CX_3CX_2CX is well-known for an iron-sulfur cluster binding motif (Sofia *et al.,* 2001). *E. coli* HemW and HemW from other organisms display this motif as well. Here, the presence and function of the iron-sulfur cluster were examined. Furthermore, the presence and function of SAM was analyzed due to the presence of a SAM-binding site of HemW.

First, the purified protein was analyzed via UV-Vis spectroscopy. A spectrum between 250 nm and 600 nm using 10 µM HemW was recorded (Figure 16, solid line). This spectrum revealed a slight shoulder at 420 nm which represents the absorption of an incorporated iron-sulfur cluster. For assessment of the Fe-S cluster incorporation rate, the ratio of the absorption at 280 nm for proteins and 420 nm for iron-sulfur cluster was used. In the case of purified HemW an A_{420}:A_{280} ratio of 0.04 was determined. This indicated a low incorporation of iron-sulfur cluster, probably due to the high-level recombinant production of HemW in *E. coli*. Another technique for the assessment of the Fe-S cluster incorporation rate is an iron and sulfur content determination of the protein. Per mol HemW 0.5 mol iron and 0 mol sulfur were detected. This result confirmed the low incorporation of iron-sulfur clusters.

3.1.2.1 Reconstitution of the Fe-S cluster of HemW

To yield a higher content of iron-sulfur clusters a chemical reconstitution was performed. For this purpose, the protein was incubated with ammonium ferric citrate and lithium sulfide. The reconstitution of the iron-sulfur cluster was followed via UV-Vis spectroscopy. In contrast to the as-isolated protein the spectra after Fe-S cluster reconstitution (Figure 16, dashed line) revealed an increase in the absorption at 420 nm. The A_{420}:A_{280} ratio increased to 0.19. Determination of the iron and sulfur content of 3.8 mol iron/2.5 mol sulfur per mol HemW confirmed the improved integration of Fe-S clusters. However, the iron and sulfur contents of 3.8 mol and 2.5 mol did not allow a prediction about the type of Fe-S cluster. Therefore, further analyses were essential.

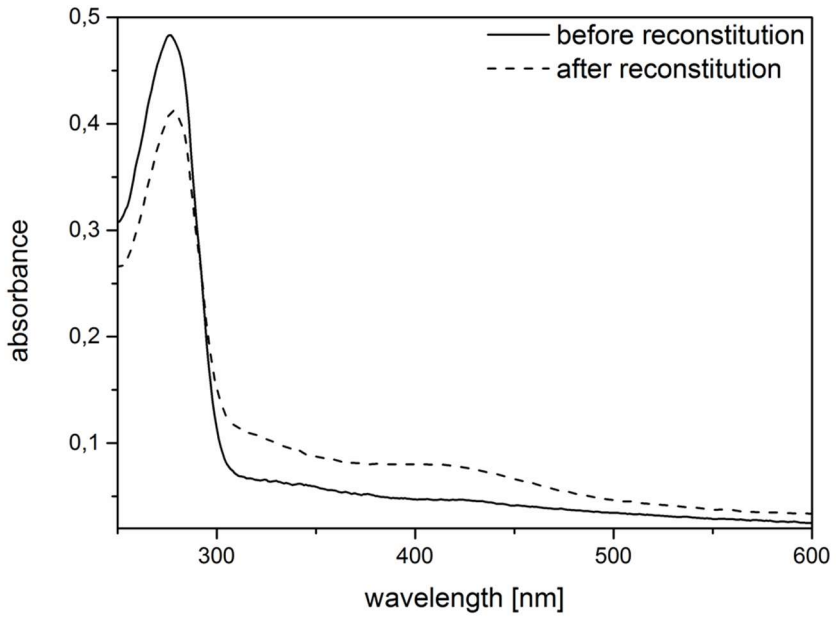

Figure 16: UV-Vis spectra of as-isolated and reconstituted HemW. Shown are UV-Vis spectra of 10 µM HemW before (solid line) and after (dashed line) reconstitution of the iron-sulfur cluster. Spectra were recorded between 250 nm and 600 nm with a V- 650 spectrophotometer (JASCO, Groß-Umstadt, Germany) under anaerobic conditions.

3.1.2.2 Biophysical Characterization of the Fe-S cluster of HemW

Powerful tools for the characterization of iron-sulfur clusters are the electron paramagnetic resonance (EPR) and the Mössbauer spectroscopy. An advantage of EPR is the direct measurement of protein solution without further additives. On the other hand, iron-sulfur clusters have to be in an unpaired electron state for signal detection. Therefore, a reduction e.g. with sodium dithionite or an oxidation e.g. with potassium ferrocyanide has to be performed. With the help of EPR the function of the [4Fe-4S] cluster and interaction of hemin and HemW were analyzed. For EPR spectroscopy 200 µl of 500 µM HemW were used. The samples were filled anaerobically into capillary tubes and frozen in liquid nitrogen. The measurements were performed by Dr. Edward J. Reijerse (Max-Planck Institute for Chemical Energy Conversion, Mülheim an der Ruhr, Germany).

Incubation with 10 mM sodium dithionite or 1 mM potassium ferrocyanide revealed no significant differences in the spectra (Figure 17, A-C). There was only a slight hint for a low potential reduced [4Fe-4S] cluster after addition of sodium dithionite (Figure 17, B). The oxidation of the cluster induced an increase in the amount of non-specific iron (III) (Figure 17, C). The addition of hemin revealed no further information of the function of the iron-sulfur cluster. Only high-spin heme was detected (Figure 17, D).

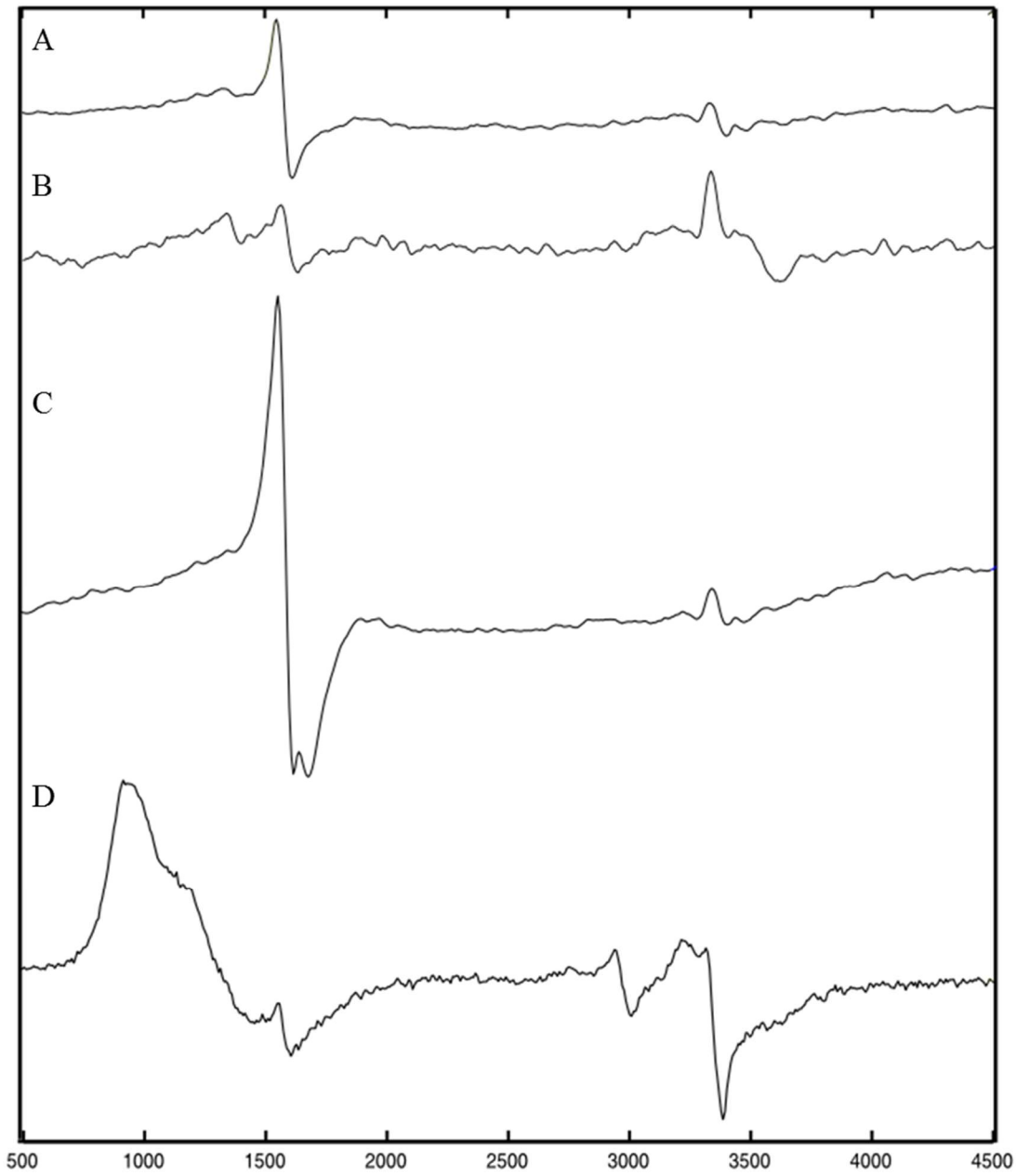

Figure 17: Electron paramagnetic resonance spectroscopy of *E. coli* HemW. Purified HemW (A), HemW reduced with sodium dithionite (B), HemW oxidized with potassium ferrocyanide (C), HemW with hemin (D), Experimental conditions: microwave frequency 9.4 GHz, microwave power 0.2 mW, T=5 K, 10 scans

The EPR technique revealed no further information about the oxidation state of the iron-sulfur cluster and the relation to heme binding. One possible explanation is a Fe-S cluster in 2+ state. In general, the presence of unpaired electrons for EPR measurements are necessary. Furthermore, this iron-sulfur cluster is only poorly reduced by sodium dithionite not really revealing an unpaired electron. The stable oxidation state suggest another function for the Fe-S cluster than involved in a radical SAM mechanism.

In this context, cyclic voltammetry experiments of HemW either with or without hemin were performed. The measurements were performed by Dr. Peter Schweyen (Institute for Inorganic and Analytical Chemistry, TU Braunschweig, Germany). The revealed half step potential of the [Fe-S] of HemW against a normal hydrogen electrode (NHE) was at around -410 mV (Figure 18/black). The addition of hemin or SAM caused no changes in the redox potential (data not shown).

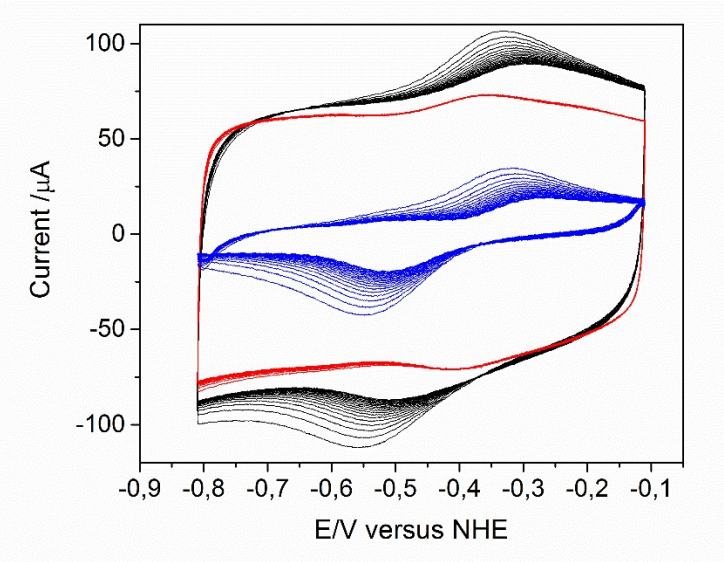

Figure 18: Cyclic voltammograms of HemW. Shown are the voltamograms of HemW (black), the protein buffer (blue) and the resulting difference of HemW and protein buffer (red).

In conclusion, the electrochemical reduction indicated clearly a reducible [Fe-S] cluster of HemW. In contrast, the EPR measurements indicated a not reducible [Fe-S] cluster. A possible explanation is that the chemical reagents had probably no access to the cluster.

Using Mössbauer spectroscopy not only iron-sulfur cluster with unpaired electrons but also with paired electrons can be analyzed. However, the incorporation of ^{57}Fe into the Fe-S cluster of interest is essential. Consequently, the protein production was performed in minimal media, e.g. M9 media with addition of ^{57}Fe. This procedure guaranteed during the production of HemW the incorporation of ^{57}Fe in the iron-sulfur clusters. First, the protein production of *E. coli* HemW was tested in M9 media with supplemented commercial ammonium ferric citrate. However, the amount of obtained recombinant protein was not sufficient for performing Mössbauer spectroscopy.

Next, the group of Prof. Dr. Martin Bröring (Institute for Inorganic and Analytical Chemistry, TU Braunschweig) provided ammonium ferric citrate containing ^{57}Fe. This synthesized compound gave the opportunity of a chemical reconstitution of the iron-sulfur cluster as described under chapter 2.6.5. The Mössbauer spectroscopical measurements were performed in cooperation with Dr. Eckhard Bill (Max-Planck Institute for Chemical Energy Conversion, Mülheim an der Ruhr, Germany).

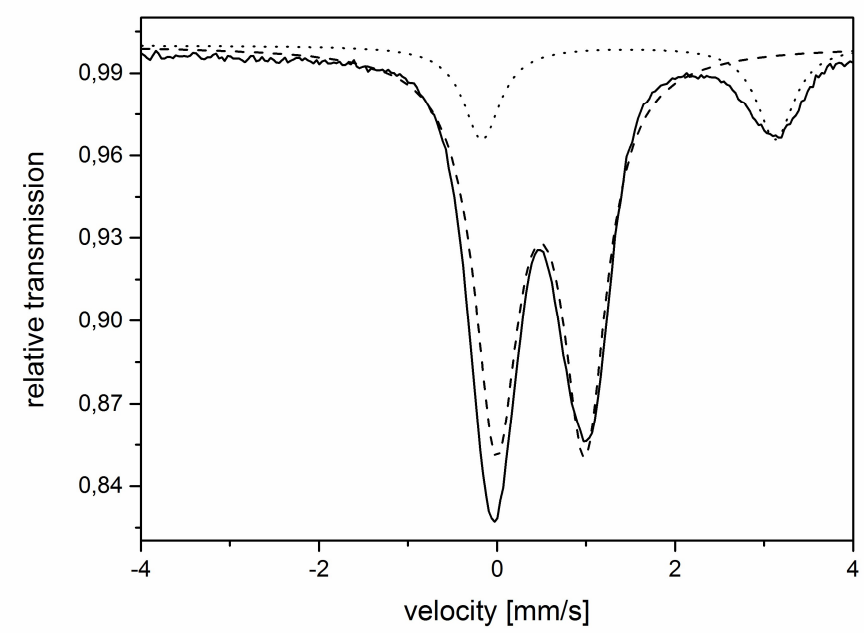

Figure 19: Mössbauer spectrum of purified HemW with an ^{57}Fe containing Fe-S cluster at 80.00 K, 0.00 T. The analysis revealed a dominant quadrupole doublet (83% of the total intensity) with an isomer shift (δ) of 0.49 mm/s and a quadrupole splitting parameter (ΔEQ) of 1.00 mm/s (dashed line). The second quadrupole doublet (17% of the total intensity) exhibited an isomer shift (δ) of 1.48 mm/s and a quadrupole splitting parameter (ΔEQ) of 3.30 mm/s (dotted line). The solid line represents the composition of the two quadrupole doublets.

The spectra of purified HemW revealed one dominant quadrupole doublet (83% of the total intensity) with an isomer shift (δ) of 0.49 mm/s and a quadrupole splitting parameter (ΔE_Q) of 1.00 mm/s, which is typical for $[4Fe\text{-}4S]^{2+}$ clusters (Figure 19, dashed line). Furthermore, a second quadrupole doublet (17% of the total intensity) with an isomer shift (δ) of 1.48 mm/s and a quadrupole splitting parameter (ΔEQ) of 3.30 mm/s, corresponding to inorganic Fe(II), was detected (Figure 19, dotted line). The solid line in Figure 19 represents the composition of the two quadrupole doublets. This spectrum indicates the coordination of the iron-sulfur cluster by three cysteine ligands and one N/O

ligand. The three cysteine residues are presumably the Cys^{16}, Cys^{20} and Cys^{23} of the CX_3CX_2C motif at the N-terminus of the protein sequence. The one N/O ligand most likely for coordination comes from SAM.

In conclusion, the presence of a $[4Fe\text{-}4S]^{2+}$ cluster in HemW was shown via Mössbauer analysis. This cluster was coordinated by three cysteines and one N/O ligand. This coordination-type resembles the type of the radical SAM-enzyme HemN (Layer *et al.,* 2003).

3.1.2.3 Influence of Fe-S cluster on the oligomerization state

Besides the analysis of the Fe-S cluster type the importance of the cluster for heme binding was questioned. Therefore, Mössbauer spectroscopy of HemW incubated with hemin was performed.

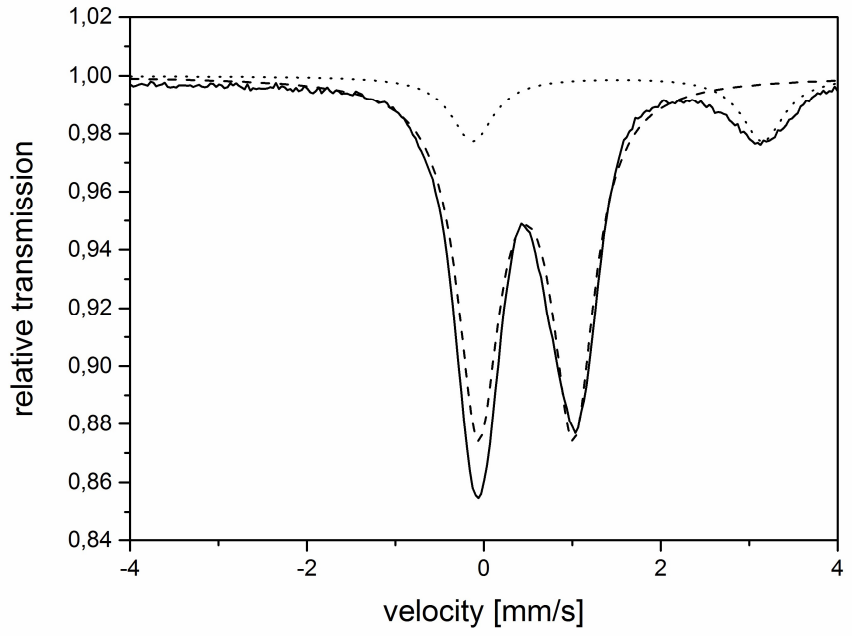

Figure 20: Mössbauer spectra of purified HemW (0.55 mM) with supplemented hemin (0.55 mM) at 80.00 K, 0.00 T. The analysis revealed a dominant quadrupole doublet (84% of the total intensity) with an isomer shift (δ) of 0.48 mm/s and a quadrupole splitting parameter (ΔEQ) of 1.08 mm/s (dashed line). The second quadrupole doublet (16% of the total intensity) exhibited an isomer shift (δ) of 1.51 mm/s and a quadrupole splitting parameter (ΔEQ) of 3.28 mm/s (dotted line). The solid line represents the composition of the two quadrupole doublets.

The Mössbauer sample preparation was performed as described (3.1.5), except the incubation with an equal amount of hemin overnight. Mössbauer spectrum of purified HemW with added Hemin (Figure 20) showed identical fit parameters compared to the spectra of HemW without further additions (Figure 19). This observation indicated no changes in the oxidation state of the $[4Fe\text{-}4S]^{2+}$ cluster nor changes in the four ligands of HemW in the presence of bound hemin. Additional UV-Vis spectroscopy revealed the same heme binding behavior of an iron-sulfur cluster amino acid mutant in comparison to wild type HemW (see Figure 38). In conclusion, there is no correlation between the iron-sulfur cluster and heme binding.

Since the iron-sulfur cluster is not involved in the initial heme binding by HemW, the function had to be clarified. To check a possible correlation between the iron-sulfur cluster and the oligomerization state of HemW an analytical gel-filtration chromatography was performed. The gel-filtration was performed under anaerobic conditions with a Superdex 200 10/300 GL (described in the method section, chapter 2.6.11). Therefore, wild type protein as-isolated and wild type protein with reconstituted iron-sulfur cluster were analyzed. Due to slight incorporation of the iron-sulfur cluster during protein production by *E. coli*, as-isolated protein was examined as iron-sulfur cluster free.

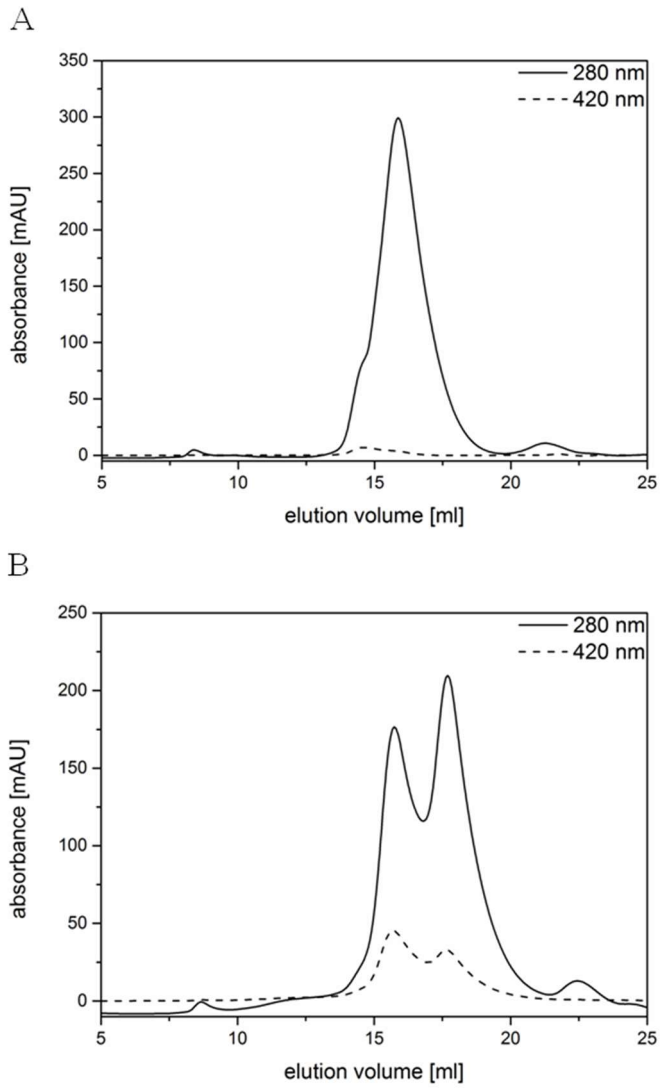

Figure 21: Analytical gel filtration of HemW as-isolated (A) and HemW with reconstituted iron-sulfur cluster (B). The chromatograms revealed after reconstitution of iron-sulfur clusters a second fraction with relative molecular masses corresponding to dimeric HemW. Solid line: absorption of protein at 280 nm; dashed line: absorption of iron-sulfur cluster at 420 nm. A 24 ml Superdex® 200 10/300 GL column (GE Healthcare, Freiburg, Germany) and an ÄKTApurifier system (GE Healthcare, Freiburg, Germany) under anaerobic conditions was used.

The chromatogram of the gel-permeation chromatography of HemW as-isolated revealed a peak corresponding to a monomeric protein (Figure 21, A). The solid line indicates the protein abundance at 280 nm and the dashed line shows the absorption at 420 nm, typical for iron-sulfur clusters. Almost no absorption at 420 nm was detected for the as-isolated protein indicating no incorporation of iron-sulfur clusters. In contrast, HemW with reconstituted iron-sulfur clusters revealed a different chromatogram. The two peaks indicated the presence of a monomeric and dimeric protein. The increase absorption at

420 nm indicated the successful iron-sulfur cluster incorporation. These results clearly showed the strict dependence of the dimerization of HemW on the presence of an intact Fe-S cluster. An additional gel filtration of a HemW variant C16S, disabled in the building of the iron-sulfur clusters, confirmed these findings (Figure 22).

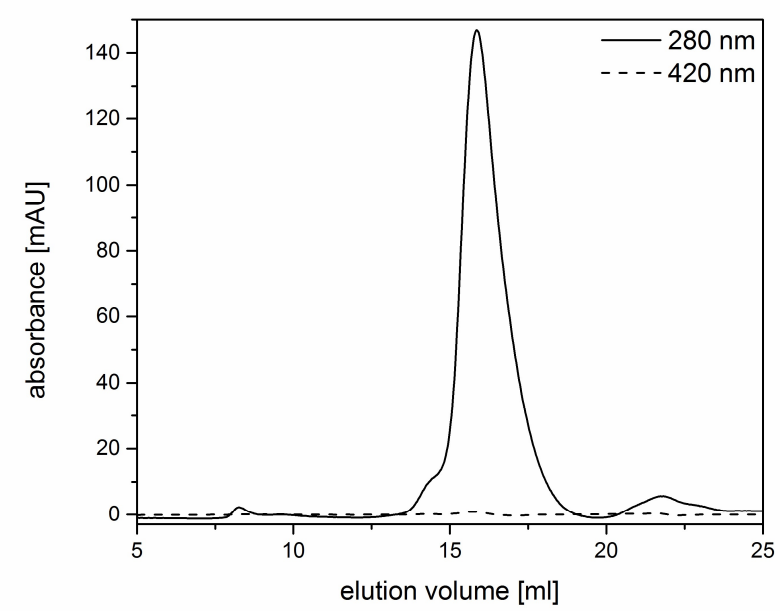

Figure 22: Analytical gel filtration of HemW-C16S. The chromatogram of this Fe-S cluster deficient HemW variant revealed a solely monomeric HemW. Solid line: absorption of protein at 280 nm; dashed line: absorption of iron-sulfur cluster at 420 nm. A 24 ml Superdex® 200 10/300 GL column (GE Healthcare, Freiburg, Germany) and an ÄKTApurifier system (GE Healthcare, Freiburg, Germany) under anaerobic conditions was used.

Altogether, these results show a direct relation of the presence of an intact [4Fe-4S] cluster on the oligomeric state of HemW. Structural function of iron-sulfur cluster is already described in literature. One example is the iron-sulfur cluster in *E. coli* MutY, essential for the structure and therefore for binding DNA (Porello *et al.,* 1998).

3.1.3 Characterization of the Radical SAM Cofactors: SAM

The amino acid sequence of HemW revealed two conserved binding sites for S-adenosyl-L-methione (SAM) similar to the radical SAM enzyme HemN from *E. coli* (Layer *et al.,* 2003). For studying SAM-binding, the protein was incubated with ^{14}C-SAM and the mixture was passed afterwards over a desalting column. Upon the chromatography,

protein-bound ^{14}C- SAM was separated from free ^{14}C- SAM**.** A liquid scintillation counter (Perkin Elmar, Waltham, USA) was used for analyzing the radioactivity of the eluates. The control experiment was carried out with BSA. Radioactivity in the control experiment with BSA were solely detected in the fractions which represented the small molecules, i.e. free ^{14}C- SAM (Figure 23, dashed line, fractions 6-14). In contrast, the ^{14}C- SAM in the assay with HemW was found in the protein-containing fractions clearly indicating the presence of a ^{14}C- SAM-HemW complex (Figure 23, solid line, fractions 1-4).

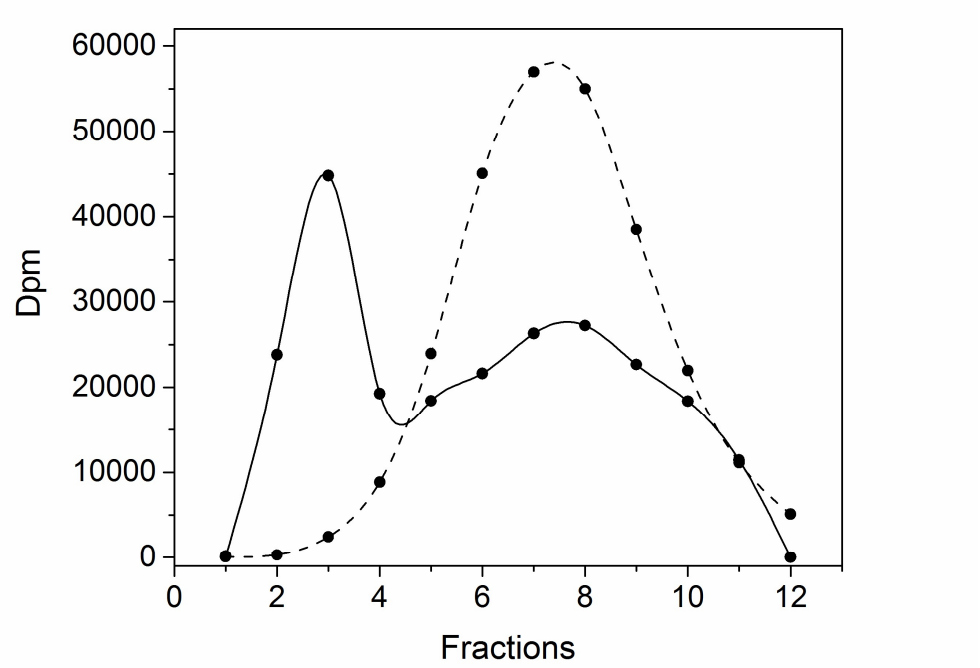

Figure 23: SAM-binding to HemW. HemW was incubated with radioactive ^{14}C-SAM and size-fractionated via a desalting column. The fractions were analyzed for radioactivity with a liquid scintillation counter (Perkin Elmar, Waltham, USA). BSA served as negative control. Solid line: HemW; dashed line: BSA+^{14}C-SAM.

SAM binding to HemW was clearly demonstrated as ^{14}C-SAM co-eluted with the protein fractions where HemW and BSA were eluting (Figure 23, solid line fractions 1-4). The control protein BSA was found unable to bind ^{14}C-SAM (Figure 23, dashed line, fractions 6-14). All ^{14}C-SAM added to BSA eluted in the small molecule fractions.

Since HemW was shown to bind SAM, a potential cleavage of SAM as shown for HemN needed to be determined. For this purpose, HemW was incubated with hemin overnight and then SAM and sodium dithionite was added. Sodium dithionite as electron donor is

important for the start of the radical SAM reaction by reduction of the iron-sulfur cluster for subsequent homolytic SAM cleavage. The assays were analyzed via high-performance liquid chromatography (HPLC). For detection of 5′-deoxyadenosine (DOA), the chromatograms were recorded at 254 nm. The HPLC chromatographs revealed for HemW with hemin and HemN peaks corresponding to residual SAM and the cleavage product (DOA) (Figure 24).

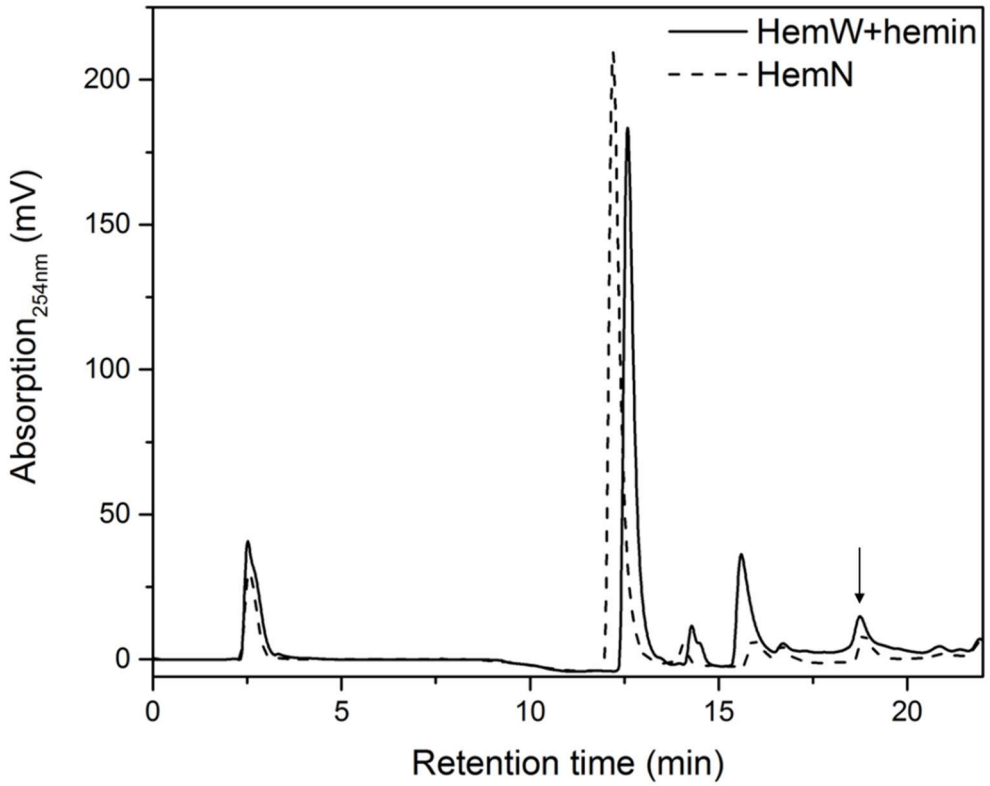

Figure 24: SAM cleavage assay. Twenty-five µM HemW with supplemented hemin was incubated with 0.6 mM sodium dithionite and 0.6 mM SAM overnight at 17 °C under anaerobic conditions. The reaction was stopped by adding 5 % formic acid. For detection of 5′- deoxyadenosine (DOA) a Hypercarb^{TM} column (Thermo Fisher Scientific, USA) at a JASCO 2000 system (JASCO, Groß-Umstadt, Germany) was used. A gradient of 0.1 % TFA in H_2O and 0.08 % TFA in acetonitrile with a flow rate of 0.2 ml/min and the absorption at 254 nm was adjusted. The peak at around 19 min indicated the presence of DOA. Solid line: HemW with bounded hemin; dashed line: HemN.

However, HemN was applied without the substrate coproporphyrinogen III. Therefore, the detected DOA (Figure 24, dashed line) indicated the background level. HemN was shown to induce to SAM cleavage in the presence of its substrate coproporphyrinogen III (Layer *et al.,* 2005). Compared to HemW with its substrate hemin also only background

levels for SAM cleavage were detected (Figure 24, solid line). A further SAM cleavage assay with sole HemW revealed the same HPLC chromatogram (data not shown).

Altogether, HemW is able to bind SAM but lost the function of SAM cleavage to generate a 5′-deoxyadenosyl radical.

3.1.4 HemW binds one molecule hemin covalently

Previous studies on *E. coli* HemW indicated its heme binding capability (Huhn, 2012), however further detailed analyses, i.e. heme binding stoichiometry and heme transfer, needed to be analyzed in more detail.

Heme binding is detectable via UV-vis spectroscopy due to shifts of absorption peaks in comparison to free unbound heme. For free heme a Soret band at around 385 nm was detected. After addition of HemW and incubation overnight, a red-shiftet Soret band at around 410 nm was observed. This shift and the visible bands at 560 nm and 584 nm indicated complex formation of HemW and hemin. The shoulder at 390 nm indicated remaining unbound hemin (Figure 25, solid line). These results are in agreement with published data for heme binding studies via UV-vis spectroscopy (Molitor *et al.,* 2013; Karnaukhova *et al.,* 2014). For comparison, a spectrum of purified HemW without added hemin was performed (Figure 25, dashed line). Only an absorption peak at 280 nm was detected indicating the sole presence of the protein.

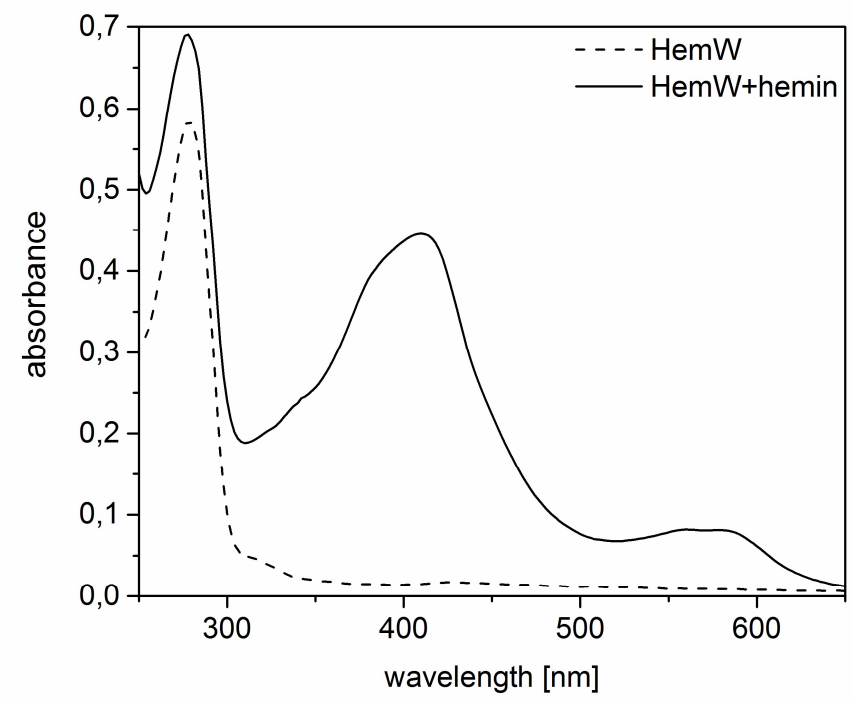

Figure 25: Absorption spectra of HemW (10 µM) with or without an equimolar amount of hemin. UV-Vis spectra of purified HemW with addition of 10 µM hemin showed a peak at 280 nm representing the protein absorption and a Soret band at 410 nm resulting from the bound heme. Peaks at 560 nm and 584 nm are typical visible bands of incorporated heme (solid line). For comparison, spectrum of purified HemW without added hemin is shown (dashed line) Spectrum was recorded between 250 nm and 600 nm with a V- 650 spectrophotometer (JASCO, Groß-Umstadt, Germany) under strict anaerobic conditions.

For detailed analysis of the stoichiometry and nature of heme binding other techniques, e.g. heme titration, heme staining and acidified butanone extraction were performed. Heme stains utilize the natural peroxidase activity of heme (Hrycay & O'Brien, 1971). After protein separation via SDS- PAGE, the peroxidase activity can be detected with a charge-coupled device (CCD) camera (CoolSNAP *HQ*^{2}, Photometrics ,Tucson, USA) due to the reaction with enhanced chemo-luminescent reagents (Feissner *et al.,* 2003). For heme staining, HemW and equimolar amounts of hemin were incubated overnight and the HemW-hemin complex was separated in duplicate by SDS- PAGE. Afterwards one half was stained with Instant*Blue*^{TM} (Expedeon Inc., San Diego, USA) for the detection of proteins (Figure 26, A) and the second half was blotted onto a nitrocellulose membrane and the amount of bound hemin was visualized using the chemo-luminescent assay (Figure 26, B). Protein detection by Instant*Blue*^{TM} staining revealed a single band with a relative molecular mass of ~ 45.000±5000, corresponding to the size of HemW. The detection of chemo-luminescence via CCD camera (CoolSNAP *HQ*^{2}, Photometrics, Tucson, USA) revealed a signal for the identical position of the HemW protein in

SDS- PAGE, indicating heme-binding by HemW. The chemiluminescent assay clearly confirmed heme-binding to HemW.

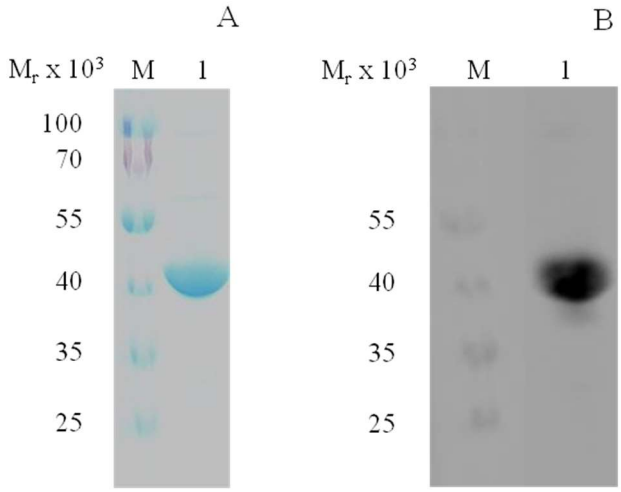

Figure 26: Heme binding assay. Twenty-five µM HemW were incubated with equimolar amount of hemin. After incubation overnight the heme staining procedure was performed. After SDS-PAGE separated proteins were stained with Instant*Blue*™ (Expedeon Inc., San Diego, USA) (A). The peroxidase activity of heme is detectable based on the reaction with ECL reagent (GE Healthcare Europe GmbH, Germany) (B); M, marker with proteins of known relative molecular weights indicated the relative molecular mass of the observed protein (PageRuler Prestained Protein Ladder; Thermo Fisher Scientific, Massachusetts, USA).

In a second approach, acidified butanone extraction was used to provide information about the chemical nature of heme binding to the HemW protein. Since the HemW-heme complex was stable during SDS-PAGE a covalent binding was under discussion. Proteins were extracted with butanone resulting either in extracted non-covalently linked heme in the organic or still bound covalently linked heme in the aqueous phase (Teale, 1959). The location of hemin either in the organic or aqueous phase was observable due to its brownish color.

For the analysis, 25 µM HemW were incubated with 15 µM hemin overnight. Less hemin than HemW was used to avoid residual free hemin in solution. Afterwards, the pH was adjusted to 1.5 - 2. After adding butanone and incubation on ice, two phases became visible. The brownish hemin was detected visually in the lower aqueous phase indicating a stable HemW-hemin complex and consequently covalently bound hemin (Figure 27, A). Butanone extraction from cytochrome *c* served as a positive control and confirmed covalently bound heme (Figure 27, B).

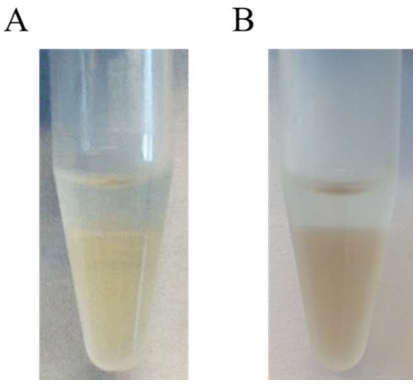

Figure 27: Butanone extraction. Twenty-five µM HemW were incubated with 15 µM hemin overnight. Afterwards the pH was adjusted to pH 1.5 - 2 with 10 % HCl. Ice-cold 2- butanone was added and carefully mixed. The remained hemin in aqueous phase indicated a covalently binding of heme to HemW (A). Butanone extraction from cytochrome *c* (horse heart, 1 mg/ml) served as a positive control and confirmed covalently bound heme (B).

The detection of hemin in denatured proteins via heme stain and the acidified butanone extraction indicated a covalently bound heme by HemW.

Next, the heme binding stoichiometry of HemW was of interest. Therefore, 10 µM HemW were titrated with increasing amounts from 5 µM to 25 µM hemin (Figure 28, lanes 1 - 5). Resulting complexes were separated via SDS-PAGE and transferred to a nitrocellulose membrane. The heme stain was performed like described before and revealed an increase of heme intensity up to a hemin concentration of 10 µM (Figure 28, lane 2). This result indicated a stoichiometry of one heme molecule per protein monomer.

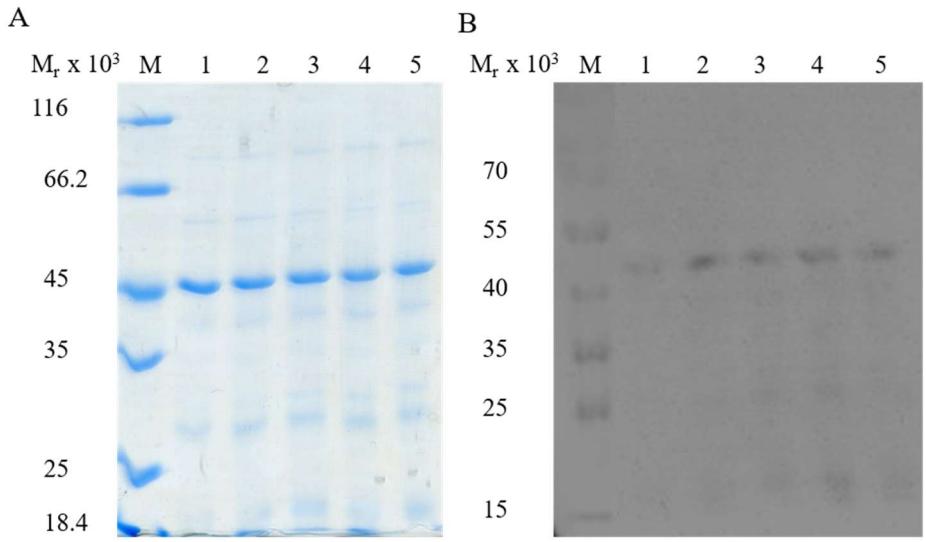

Figure 28: Heme titration experiments with HemW. Purified protein (10 µM) was titrated with increasing amounts of hemin (5 µM (lane 1), 10 µM (lane 2), 15 µM (lane 3), 20 µM (lane 4) and 25 µM (lane5)). The SDS-PAGE was stained with Instant*Blue*™ (Expedeon Inc., San Diego, USA) for proteins (A) and the blotted membrane with ECL reagent (GE Healthcare Europe GmbH, Germany) for heme (B). A marker with proteins of known relative molecular masses indicated the relative molecular mass of the separated proteins (Pierce™ Unstained protein molecular weight marker, PageRuler Prestained Protein Ladder; Thermo Fisher Scientific, Massachusetts, USA).

To further quantify the binding stoichiometry a second heme titration experiment was performed. Different amounts of hemin were added to 20 µM HemW. After incubation overnight, the absorption at 411 nm was recorded with the help of a V- 650 spectrophotometer (JASCO, Groß-Umstadt, Germany) under anaerobic conditions. Afterwards, the absorption at 411 nm, representing bound hemin (Guo *et al.,* 2008) was plotted against the added amount of hemin (Figure 29). The intersection of the two interpolated linear slopes indicated a saturation of heme binding at 20 µM hemin. Due to added 20 µM HemW, a 1:1 binding stoichiometry of hemin by HemW was verified.

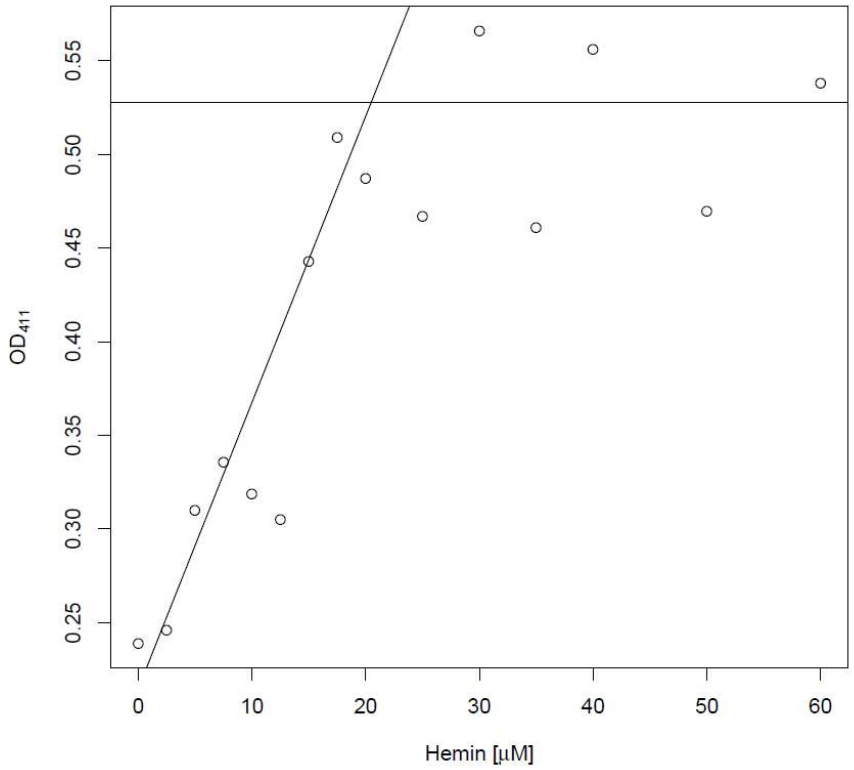

Figure 29: Heme titration experiment. 20 µM HemW were incubated with different amounts of hemin. Absorption at 411 nm was recorded with a V- 650 spectrophotometer (JASCO, Groß-Umstadt, Germany) under anaerobic conditions. The absorption at 411 nm is plotted against concentrations of hemin. The intersection of the two linear slopes indicates the saturation of heme binding at 20 µM hemin.

Altogether, this work confirmed the heme binding of HemW. Furthermore, the binding stoichiometry of one molecule hemin to one molecule HemW was determined. Hemin binding behavior by HemW was identified as a covalent bondage. In the past, specific binding of solely hemin and not of biosynthetic heme precursors was shown (Huhn, 2012). Taken these results together, a selective binding of heme by HemW confirms the discovery of a "new" heme-binding protein.

3.1.5 Potential Amino Acids of HemW involved in Heme Binding

The previous outlined experiments displayed a covalent heme binding of one heme molecule per protein, but no details of the binding location in HemW. The generation and characterization of HemW variants carrying exchanges of amino acids potentially involved in heme binding can provide information about the mode of heme binding. In literature, several heme binding motifs have been previously discussed (Li *et al.,* 2011).

Histidine residues play an important role in the coordination of the central iron of the tetrapyrrole heme. Therefore, several histidine residues conserved between multiple HemW proteins were exchanged via site-directed mutagenesis either into an alanine or into an arginine residue. Histidine is an aromatic amino acid with a positive charged side chain. In contrast, alanine carries a non-polar side chain. Arginine has a positive charged side chain but no imidazole functional group similar to histidine. The exchange of histidine to alanine should cause a different electrical or in the case of arginine a steric problem. In this work, the following amino acid exchanges of HemW were constructed via site-directed mutagenesis: H140A, H190A, H250A, H268A, H268R and W255L, respectively. Besides histidine, the aromatic amino acid tryptophan can be involved in heme binding (Smith *et al.,* 2010). Tryptophan is an aromatic amino acid with a hydrophobic side chain, while leucine exhibits a hydrophobic side chain, but it carries no indole function. Abicht and colleagues analyzed heme-binding affinity for *L. lactis* HemW by fluorescence quenching using an tryptophan close to the bound heme (Abicht *et al.,* 2012). They identified the presence of an HNXXYW amino acid motif in all HemW proteins. In *E. coli* HemW, this motif is also present and the tryptophan at position 255 was exchanged against leucine in this study. However, the selection of the amino acids were chosen by means of the tool SNAP2 (Yachdav *et al.,* 2014). This tool predict functional effects due to changed amino acid residues.

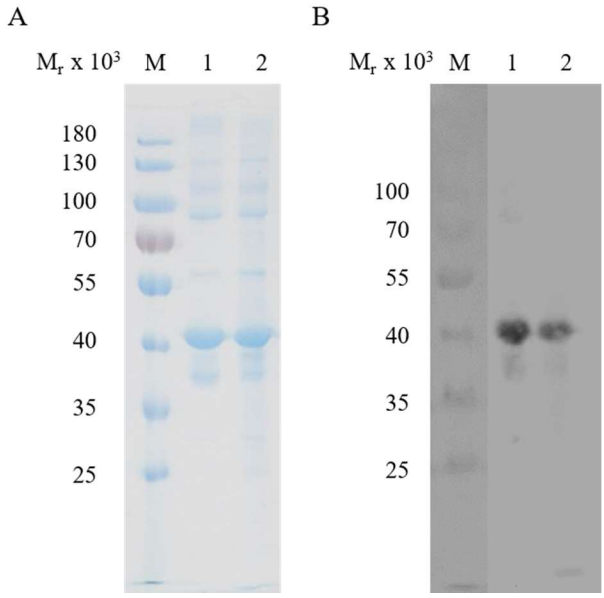

Figure 30: Heme binding assay of HemW and HemW-W255L. Twenty-five µM of each protein were incubated with equimolar amount of hemin. After incubation overnight the heme staining procedure was performed. Proteins were stained with Instant*Blue*™ (Expedeon Inc., San Diego, USA) (A). The peroxidase activity of heme was detectable based on the reaction with ECL reagent (GE Healthcare Europe GmbH, Germany) (B). Lane 1 display HemW and lane 2 HemW-W255L; M, marker with proteins of known relative molecular masses indicated the relative molecular mass of the separated proteins (PageRuler Prestained Protein Ladder; Thermo Fisher Scientific, Massachusetts, USA).

The mutant proteins were produced and purified like the wild type protein and the heme binding behavior was tested via heme staining. Exemplary, a heme stain experiment performed with wild type HemW and HemW-W255L is shown in Figure 30. Heme binding studies of HemW-W255L indicated a decrease in heme binding but no complete loss in the heme binding ability. In contrast, the other HemW variants indicated no differences in heme binding behavior.

However, a double mutant in the HNLNYW motif was constructed to provide further information about heme coordination e.g. deficiency in heme binding. The HemW- H250R-W255L variant was purified and the heme binding behavior was analyzed via UV-vis spectroscopy (Figure 31). For comparison, the wildtype HemW was recorded in parallel. As a result, the HemW-H250R-W255L mutant protein indicated a difference in heme binding compared to the wildtype HemW protein.

A more sensitive technique than UV-vis spectroscopy should be of an advantage. EPR spectroscopy could provide further detailed information about the oxidation state of bound heme in the HemW-H250R-W255L mutant protein.

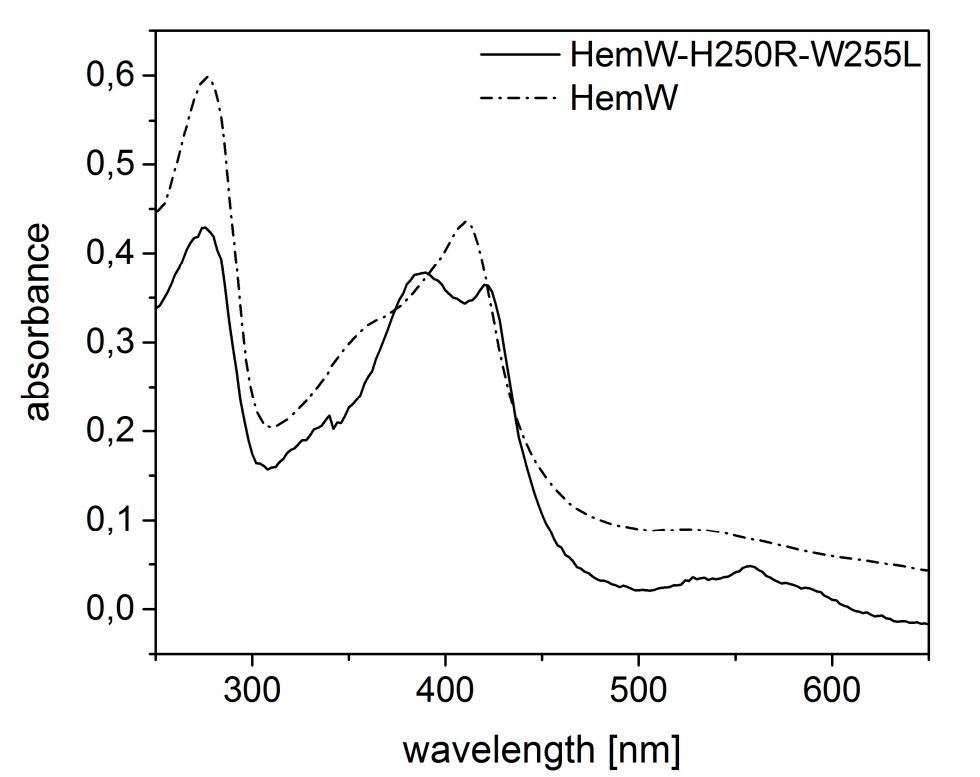

Figure 31: Absorption spectra of HemW, HemW-H250R-W255L (each 10 µM) with an equimolar amount of hemin. UV-Vis spectra of purified HemW with addition of 10 µM hemin showed a peak at 280 nm representing the protein absorption and a Soret band at 416 nm resulting from the bound heme (dashed-dotted line). The mutant protein HemW- H250R-W255L indicated a red-shift to 422 nm (solid line). Peaks at 530 nm and 558 nm are typical visible bands of incorporated heme. Spectrum was recorded between 250 nm and 700 nm with a V- 650 spectrophotometer (JASCO, Groß-Umstadt, Germany) under strict anaerobic conditions.

3.1.6 Heme Binding to HemW Induces Dimer Formation

Initial studies on heme binding to HemW revealed the heme dependent dimerization of HemW (Huhn, 2012). To confirm and quantify these results gel permeation chromatography of HemW was performed. HemW was analyzed either as-isolated or after incubation with hemin (Figure 32). A 24 ml Superdex® 200 10/300 GL column (GE Healthcare, Freiburg, Germany) and an ÄKTApurifier system (GE Healthcare, Freiburg, Germany) was used for the gel permeation chromatography under anaerobic conditions. The process was monitored by a UV detector at 280 nm and 410 nm. The absorption at 280 nm indicated the protein amount and the absorption at 410 nm showing the heme content. HemW as-isolated revealed one dominant peak at around 17 ml elution volume corresponding to a relative mass of 45.000±5000 corresponding to a monomeric protein

(Figure 32, A). After adding hemin in equimolar amounts and incubation overnight the oligomeric status of the protein remained monomeric (Figure 32, B).

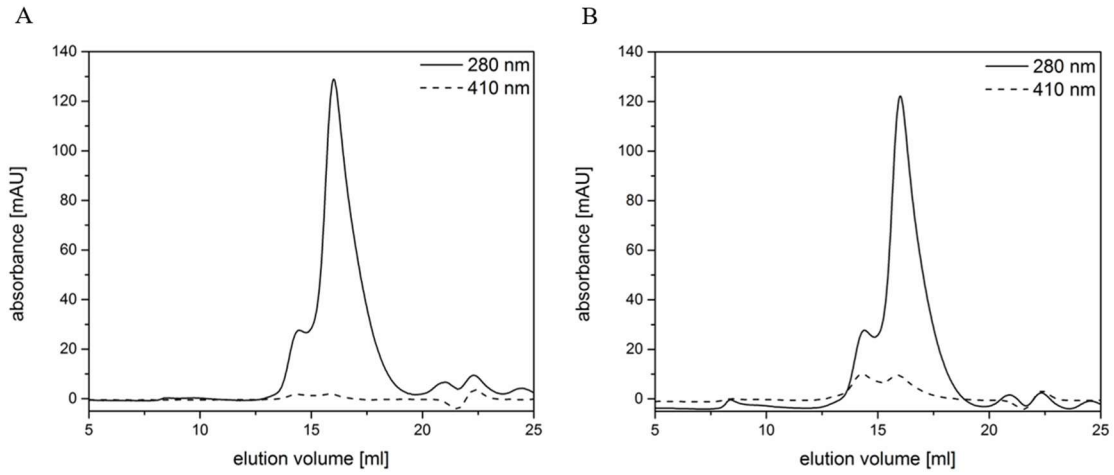

Figure 32: Analysis of heme binding-dependent oligomerization of HemW. The analytical gel permeation chromatography was performed with HemW as-isolated (A) and HemW incubated with hemin (B) under anaerobic conditions. Solid line: absorption of protein at 280 nm; dashed line: absorption of hemin at 410 nm. A 24 ml Superdex® 200 10/300 GL column (GE Healthcare, Freiburg, Germany) and an ÄKTApurifier system (GE Healthcare, Freiburg, Germany) were used.

In contrast to previous studies, this experiment revealed an independency between heme binding and the oligomeric state of HemW. The protein remained dominantly monomeric.

3.1.7 Heme Transfer to Nitrate Oxidoreductase

After characterizing heme binding to *E. coli* HemW (see chapter 3.1.4), the assumed function as heme chaperone had to be validated. First of all, an appropriate heme acceptor protein was needed. Abicht *et al.* showed the heme release from *L. lactis* HemW in the presence of *L. lactis* membrane vesicles (Abicht *et al.,* 2012). For this reason, a membrane-anchored or membrane-associated heme containing protein was searched as an appropriate acceptor protein for HemW. This acceptor protein had to bind heme as a cofactor. Moreover, it had to be produced without heme cofactor to allow for its functional complementation. Finally, an assay for detecting the heme transfer was required. We selected the quinol-nitrate oxidoreductase (NarGHI), a heme containing terminal oxidase of the anaerobic respiration of *E. coli*. In cooperation with the group of Prof. Dr. Axel Magalon (Laboratoire de Chimie Bacterienne, CNRS, Marseille) we

established the expression of heme-free NarGHI. They provided *E. coli* heme-free membrane vesicles prepared from an *E. coli* Δ*hemA* mutant with overexpressed *narGHJI* (Figure 33). UV- Vis spectroscopic analysis of the NarGHI preparation from the heme-deficient strain (*E. coli* Δ*hemA*) revealed the absence of heme cofactor in the membrane vesicles indicated by the loss of the heme specific absorption at around 425 nm (Figure 33, A). Furthermore, the pale color of heme-free membrane vesicles indicated the depletion of heme. In contrast, membrane vesicles prepared from *E. coli* wild type MC4100 still possessed the brownish color from the inserted heme cofactor in NarI (Figure 33, B).

An established assay for measuring the NarGHI activity was employed to test for functional complementation of NarGHI activity via heme insertion mediated by HemW (Lanciano *et al.,* 2007). This activity assay was based on the nitrate-dependent oxidation of the electron donating menaquinol to menadione with the corresponding changes in absorption at 260 nm. First experiments with heme-free NarGHI revealed the expected and required loss of activity for the heme-transfer experiments. Loss of activity is caused by missing heme cofactor and thereby failed electron transfer to nitrate, essential for the oxidation of menaquinol.

The rationale of our approach was that HemW provides heme for incorporation into heme-free NarGHI, resulting in a reconstitution of NarGHI activity. Such observation would verifying the function as a heme chaperone for HemW.

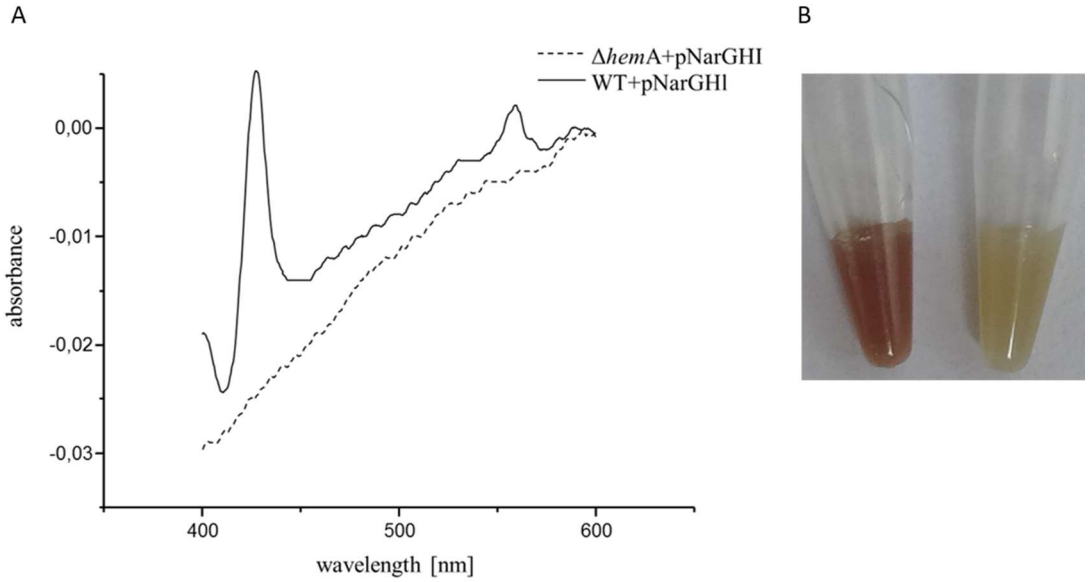

Figure 33: Comparative spectroscopic analysis of prepared membrane vesicles from *E. coli* wild type MC4100 and *E. coli* Δ*hemA* mutant. The clear out decrease of absorption at around 425 nm indicated the absence of bound heme cofactor in NarGHI produced by *E. coli* Δ*hemA* mutant (A). The decolorization of the prepared membrane vesicles (left tube wildtype, right tube Δ*hemA* mutant) due to the depletion of heme is optically visible (B). The experiments were performed in cooperation with the group of Prof. Dr. Axel Magalon (Laboratoire de Chimie Bacterienne, CNRS, Marseille).

For testing the heme transfer to NarGHI mediated by HemW, HemW was first incubated with hemin in an equimolar ratio overnight under anaerobic conditions. Next, different experiments were set up, e.g. negative controls were prepared and the membrane vesicles either with heme cofactor or without were added and incubated at 30 °C for two hours.

The Nar activity assay was executed directly in a quartz cuvette under anaerobic conditions. Initially, a basal slope for absorption at 260 nm was recorded by a V-650 spectrophotometer (JASCO, Groß-Umstadt, Germany). The reaction was started with the addition of nitrate and the UV-Vis measurements was continued. The measured changes in absorption at 260 nm were used afterwards to deduce the corresponding NarGHI activity using the Kinetic Analysis Program (JASCO, Groß-Umstadt, Germany). For determination of the increase of absorption the area of a constant curve was chosen. Figure 34 shows the absorption at 260 nm, indicating the translation of menaquinol to menadione, mediated by NarGHI isolated from *E. coli* wild type strain.

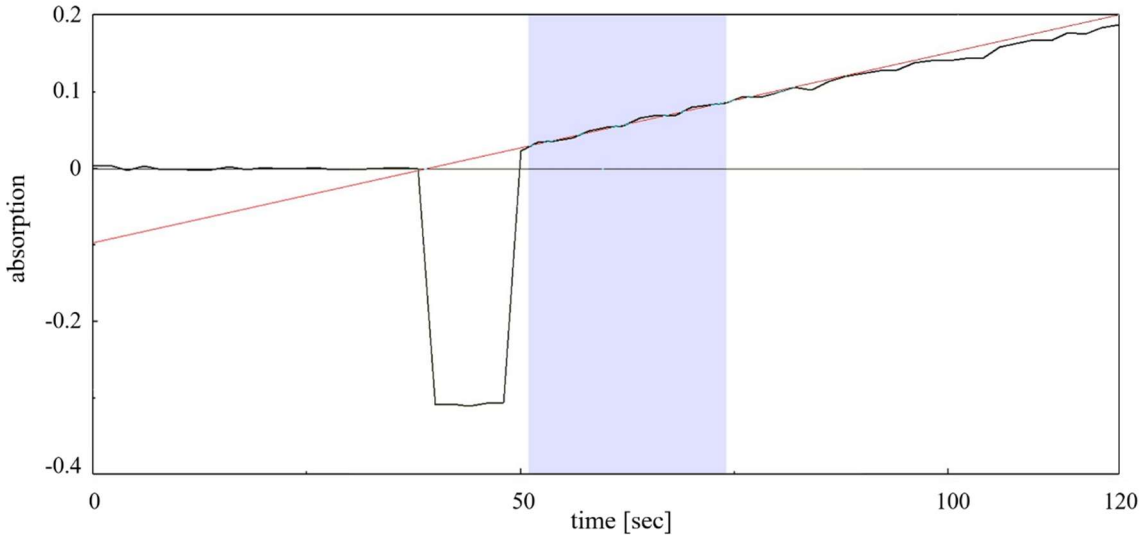

Figure 34: Utilization of increase of absorption at 260 nm by Kinetic Analysis Program to calculate NarGHI activity. This approach visualized the activity of NarGHI isolated from *E. coli* wild type strain. The blue-marked area was used for calculating NarGHI activity.

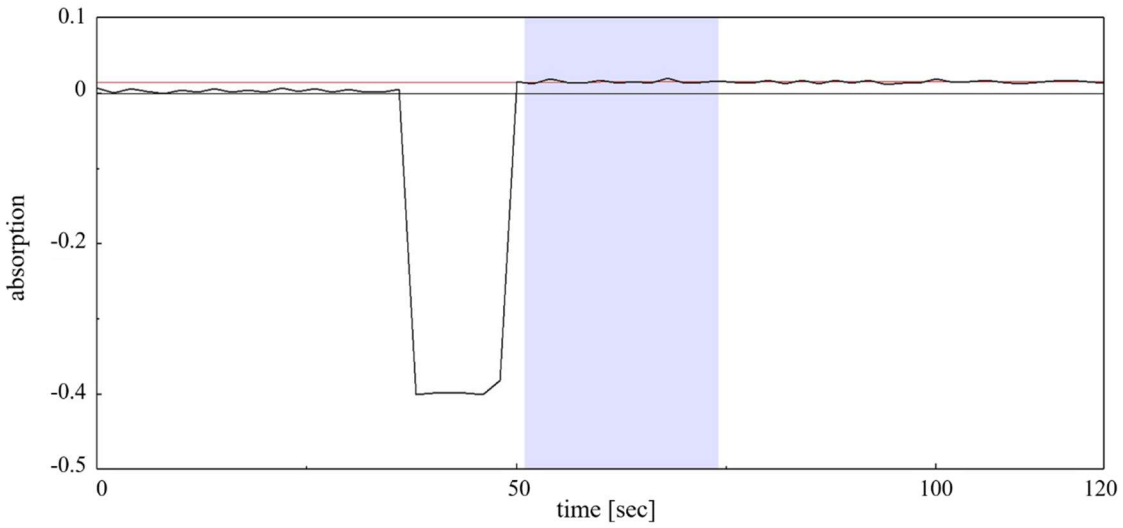

Figure 35: Verification of the loss of activity of membrane vesicles isolated from *E. coli* Δ*hemA*. The red line indicates no increase of absorption corresponding to missing conversion of menaquinol.

As mentioned, a total loss of activity of NarGHI prepared from the heme deficient Δ*hemA* mutant was an essential requirement for the desired test system. For determination of this basal activity, an activity assay of membrane vesicles isolated from *E. coli* Δ*hemA* was performed (Figure 35). As expected no NarGHI activity was observed.

Results for the NarGHI activity assays for different approaches are shown in Figure 36. The assays were performed at least five times in triplicate and statistically evaluated. The

columns represent the mean and the appropriate standard errors. First, the result for NarGHI with inserted heme cofactor isolated from *E. coli* wild type MC4100, named wild type is shown, indicating the maximal activity of 16.7 µmol/min*ml.

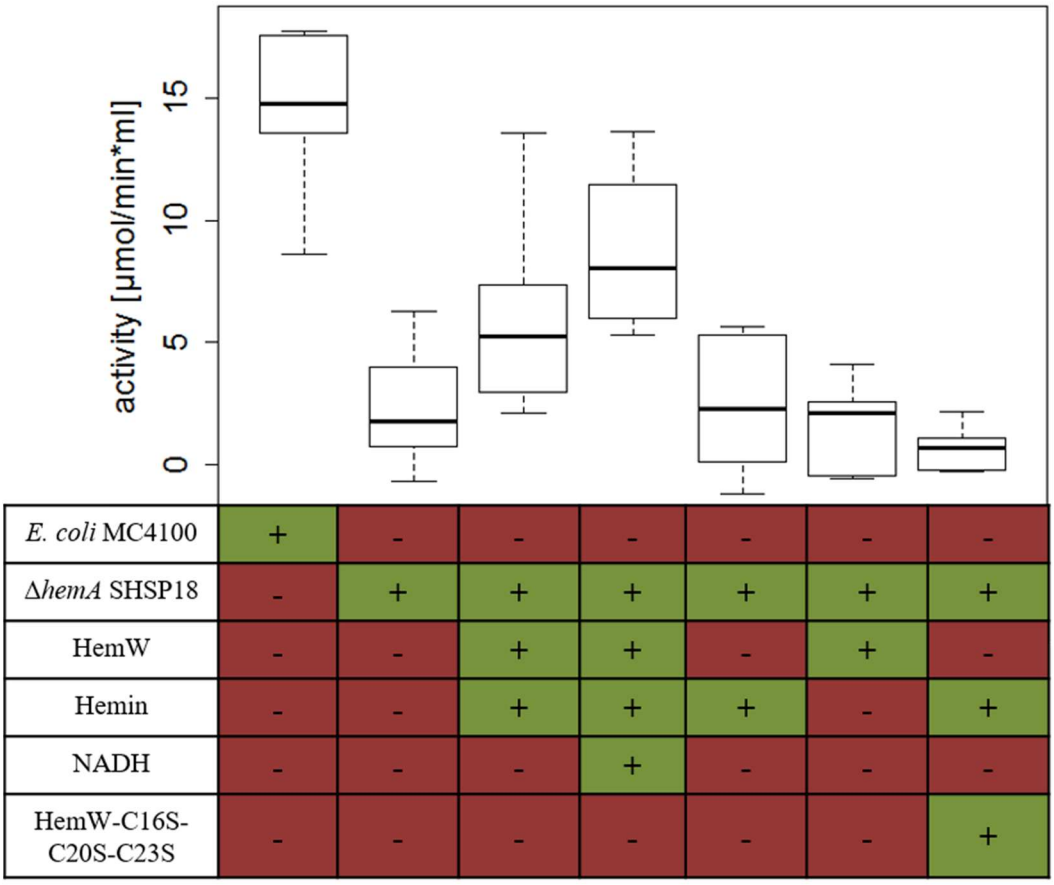

Figure 36: Quinol nitrate oxidoreductase assays. Assays were performed with membrane vesicles isolated from *E. coli* MC4100/pVA700 overexpressing *narGHJI* (labelled *E. coli* MC4100) and membrane vesicles with overproduced heme-depleted nitrate oxidoreductase isolated from *E. coli* Δ*hemA*/pVA700 (labeled Δ*hemA* SHSP18). The heme-depleted nitrate oxidoreductase was incubated with HemW-hemin, HemW-hemin+NADH or with HemW- C16S-C20S-C23S-hemin and as negative controls solely with hemin or HemW. The range between -1 and 18 µmol/min*ml is shown.

Membrane vesicles isolated from *E. coli* Δ*hemA* with overexpressed NarGHI lacking the heme cofactor showed a basal activity of 2.4 µmol/min*ml. The negative controls, Δ*hemA* vesicles with added hemin and Δ*hemA* vesicles with added HemW but without hemin showed an identical basal activity (2.4 µmol/min*ml, 1.7 µmol/min*ml).

Only the addition of HemW with bounded hemin to Δ*hemA* membrane vesicles resulted in a significant increase in the nitrate dependent conversion of menaquinol. The measurements revealed a NarGHI activity of 6.1 µmol/min*ml. The measurements are

exemplary shown in Figure 37. The red line clearly indicates an increase in absorption and within restored activity of NarGHI isolated from *E. coli* Δ*hemA* after addition of HemW with bounded hemin. In conclusion, heme cofactor was transferred from HemW to NarGHI and was functional inserted.

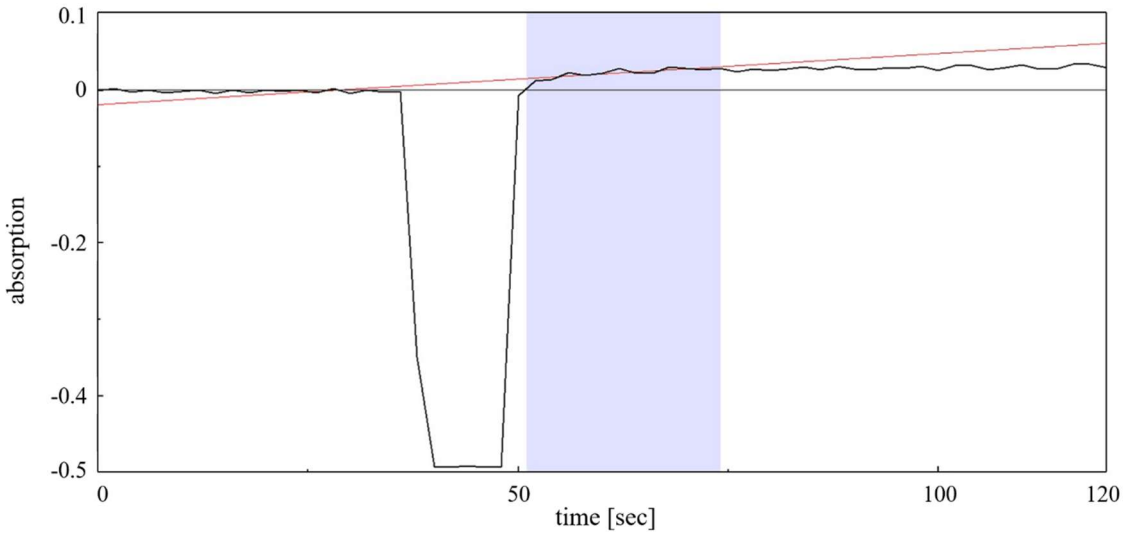

Figure 37: Increase in absorption at 260 nm and within conversion of menaquinol of membrane vesicles isolated from *E. coli* Δ*hemA* after incubation with HemW loaded with hemin. NADH was added to this approach.

The influence of NADH was also analyzed due to a proposal NADH-dependent mode of heme release of *L. lactis* HemW after incubation with membrane vesicles in presence of NADH (Abicht *et al.,* 2012). NADH may play an important role in the electron transfer required for the release of hemin from HemW. Abicht and colleagues suggested for NADH a function as electron donor required for the bond breakage during heme release (Abicht *et al.,* 2012).

In this study, NADH also exhibited a positive role in the complex heme transfer from HemW to NarGHI due to an observed raised activity of up to 8.7 µmol/min*ml in contrast to 6.1 µmol/min*ml without NADH (Figure 36).

Finally, the function of the iron-sulfur cluster in heme release was analyzed. The amino acids involved in iron-sulfur coordination at positions 16, 20 and 23 were exchanged from cysteine to serine. This protein was prepared and purified analogously to the wildtype protein. The protein was heme loaded and the heme transfer assay was also performed as

previously described. Interestingly, the activity of NarGHI was not restored by the HemW variant (0.7 µmol/min*ml) (Figure 36).

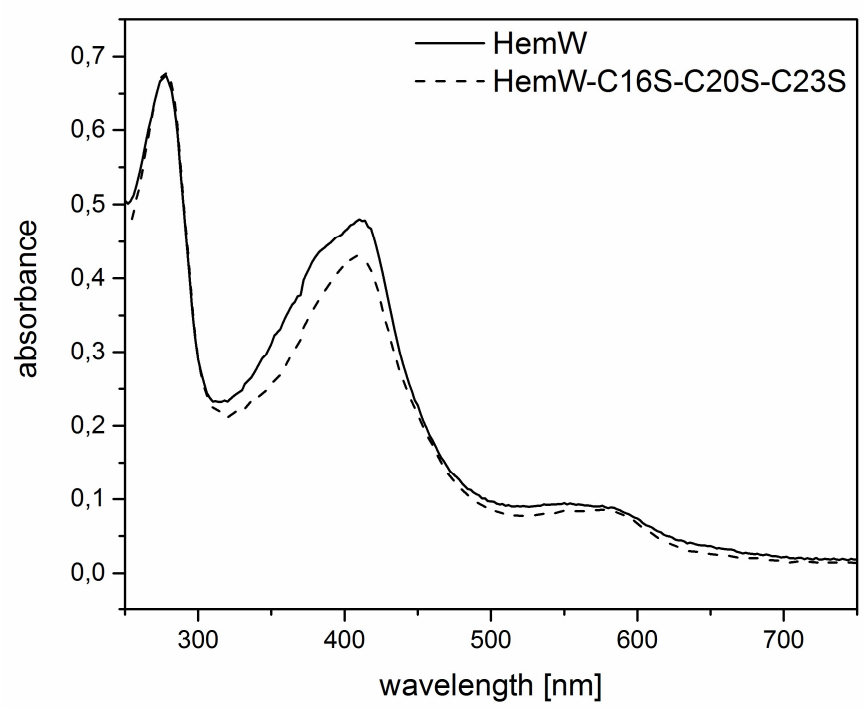

Figure 38: Spectroscopical analysis of HemW and HemW-C16S-C20S-C23S. Ten µM protein and 10 µM hemin were incubated overnight under anaerobic conditions. The spectra were recorded under anaerobic conditions. Peaks at 410 nm indicated a coordinated heme by HemW (solid line) and HemW-C16S-C20S-C23S (dashed line). Spectra were recorded between 250 nm and 750 nm with a V- 550 spectrophotometer (JASCO, Groß-Umstadt, Germany) under anaerobic conditions.

To exclude an influence deficient heme binding by the mutant protein, heme binding was analyzed by UV-Vis (Figure 38). The spectra indicated successful heme binding for wildtype HemW and HemW-C16S-C20S-C23S. In conclusion, the iron-sulfur cluster has no influence on heme binding, but on the heme transfer.

Altogether, HemW transferred heme to heme-free NarGHI *in vitro* and restored the nitrate reductase activity. Furthermore, the coordination of an iron-sulfur cluster in HemW is essential for the heme transfer. Above all, NADH enhanced the heme transfer or the insertion of heme. The detailed heme release, e.g. heme binding site and structural formation of HemW remains to be analyzed. For example, the probable structural changes of HemW during heme release can be studied via circular dichroism spectroscopy.

However, the activity of rescued NarGHI was not restored to wild type level whether in NADH absence or presence. One possibility might be the limitation of the *in vitro* environment. Furthermore, isolated membrane vesicles and not cells were used, resulting in a probable absence of other necessary participants, e.g electron donors or electron acceptors. NarGHI possesses two heme cofactors. One heme cofactor is located in NarI distal to the subunits NarGH. In contrast, the second heme cofactor is located proximal to NarGH and thereby deeper inside the protein. For the oxidation of menaquinol both hemes are essential. An incomplete *in vitro* insertion of one heme might result in a not fully restored active protein. If the observed lower activity was dependent on not completely inserted heme molecules by HemW, a quantification and thereby normalization would have led to values closer to wild type levels. This approach should be pursued in further studies.

Recently, *in vivo* interaction studies of HemW with probable interaction partners were performed by Katrin Müller (Institute for Microbiology, TU Braunschweig, Germany, unpublished work). These studies were performed with the help of the BACTH system (EUROMEDEX, Souffelweyersheim, France). HemW from *Pseudomonas aeruginosa* was chosen for this experiments due to the established technology for this organism in our laboratory. As a result, an interaction between HemW and the heme-binding subunit of nitrate reductase NarI both from *P. aeruginosa* was clearly detected. These findings experimentally emphasized the detected heme transfer from HemW to NarGHI.

In conclusion, the reconstituted enzyme activity of NarGHI after heme transfer from HemW provides the final proof for the discovery of the first heme chaperone transferring heme b to energy generating systems in the membrane of Gram negative bacteria. To declare HemW as a general heme chaperone its function needs to be analyzed in other organisms. Here, first studies were performed with human HemW and localization studies with the model organism zebrafish (see chapter 3.2 Localization studies with *Danio rerio* HemW). Therefore, human HemW was expressed in *E. coli* and afterwards the heme binding was shown via heme stain and UV-Vis spectroscopy (Knobel, 2015; Heine, 2012). The proof of heme transfer by human HemW needs to be analyzed. Further on, the analysis of HemW from *Bacillus subtilis* is still in progress and will serve further information about the heme chaperone in Gram positive bacteria.

3.2 Localization studies with *Danio rerio* HemW

In this work, biochemical experiments with HemW identified the protein as bacterial heme chaperone. In contrast to the coproporphyrinogen III dehydrogenase HemN, the HemW protein is also found in almost all eukaryots with exception of the fungi. In order to proof the heme chaperone function for eukaryotes, the respective zebrafish protein was tested in protein location studies.

In zebrafish, the *hemW* gene is annotated as *rsad1* (radical S-adenosyl methionine domain containing 1, ZDB-GENE-030131-2508) and is located on chromosome 3. Two transcripts from *rsad1* of different lengths were detected. The first transcript possessed a length of 1510 bp and the second one of 822 bp. The longer transcript covered the corresponding bacterial *hemW* transcript and encoded most likely a functional protein and was therefore chosen in this work.

3.2.1 RSAD1 is localized in mitochondria

Localization studies of RSAD1 were performed by transfection of a zebrafish *rsad1* construct into an eukaryotic cell line. In detail, cDNA of *rsad1* was synthesized from isolated RNA of 24 hpf zebrafish embryos by RT-PCR and afterwards cloned into pCS2+ vector. Two constructs of *rsad1* cDNA with either the fluorescent proteins Venus or mTFP were generated. Afterwards, COS7 cells, derived from the kidney of the African green monkey *Chlorocebus aethiops*, were transfected with this construct. COS7 cells are often employed for this purpose due to resemble the fibroblast cells in humans. For identifying the supposed cellular location of HemW, a tracker for mitochondria (pCS-mitoRFP) was co-transfected. This construct carries the mitochondrial targeting sequence from subunit VIII of the human cytochrome *c* oxidase cDNA. Cells were then analyzed using a Leica TCS SP8 confocal laser scanning microscope. These experiments were performed in cooperation with Dr. Wiebke Sassen of the group of Prof. Dr. Reinhard Köster (Division of Cellular and Molecular Neurobiology, Institute of Zoology, TU Braunschweig, Germany).

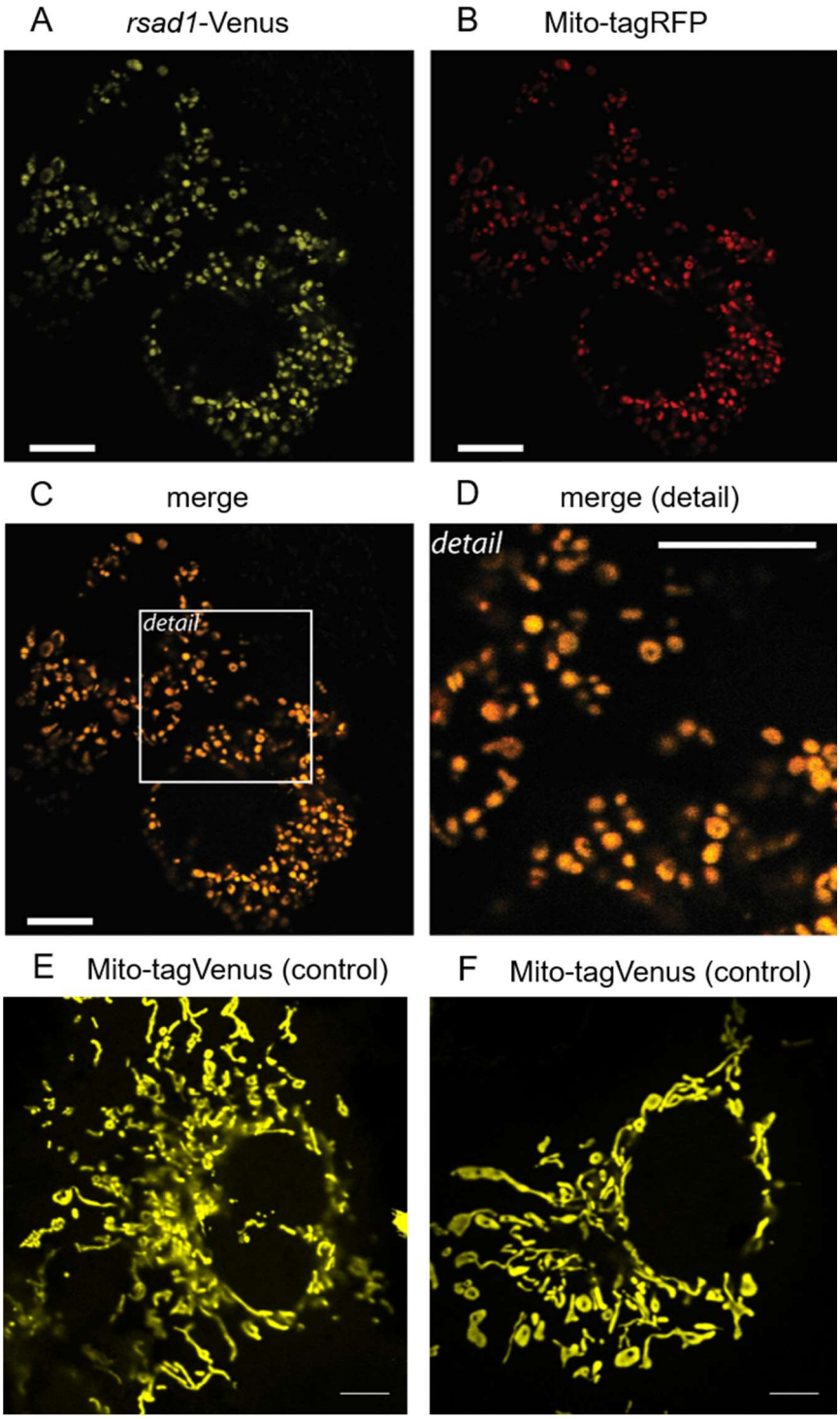

Figure 39: Localization studies of HemW in COS7 fibroblast cells. Microscopy images of the mitochondria of transfected COS7 cells. The construct *rsad1*-Venus (A) and a mito-tagRFP construct (B) were transfected in COS7 cells. The merged image (C) revealed the mitochondrial localization of eukaryotic HemW (RSAD1). The detail (D) demonstrates the altered phenotype of mitochondria. Transfection of COS7 cells with a mito-tagVenus construct served as control and showed no altered phenotype of mitochondria (F, E); metering bar is equivalent to 10 µm.

The analyses via a confocal laser scanning microscope are shown in Figure 39. Localization of RSAD1 was illustrated in yellow (Figure 39, A) in dependence on the emission wavelength of the fusion protein venus. The mito-RFP tracker was likewise illustrated in red (Figure 39, B). A co-localization of these signals resulted in an orange signal.

The signals derived from the pCS-*rsad1*-Venus construct and the mito-tracker revealed a 100 % co-localization (Figure 39, C).

Interestingly, the *rsad1*-transfected cells showed an altered phenotype of the mitochondria (Figure 39, D). Mitochondria were shorter than the normal long tubular forms. In detail, mitochondria of untreated cells exhibit a length of 3.24 µm and cells transfected with 1.5 µg pCS-*rsad1*-Venus were 1.22 µm in length (n = 150, measurement was performed by Dr. Simone Karrie (Division of Cellular and Molecular Neurobiology, Institute of Zoology, TU Braunschweig, Germany). These altered mitochondrial morphology was probably based on a mitochondrial dysfunction which might be caused for example by an impaired fission-fusion balance or increased oxidative stress (Henchcliffe & Beal, 2008).

Altogether, transfection of cells with a *rsad1* construct indicated the presence of RSAD1 in the mitochondria, the place of the final steps of heme biosynthesis and the respiratory chain. Furthermore, the altered phenotype of mitochondria suggest an important function of RSAD1 in mitochondrial performance.

3.2.2 Localization of RSAD1 in the model organism *Danio rerio*

Transfection of COS7 cells showed a localization of HemW (RSAD1) in the mitochondria (3.2.1). This observation points to an involvement of HemW (RSAD1) in delivering heme to the mitochondrial membrane- anchored respiratory chain proteins. Further evidence for this hypothesis would be the presence of HemW in organs with high levels of energy generation. The model organism zebrafish, *Danio rerio*, is well suited for such analysis due to the transparency of embryos. Consequently, an *in-situ* hybridization in 24 hpf, 48 hpf, 72 hpf and 96 hpf zebrafish embryos for detection of mRNA of *rsad1* was performed. In detail, RNA from zebrafish embryos was extracted and the cDNA of *rsad1* was synthesized. Afterwards, antisense and sense RNA labeled with digoxigenin were prepared. The detection of hybridized probe was performed immunohistochemically via an anti-digoxigenin antibody (Roche, Basel, Switzerland). These experiments were performed in cooperation with Dr. Simone Karrie (Division of Cellular and Molecular Neurobiology, Institute of Zoology, TU Braunschweig, Germany).

In the early steps of embryonal development, RSAD1 was present in the whole 24 hpf zebrafish embryo with especially strong expression in the head (Figure 40, A/left) indicating an overall function of HemW (RSAD1) in development.

In later developmental stages (Figure 40, B-D/left), RSAD1 mRNA was mainly detected in the head, gills and heart of the embryos. These organs are characterized by high-energy conversion and thus supported the hypothesis of HemW involved in heme transfer to heme-binding proteins of the respiratory chain. As control, the same experiments were performed with a sense mRNA probe indicating no unspecific staining (Figure 40, A- D/right).

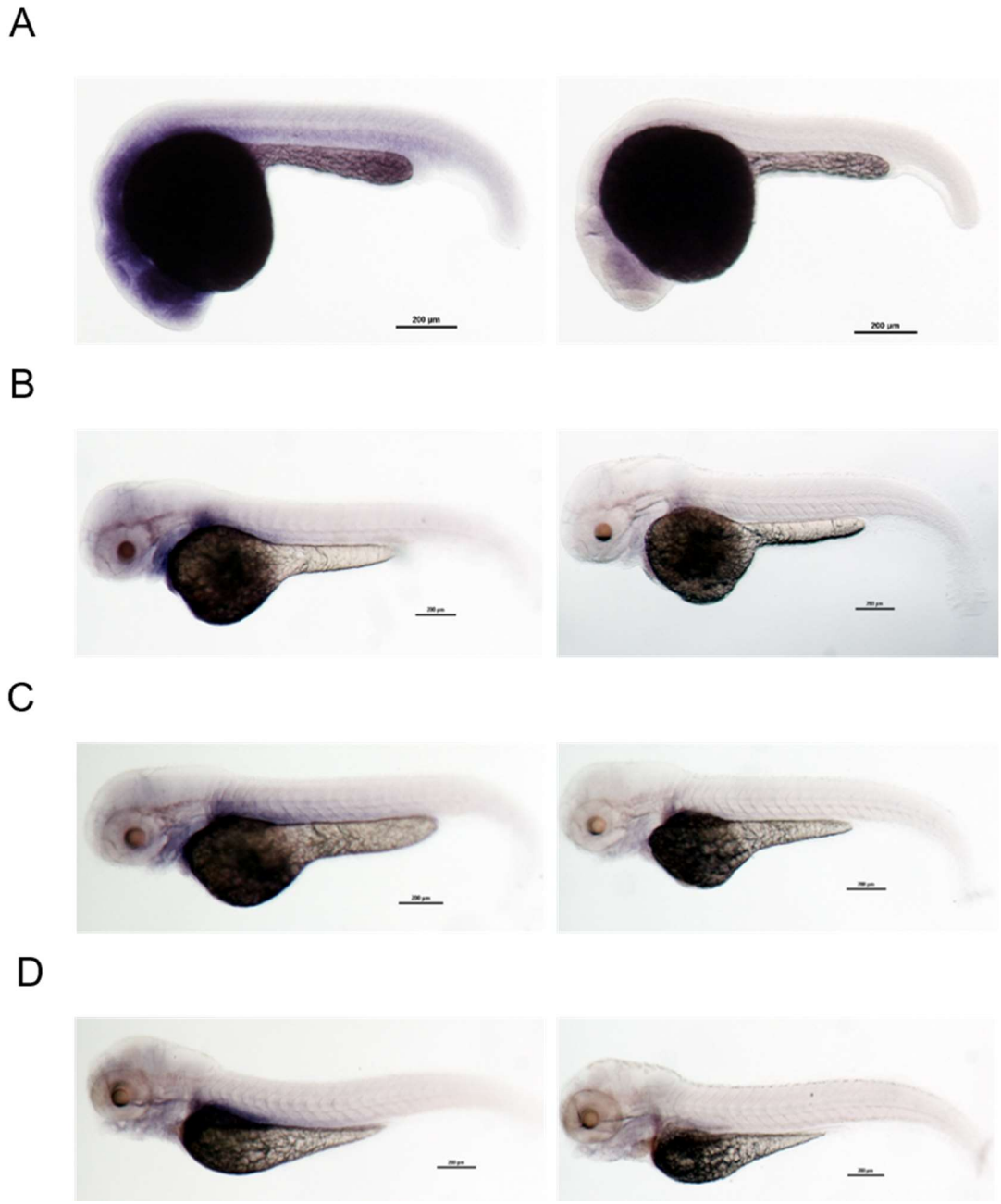

Figure 40: In-situ hybridization of 24 hpf, 48 hpf, 72 hpf and 96 hpf zebrafish embryos with a mRNA complementary probe of RSAD1. In 24 hpf embryos, RSAD1 was detected in the whole embryo with strong expression in the head (A, left). Sense mRNA probe served as control (A, right). In 48 hpf embryos, RSAD1 was detected in the heart und gills with additional weak expression in the brain (B, left). Sense mRNA probe served as control (B, right). In 72 hpf embryos, RSAD1 was detected in the heart and gills (C, left). Sense mRNA probe served as control (C, right). In 96 hpf embryos, weak RSAD1 expression was detected in the gills (D, left; control D, right). The metering bar is equivalent to 200 µm.

3.3 HemW reaction mechanism

In this work, several hints for elucidation of the reaction mechanism of HemW were generated. Currently, only a hypothetical reaction mechanism can be constructed. First of all, heme binding is independent due to the oligomeric state in contrast to the heme transfer. These results indicate a possible storage function of heme in absence of possible heme acceptor proteins. In the presence of acceptor proteins, e.g. NarGHI, HemW dimerizes and the heme is transferred. The dimerization is correlated with an incorporated [Fe- S] cluster and results in a changed conformation of HemW. This conformational change is necessary for the location of heme on the protein surface and the removal. An electron donor e.g. NADH is necessary for heme release. For *L. lactis* HemW, NADH serving as electron donor was also discussed (Abicht *et al.,* 2012). In conclusion, the [Fe- S] cluster of HemW is, unlikely to HemN, not involved in electron transfer but in dimerization. This hypothesis is supported by the disabled reduction of the [Fe-S] cluster by reducing agents. The disabled reduction is explained by different amino acids involved in [Fe-S] cluster binding. In HemN, F68, D147 and R149 plays an important role in cluster binding (Layer *et al.,* 2003). In contrast, for HemW the phenylalanine is exchanged to tyrosine, aspartic acid to asparagine and arginine to glycine. The changes of amino acids with hydrophobic or electrically charged side chains to amino acids with less hydrophobic or uncharged side chains probably results in a different environment of the [Fe-S] cluster and thereupon in the changed function. An amino acid mutant of MoaA, disabled in coordinating the [Fe-S] cluster, also showed SAM binding but no cleavage due to disabled cluster reduction (Hanzelmann & Schindelin, 2006). MoaA is a radical SAM protein catalyzing together with MoaC the first step in Moco biosynthesis, the conversion of 5´-GTP to precursor Z (Hanzelmann & Schindelin, 2006; Hanzelmann *et al.,* 2002). However, a direct relation between iron-sulfur cluster assembly and thereupon dimerization is not known until now and should be further investigated.

4 Summary

The HemW protein, found in bacteria, animals and plants, and wrongly annotated as coproporphyrinogen III dehydrogenase, was identified as a general heme chaperone catalyzing the insertion of heme into membrane localized respiratory chain enzymes. In this work we demonstrated that HemW of *E. coli* transfers heme to the corresponding heme-dependent nitrate oxidoreductase *in vitro*. It is the first heme chaperone working in the cytoplasm of bacteria and most likely in the eukaryotic mitochondrial lumen. Surprisingly, the intact radical SAM scaffold of HemW consisting of a three cysteine and one SAM coordinated [4Fe-4S] cluster was not employed for radical generation and catalysis. Therefore, HemW represents a novel class of radical SAM proteins without radical SAM catalysis. The Mössbauer studies and heme transfer experiments failed to identify influence of the iron-sulfur cluster on heme binding to HemW. However, the [4Fe-4S] cluster was essential for the delivery of heme to nitrate reductase. Furthermore, the iron-sulfur cluster is responsible for the dimerization of HemW. We propose that the translocation of HemW to its reaction place, the cytoplasmic membrane, is dependent on the formation of the HemW dimer.

Eukaryotic HemW termed RSAD1 from *D. rerio* was found in mitochondria and in zebrafish embryos in the head, heart and gills.

Overall, a novel heme chaperone termed HemW/RSAD1 present in almost all prokaryotes and eukaryotes with the exception of the fungi, was discovered and functionally characterized as a radical SAM protein without radical based catalysis.

5 Outlook

In this work, new biochemical and functional insights in the heme chaperone HemW were obtained. For elucidation of the detailed reaction mechanism further questions have to be investigated.

Characterization of heme binding and heme transfer

- Identification of the amino acid residues involved in heme binding
- Verification of heme transfer to other heme-binding proteins e.g. catalase or bacterioferritin via immunoprecipitation experiments
- The crystal structure of HemW would give further information about the mode of heme binding

Function of cofactors

- Elucidation of the function of the SAM cofactor via binding site mutations
- Detailed characterization of the iron-sulfur cluster dependent dimerization and the necessity for protein function

RSAD1 in zebrafish

- Analysis of a CRISPR/Cas- mediated zebrafish mutant to determine the importance of the heme chaperone in this organism

6 References

Abicht, H. K., **Martinez, J.**, **Layer, G.**, **Jahn, D. & Solioz, M. (2012).** *Lactococcus lactis* HemW (HemN) is a haem-binding protein with a putative role in haem trafficking. *The Biochemical Journal* **442**, 335–343.

Aft, R. L. & Mueller, G. C. (1984). Hemin-mediated oxidative degradation of proteins. *The Journal of Biological Chemistry* **259**, 301–305.

Al-Karadaghi, S., **Franco, R.**, **Hansson, M.**, **Shelnutt, J. A.**, **Isaya, G. & Ferreira, G. C. (2006).** Chelatases: distort to select? *Trends in Biochemical Sciences* **31**, 135–142.

Astner, I., **Schulze, J. O.**, **van den Heuvel, J.**, **Jahn, D.**, **Schubert, W.-D. & Heinz, D. W. (2005).** Crystal structure of 5-aminolevulinate synthase, the first enzyme of heme biosynthesis, and its link to XLSA in humans. *The EMBO Journal* **24**, 3166–3177.

Bagg, A. & Neilands, J. B. (1987). Molecular Mechanism of Regulation of Siderophore-Mediated Iron Assimilation. *Microbiological Reviews* **51**, 509–518.

Beale, S. I. & Castelfranco, P. A. (1974). The Biosynthesis of delta-Aminolevulinic Acid in Higher Plants: II. Formation of C-delta-Aminolevulinic Acid from Labeled Precursors in Greening Plant Tissues. *Plant Physiology* **53**, 297–303.

Beinert, H. (1983). Semi-micro methods for analysis of labile sulfide and of labile sulfide plus sulfane sulfur in unusually stable iron-sulfur proteins. *Analytical Biochemistry* **131**, 373–378.

Beinert, H. (2000). Iron-sulfur proteins. Ancient structures, still full of surprises. *Journal of Biological Inorganic Chemistry* **5**, 2–15.

Berks, B. C., **Ferguson, S. J.**, **Moir, J. W. & Richardson, D. J. (1995).** Enzymes and associated electron transport systems that catalyse the respiratory reduction of nitrogen oxides and oxyanions. *Biochimica et Biophysica Acta* **1232**, 97–173.

Berman, J., **Hsu, K. & Look, A. T. (2003).** Zebrafish as a model organism for blood diseases. *British Journal of Haematology* **123**, 568–576.

Bertani, G. (1951). Studies on lysogenesis. I. The mode of phage liberation by lysogenic *Escherichia coli*. *Journal of Bacteriology* **62**, 293–300.

Bertero, M. G., **Rothery, R. A.**, **Palak, M.**, **Hou, C.**, **Lim, D.**, **Blasco, F.**, **Weiner, J. H. & Strynadka, N. C. (2003).** Insights into the respiratory electron transfer pathway from the structure of nitrate reductase A. *Nature Structural Biology* **10**, 681–687.

Booker, S. J. & Grove, T. L. (2010). Mechanistic and functional versatility of radical SAM enzymes. *F1000 Biology Reports* **2**, 52.

Bradford, M. M. (1976). A rapid and sensitive method for the quantitation of microgram quantities of protein utilizing the principle of protein-dye binding. *Analytical Biochemistry* **72**, 248–254.

Buchenau, B., **Kahnt, J.**, **Heinemann, I. U.**, **Jahn, D. & Thauer, R. K. (2006).** Heme biosynthesis in *Methanosarcina barkeri* via a pathway involving two methylation reactions. *Journal of Bacteriology* **188**, 8666–8668.

Casadaban, M. J. (1976). Transposition and fusion of the lac genes to selected promoters in *Escherichia coli* using bacteriophage lambda and Mu. *Journal of Molecular Biology* **104**, 541–555.

Chakravarti, R., **Aulak, K. S.**, **Fox, P. L. & Stuehr, D. J. (2010).** GAPDH regulates cellular heme insertion into inducible nitric oxide synthase. *Proceedings of the National Academy of Sciences of the United States of America* **107**, 18004–18009.

Chen, M. W., **Jahn, D.**, **O'Neill, G. P. & Söll, D. (1990).** Purification of the glutamyl-tRNA reductase from *Chlamydomonas reinhardtii* involved in delta-aminolevulinic acid formation during chlorophyll biosynthesis. *The Journal of Biological Chemistry* **265**, 4058–4063.

Conejero, V. & Semancik, J. S. (1977). Analysis of the proteins in crude plant extracts by polyacrylamide slab gel electrophoresis. *Phytopathology*, 1424–1426.

Cope, L. D., **Love, R. P.**, **Guinn, S. E.**, **Gilep, A.**, **Usanov, S.**, **Estabrook, R. W.**, **Hrkal, Z. & Hansen, E. J. (2001).** Involvement of HxuC outer membrane protein in utilization of hemoglobin by *Haemophilus influenzae*. *Infection and Immunity* **69**, 2353–2363.

Cope, L. D., **Yogev, R.**, **Muller-Eberhard, U. & Hansen, E. J. (1995).** A gene cluster involved in the utilization of both free heme and heme:hemopexin by *Haemophilus influenzae* type b. *Journal of Bacteriology* **177**, 2644–2653.

Dailey, H. A. (1990). *Biosynthesis of Heme and Chlorophylls:* McGraw-Hill.

Dailey, H. A., **Gerdes, S.**, **Dailey, T. A.**, **Burch, J. S. & Phillips, J. D. (2015).** Noncanonical coproporphyrin-dependent bacterial heme biosynthesis pathway that does not use protoporphyrin. *Proceedings of the National Academy of Sciences of the United States of America* **112**, 2210–2215.

D'Costa, A. & Shepherd, I. T. (2009). Zebrafish development and genetics: introducing undergraduates to developmental biology and genetics in a large introductory laboratory class. *Zebrafish* **6**, 169–177.

de Vries, S. P. W., **Burghout, P.**, **Langereis, J. D.**, **Zomer, A.**, **Hermans, P. W. M. & Bootsma, H. J. (2013).** Genetic requirements for *Moraxella catarrhalis* growth under iron-limiting conditions. *Molecular Microbiology* **87**, 14–29.

Desuzinges-Mandon, E., **Arnaud, O.**, **Martinez, L.**, **Huché, F.**, **Di Pietro, A. & Falson, P. (2010).** ABCG2 transports and transfers heme to albumin through its large extracellular loop. *The Journal of Biological Chemistry* **285**, 33123–33133.

Duffy, S. P., **Shing, J.**, **Saraon, P.**, **Berger, L. C.**, **Eiden, M. V.**, **Wilde, A. & Tailor, C. S. (2010).** The Fowler syndrome-associated protein FLVCR2 is an importer of heme. *Molecular and Cellular Biology* **30**, 5318–5324.

Feissner, R., **Xiang, Y. & Kranz, R. G. (2003).** Chemiluminescent-based methods to detect subpicomole levels of c-type cytochromes. *Analytical Biochemistry* **315**, 90–94.

Fish, W. W. (1988). Rapid colorimetric micromethod for the quantitation of complexed iron in biological samples. *Methods in Enzymology* **158**, 357–364.

Frey, P. A. & Booker, S. J. (2001). Radical mechanisms of S-adenosylmethionine-dependent enzymes. *Advances in Protein Chemistry* **58**, 1–45.

Gibson, K. D., **Laver, W. G. & Neuberger, A. (1958).** Initial stages in the biosynthesis of porphyrins. 2. The formation of delta-aminolaevulic acid from glycine and succinyl-coenzyme A by particles from chicken erythrocytes. *The Biochemical Journal* **70**, 71–81.

Gilbert, S. F., Singer, S. R. & Tyler, M. S. (2006). *Developmental biology*, 8th edn.: Sinauer.

Gluzman, Y. (1981). SV40-transformed simian cells support the replication of early SV40 mutants. *Cell* **23**, 175–182.

González, P. J., **Correia, C.**, **Moura, I.**, **Brondino, C. D. & Moura, J. J. (2006).** Bacterial nitrate reductases: Molecular and biological aspects of nitrate reduction. *Journal of Inorganic Biochemistry* **100**, 1015–1023.

Grage, K. (2005). *Oxygen-independent coproporphyrinogen III oxidase : Characterization of* Escherichia coli *HemN and investigation of proposed functional analogs*. Dissertation, Technische Universität Braunschweig, Germany.

Guigliarelli, B., **Asso, M.**, **More, C.**, **Augier, V.**, **Blasco, F.**, **Pommier, J.**, **Giordano, G. & Bertrand, P. (1992).** EPR and redox characterization of iron-sulfur centers in nitrate reductases A and Z from *Escherichia coli*. Evidence for a high-potential and a low-potential class and their relevance in the electron-transfer mechanism. *European Journal of Biochemistry* **207**, 61–68.

Guigliarelli, B., **Magalon, A.**, **Asso, M.**, **Bertrand, P.**, **Frixon, C.**, **Giordano, G. & Blasco, F. (1996).** Complete coordination of the four Fe-S centers of the beta subunit from *Escherichia coli* nitrate reductase. Physiological, biochemical, and EPR characterization of site-directed mutants lacking the highest or lowest potential [4Fe-4S] clusters. *Biochemistry* **35**, 4828–4836.

Guo, Y., **Guo, G.**, **Mao, X.**, **Zhang, W.**, **Xiao, J.**, **Tong, W.**, **Liu, T.**, **Xiao, B. & Liu, X. & other authors (2008).** Functional identification of HugZ, a heme oxygenase from *Helicobacter pylori*. *BMC microbiology* **8**, 226.

Hanson, M. S., **Pelzel, S. E.**, **Latimer, J.**, **Muller-Eberhard, U. & Hansen, E. J. (1992).** Identification of a genetic locus of *Haemophilus influenzae* type b necessary for the binding and utilization of heme bound to human hemopexin. *Proceedings of the National Academy of Sciences of the United States of America* **89**, 1973–1977.

Hanzelmann, P. & Schindelin, H. (2006). Binding of 5'-GTP to the C-terminal FeS cluster of the radical S-adenosylmethionine enzyme MoaA provides insights into its mechanism. *Proceedings of the National Academy of Sciences of the United States of America* **103**, 6829–6834.

Hanzelmann, P., **Schwarz, G. & Mendel, R. R. (2002).** Functionality of alternative splice forms of the first enzymes involved in human molybdenum cofactor biosynthesis. *The Journal of Biological Chemistry* **277**, 18303–18312.

Heine, S. (2012). *Charakterisierung des humanen potentiellen Häm-Chaperons HemW*. Masterarbeit, Technische Universität Braunschweig, Germany.

Heinemann, I. U., **Jahn, M. & Jahn, D. (2008).** The biochemistry of heme biosynthesis. *Archives of biochemistry and biophysics* **474**, 238–251.

Henchcliffe, C. & Beal, M. F. (2008). Mitochondrial biology and oxidative stress in Parkinson disease pathogenesis. *Nature clinical practice. Neurology* **4**, 600–609.

Ho, W. W., **Li, H.**, **Eakanunkul, S.**, **Tong, Y.**, **Wilks, A.**, **Guo, M. & Poulos, T. L. (2007).** Holo- and apo-bound structures of bacterial periplasmic heme-binding proteins. *Journal of Biological Chemistry* **282**, 35796–35802.

Hrycay, E. G. & O'Brien, P. J. (1971). The peroxidase nature of cytochrome P-420 utilizing a lipid peroxide substrate. *Archives of biochemistry and biophysics*, 28–35.

Huhn, S. (2012). *Einbau von prosthetischem Häm in cytoplasmatische und membrangebundene Proteine*. Dissertation, Technische Universität Braunschweig, Germany.

Hung, H.-I., **Schwartz, J. M.**, **Maldonado, E. N.**, **Lemasters, J. J. & Nieminen, A.-L. (2013).** Mitoferrin-2-dependent mitochondrial iron uptake sensitizes human head and neck squamous carcinoma cells to photodynamic therapy. *The Journal of Biological Chemistry* **288**, 677–686.

Jackson, A. H., **Sancovich, H. A. &** Ferramola de Sancovich, A.M. **(1980).** Synthetic and biosynthetic studies of porphyrins: III. Structures of the intermediates between uroporphyrinogen-III and coproporphyrinogen-III: Synthesis of fourteen heptacarboxylic, hexacarboxylic, and pentacarboxylic porphyrins related to uroporphyrin-III. *Bioinorganic Chemistry* **9**, 71–120.

Jacobson, M. R., **Cash, V. L.**, **Weiss, M. C.**, **Laird, N. F.**, **Newton, W. E. & Dean, D. R. (1989).** Biochemical and genetic analysis of the nifUSVWZM cluster from *Azotobacter vinelandii*. *Molecular and General Genetics* **219**, 49–57.

Jahn, D., **Chen, M. W. & Söll, D. (1991).** Purification and functional characterization of glutamate-1-semialdehyde aminotransferase from *Chlamydomonas reinhardtii*. *The Journal of Biological Chemistry* **266**, 161–167.

Jahn, M. & Jahn, D. (2012). Tetrapyrroles. In *Biochemical Pathways. An Atlas of Biochemistry and Molecular Biology*, pp. 82–92. Edited by G. Michal & D. Schomburg, 2nd edn.: John Wiley & Sons.

Johnson, D. C., **Dean, D. R.**, **Smith, A. D. & Johnson, M. K. (2005).** Structure, Function, and Formation of Biological Iron-Sulfur Clusters. *Annual Review of Biochemistry* **74**, 247–281.

Kadish, K. M., Smith, K. M. & Guilard, R. (2011). *Handbook of Porphyrin Science. With applications to chemistry, physics, materials science, engineering, biology and medicine:* World Scientific.

Karnaukhova, E., **Rutardottir, S.**, **Rajabi, M.**, **Wester Rosenlof, L.**, **Alayash, A. I. & Akerstrom, B. (2014).** Characterization of heme binding to recombinant alpha1-microglobulin. *Frontiers in Physiology* **5**, 465.

Kaufholz, A.-L., **Layer, G.**, **Heinz, D.**, **Jahn, M. & Jahn, D. (2013).** The Structural Basis of Porphyrias - Defects of Heme Biosynthetic Enzymes. In *Handbook of porphyrin science (volume 26 - 30). With applications to chemistry, physics, materials science, engineering, biology and medicine*, pp. 1–42. Edited by G. C. Ferreira: World Scientific.

Kikuchi, G., **Kumar, A.**, **Talmage, P. & Shemin, D. (1958).** The enzymatic synthesis of delta-aminolevulinic acid. *The Journal of Biological Chemistry* **233**, 1214–1219.

Kimmel, C. B., **Ballard, W. W.**, **Kimmel, SR**, **Ullmann, B. & Schilling, T. F. (1995).** Stages of embryonic development of the zebrafish. *Developmental Dynamics* **203**, 253–310.

Knobel, H. B. (2015). *Charakterisierung des* Homo sapiens *Chaperons RSAD1*. Bachelorarbeit, Technische Universität Braunschweig, Germany.

Koch, M., **Breithaupt, C.**, **Kiefersauer, R.**, **Freigang, J.**, **Huber, R. & Messerschmidt, A. (2004).** Crystal structure of protoporphyrinogen IX oxidase: a key enzyme in haem and chlorophyll biosynthesis. *The EMBO Journal* **23**, 1720–1728.

Kühner, M., **Schweyen, P.**, **Hoffmann, M.**, **Ramos, J. V.**, **Reijerse, E. J.**, **Lubitz, W.**, **Bröring, M. & Layer, G. (2016).** The auxiliary [4Fe–4S] cluster of the Radical SAM heme synthase from *Methanosarcina barkeri* is involved in electron transfer. *Chemical Science* **7**, 4633–4643.

Kühner, M. T. (2015). *Die letzten Schritte der alternativen Häm-Biosynthese in Archaea: Charakterisierung der Proteine AhbA, AhbB, AhbC und des Radical SAM Enzyms AhbD aus* Methanosarcina barkeri. Dissertation, Technische Universität Braunschweig, Germany.

Lanciano, P., **Magalon, A.**, **Bertrand, P.**, **Guigliarelli, B. & Grimaldi, S. (2007).** High-stability semiquinone intermediate in nitrate reductase A (NarGHI) from *Escherichia coli* is located in a quinol oxidation site close to heme b_D. *Biochemistry* **46**, 5323–5329.

Lansky, I. B., **Lukat-Rodgers, G. S.**, **Block, D.**, **Rodgers, K. R.**, **Ratliff, M. & Wilks, A. (2006).** The cytoplasmic heme-binding protein (PhuS) from the heme uptake system of *Pseudomonas aeruginosa* is an intracellular heme-trafficking protein to the delta-regioselective heme oxygenase. *The Journal of Biological Chemistry* **281**, 13652–13662.

Layer, G., **Grage, K.**, **Teschner, T.**, **Schünemann, V.**, **Breckau, D.**, **Masoumi, A.**, **Jahn, M.**, **Heathcote, P.**, **Trautwein, A. X. & Jahn, D. (2005).** Radical S-adenosylmethionine enzyme coproporphyrinogen III oxidase HemN: functional features of the [4Fe-4S] cluster and the two bound S-adenosyl-L-methionines. *The Journal of Biological Chemistry* **280**, 29038–29046.

Layer, G., **Moser, J.**, **Heinz, D. W.**, **Jahn, D. & Schubert, W. D. (2003).** Crystal structure of coproporphyrinogen III oxidase reveals cofactor geometry of Radical SAM enzymes. *The EMBO Journal* **22**, 6214–6224.

Layer, G., **Reichelt, J.**, **Jahn, D. & Heinz, D. W. (2010).** Structure and function of enzymes in heme biosynthesis. *Protein Science* **19**, 1137–1161.

Layer, G., **Verfürth, K.**, **Mahlitz, E. & Jahn, D. (2002).** Oxygen-independent coproporphyrinogen-III oxidase HemN from *Escherichia coli*. *The Journal of Biological Chemistry* **37**, 34136–34142.

Lechardeur, D., **Fernandez, A.**, **Robert, B.**, **Gaudu, P.**, **Trieu-Cuot, P.**, **Lamberet, G. & Gruss, A. (2010).** The 2-Cys peroxiredoxin alkyl hydroperoxide reductase c binds heme and participates in its intracellular availability in *Streptococcus agalactiae*. *Journal of Biological Chemistry* **285**, 16032–16041.

Létoffé, S., **Nato, F.**, **Goldberg, M. E. & Wandersman, C. (1999).** Interactions of HasA, a bacterial haemophore, with haemoglobin and with its outer membrane receptor HasR. *Molecular Microbiology* **33**, 546–555.

Létoffé, S., **Redeker, V. & Wandersman, C. (1998).** Isolation and characterization of an extracellular haem-binding protein from *Pseudomonas aeruginosa* that shares function and sequence similarities with the *Serratia marcescens* HasA haemophore. *Molecular Microbiology* **28**, 1223–1234.

Li, T., **Bonkovsky, H. L. & Guo, J.-t. (2011).** Structural analysis of heme proteins: implications for design and prediction. *BMC Structural Biology* **11**, 13.

Lill, R., **Dutkiewicz, R.**, **Elsässer, H.-P.**, **Hausmann, A.**, **Netz, D. J. A.**, **Pierik, A. J.**, **Stehling, O.**, **Urzica, E. & Mühlenhoff, U. (2006).** Mechanisms of iron-sulfur protein maturation in mitochondria, cytosol and nucleus of eukaryotes. *Biochimica et Biophysica Acta* **1763**, 652–667.

Liu, X., **Gong, J.**, **Wei, T.**, **Wang, Z.**, **Du, Q.**, **Zhu, D.**, **Huang, Y.**, **Xu, S. & Gu, L. (2012).** Crystal structure of HutZ, a heme storage protein from *Vibrio cholerae*: A structural mismatch observed in the region of high sequence conservation. *BMC Structural Biology* **12**, 23.

Lobo, S. A. L., **Scott, A.**, **Videira, M. A. M.**, **Winpenny, D.**, **Gardner, M.**, **Palmer, M. J.**, **Schroeder, S.**, **Lawrence, A. D. & Parkinson, T. & other authors (2015).** *Staphylococcus aureus* haem biosynthesis: characterisation of the enzymes involved in final steps of the pathway. *Mol Microbiol* **97**, 472–487.

Lüer, C., **Schauer, S.**, **Möbius, K.**, **Schulze, J.**, **Schubert, W. D.**, **Heinz, D. W.**, **Jahn, D. & Moser, J. (2005).** Complex formation between glutamyl-tRNA reductase and glutamate-1-semialdehyde 2,1-aminomutase in *Escherichia coli* during the initial reactions of porphyrin biosynthesis. *The Journal of Biological Chemistry* **280**, 18568–18572.

Möbius, K., **Arias-Cartin, R.**, **Breckau, D.**, **Hannig, A.-L.**, **Riedmann, K.**, **Biedendieck, R.**, **Schroder, S.**, **Becher, D. & Magalon, A. & other authors (2010).** Heme biosynthesis is coupled to electron transport chains for energy generation. *Proceedings of the National Academy of Sciences of the United States of America* **107**, 10436–10441.

Molitor, B., **Stassen, M.**, **Modi, A.**, **El-Mashtoly, S. F.**, **Laurich, C.**, **Lubitz, W.**, **Dawson, J. H.**, **Rother, M. & Frankenberg-Dinkel, N. (2013).** A heme-based redox sensor in the methanogenic archaeon *Methanosarcina acetivorans*. *Journal of Biological Chemistry* **288**, 18458–18472.

Morero, N. R., **Botti, H.**, **Nitta, K. R.**, **Carrion, F.**, **Obal, G.**, **Picardeau, M. & Buschiazzo, A. (2014).** HemR is an OmpR/PhoB-like response regulator from *Leptospira*, which simultaneously effects transcriptional activation and repression of key haem metabolism genes. *Molecular Microbiology* **94**, 340–352.

Moser, J., **Schubert, W. D.**, **Beier, V.**, **Bringemeier, I.**, **Jahn, D. & Heinz, D. W. (2001).** V-shaped structure of glutamyl-tRNA reductase, the first enzyme of tRNA-dependent tetrapyrrole biosynthesis. *The EMBO Journal* **20**, 6583–6590.

O'Neill, M. J. & Wilks, A. (2013). The *P. aeruginosa* Heme Binding Protein PhuS is a Heme Oxygenase Titratable Regulator of Heme Uptake. *ACS Chemical Biology* **8**, 1794–1802.

Oakes, E. H. (2007). *Encyclopedia of World Scientists. 2-Volume Set (Revised Edition):* Infobase Publishing.

O'Neill, M. J., **Bhakta, M. N.**, **Fleming, K. G. & Wilks, A. (2012).** Induced fit on heme binding to the *Pseudomonas aeruginosa* cytoplasmic protein (PhuS) drives interaction with heme oxygenase (HemO). *Proceedings of the National Academy of Sciences of the United States of America* **109**, 5639–5644.

Owens, C. P., **Du, J.**, **Dawson, J. H. & Goulding, C. W. (2012).** Characterization of heme ligation properties of Rv0203, a secreted heme binding protein involved in *Mycobacterium tuberculosis* heme uptake. *Biochemistry* **51**, 1518–1531.

Porello, S. L., **Cannon, M. J. & David, S. S. (1998).** A Substrate Recognition Role for the [4Fe-4S]2+ Cluster of the DNA Repair Glycosylase MutY. *Biochemistry* **37**, 6465–6475.

Rajagopal, A., **Rao, A. U.**, **Amigo, J.**, **Tian, M.**, **Upadhyay, S. K.**, **Hall, C.**, **Uhm, S.**, **Mathew, M. K. & Fleming, M. D. & other authors (2008).** Haem homeostasis is regulated by the conserved and concerted functions of HRG-1 proteins. *Nature* **453**, 1127–1131.

Roche, B., **Aussel, L.**, **Ezraty, B.**, **Mandin, P.**, **Py, B. & Barras, F. (2013).** Iron/sulfur proteins biogenesis in prokaryotes: formation, regulation and diversity. *Biochimica et Biophysica Acta* **1827**, 455–469.

Rothery, R. A., **Blasco, F.**, **Magalon, A. & Weiner, J. H. (2001).** The diheme cytochrome b subunit (Narl) of *Escherichia coli* nitrate reductase A (NarGHI): structure,

function, and interaction with quinols. *Journal of Molecular Microbiology and Biotechnology* **3**, 273–283.

Rupp, R. A., **Snider, L. & Weintraub, H. (1994).** *Xenopus* embryos regulate the nuclear localization of XMyoD. *Genes & Development* **8**, 1311–1323.

Săsărman, A., **Surdeanu, M. & Horodniceanu, T. (1968).** Locus determining the synthesis of delta-aminolevulinic acid in *Escherichia coli* K-12. *Journal of Bacteriology* **96**, 1882–1884.

Schmitt, T. H., **Frezzatti, W. A., JR. & Schreier, S. (1993).** Hemin-induced lipid membrane disorder and increased permeability: a molecular model for the mechanism of cell lysis. *Archives of biochemistry and biophysics* **307**, 96–103.

Schulze, J. O., **Schubert, W.-D.**, **Moser, J.**, **Jahn, D. & Heinz, D. W. (2006).** Evolutionary relationship between initial enzymes of tetrapyrrole biosynthesis. *Journal of Molecular Biology* **358**, 1212–1220.

Shayeghi, M., **Latunde-Dada, G. O.**, **Oakhill, J. S.**, **Laftah, A. H.**, **Takeuchi, K.**, **Halliday, N.**, **Khan, Y.**, **Warley, A. & McCann, F. E. & other authors (2005).** Identification of an intestinal heme transporter. *Cell* **122**, 789–801.

Shemin, D. & Russell, C. S. (1953). Delta-aminolevulinic acid, its role in the biosynthesis of porphyrins and purines. *Journal of the American Chemical Society* **75**, 4873–4874.

Sievers, F., **Wilm, A.**, **Dineen, D.**, **Gibson, T.**, **Karplus, K.**, **Li, W.**, **Lopez, R.**, **McWilliam, H. & Remmert, M. & other authors (2011).** Fast, scalable generation of high-quality protein multiple sequence alignments using Clustal Omega. *Molecular Systems Biology* **7**, 539.

Smith, L. J., **Kahraman, A. & Thornton, J. M. (2010).** Heme proteins-diversity in structural characteristics, function, and folding. *Proteins* **78**, 2349–2368.

Sofia, H. J., **Chen, G.**, **Hetzler, B. G.**, **Reyes-Spindola, J. F. & Miller, N. E. (2001).** Radical SAM, a novel protein superfamily linking unresolved steps in familiar biosynthetic pathways with radical mechanisms: functional characterization using new analysis and information visualization methods. *Nucleic acids research* **29**, 1097–1106.

Stojanovski, B. M., **Breydo, L.**, **Hunter, G. A.**, **Uversky, V. N. & Ferreira, G. C. (2014).** Catalytically active alkaline molten globular enzyme: Effect of pH and

temperature on the structural integrity of 5-aminolevulinate synthase. *Biochimica et Biophysica Acta* **1844**, 2145–2154.

Stojiljkovic, I. & Hantke, K. (1992). Hemin uptake system of *Yersinia enterocolitica*: similarities with other TonB-dependent systems in gram-negative bacteria. *EMBO Journal* **11**, 4359–4367.

Stojiljkovic, I. & Hantke, K. (1994). Transport of haemin across the cytoplasmic membrane through a haemin-specific periplasmic binding-protein-dependent transport system in *Yersinia enterocolitica*. *Molecular Microbiology* **13**, 719–732.

Storbeck, S., **Walther, J.**, **Muller, J.**, **Parmar, V.**, **Schiebel, H. M.**, **Kemken, D.**, **Dulcks, T.**, **Warren, M. J. & Layer, G. (2009).** The *Pseudomonas aeruginosa* nirE gene encodes the S-adenosyl-L-methionine-dependent uroporphyrinogen III methyltransferase required for heme d_1 biosynthesis. *FEBS Journal* **276**, 5973–5982.

Teale, F. W. (1959). Cleavage of the haem-protein link by acid methylethylketone. *Biochimica et Biophysica Acta* **35**, 543.

Thompson, D. K., **Beliaev, A. S.**, **Giometti, C. S.**, **Tollaksen, S. L.**, **Khare, T.**, **Lies, D. P.**, **Nealson, K. H.**, **Lim, H. & Yates, J. & other authors (2002).** Transcriptional and Proteomic Analysis of a Ferric Uptake Regulator (Fur) Mutant of *Shewanella oneidensis*. Possible Involvement of Fur in Energy Metabolism, Transcriptional Regulation, and Oxidative Stress. *Applied and Environmental Microbiology* **68**, 881–892.

Thöny-Meyer, L. (2009). Heme transport and incorporation into proteins. In *Tetrapyrroles. Birth, Life and Death*, pp. 149–159. Edited by M. J. Warren & A. G. Smith: Springer-Verlag New York.

Towbin, H., **Staehelin, T. & Gordon, J. (1979).** Electrophoretic transfer of proteins from polyacrylamide gels to nitrocellulose sheets: procedure and some applications. *Proceedings of the National Academy of Sciences of the United States of America* **76**, 4350–4354.

Uchida, T., **Sekine, Y.**, **Matsui, T.**, **Ikeda-Saitoc, M. & Ishimori, K. (2012).** A heme degradation enzyme, HutZ, from *Vibrio cholerae*. *Chemical Communications* **48**, 6741–6743.

Ursini, F., **Maiorino, M.**, **Ferri, L.**, **Valente, M. &** Gregolin C. **(1981).** Hydrogen peroxide and hematin in microsomal lipid peroxidation. *Journal of Inorganic Biochemistry* **15**, 163–169.

Vasudevan, D. M., Sreekumari, S. & Vaidyanathan, K. (2013). *Textbook of Biochemistry for Medical Students*, 7th edn.: Jaypee Brothers Medical Pub.

Walsby, C. J., **Ortillo, D.**, **Broderick, W. E.**, **Broderick, J. B. & Hoffman, B. M. (2002).** An Anchoring Role for FeS Clusters: Chelation of the Amino Acid Moiety of S-Adenosylmethionine to the Unique Iron Site of the [4Fe−4S] Cluster of Pyruvate Formate-Lyase Activating Enzyme. *Journal of the American Chemical Society* **124**, 11270–11271.

Wandersman, C. & Delepelaire, P. (2004). Bacterial iron sources: from siderophores to hemophores. *Annual Review of Microbiology* **58**, 611–647.

Wang, K. F., **Dailey, T. A. & Dailey, H. A. (2001).** Expression and characterization of the terminal heme synthetic enzymes from the hyperthermophile *Aquifex aeolicus*. *FEMS Microbiology Letters* **202**, 115–119.

Wang, S. C. & Frey, P. A. (2007). S-adenosylmethionine as an oxidant: the radical SAM superfamily. *Trends in Biochemical Sciences* **32**, 101–110.

Westerfield, M. (2000). *The zebrafish book: a guide for the laboratory use of zebrafish* (Danio rerio): University of Oregon press.

Wu, C. K., **Dailey, H. A.**, **Rose, J. P.**, **Burden, A.**, **Sellers, V. M. & Wang, B. C. (2001).** The 2.0 A structure of human ferrochelatase, the terminal enzyme of heme biosynthesis. *Nature Structural Biology* **8**, 156–160.

Wyckoff, E.E., **Schmitt, M.**, **Wilks, A. & Payne, S. M. (2004).** HutZ is required for efficient heme utilization in *Vibrio cholerae*. *Journal of Bacteriology* **186**, 4142–4151.

Yachdav, G., **Kloppmann, E.**, **Kajan, L.**, **Hecht, M.**, **Goldberg, T.**, **Hamp, T.**, **Hönigschmid, P.**, **Schafferhans, A. & Roos, M. & other authors (2014).** PredictProtein--an open resource for online prediction of protein structural and functional features. *Nucleic acids research* **42**, W337-43.

Yanga, R., **Yana, S.**, **Zhua, X.**, **Lia, C.-Y.**, **Liub, Z. & Xiong, J.-W. (2015).** Antimalarial drug artemisinin depletes erythrocytes by activating apoptotic pathways in zebrafish. *Experimental Hematology* **43**, 331–341.

Yuan, X., **Fleming, M. D. & Hamza, I. (2013).** Heme transport and erythropoiesis. *Current Opinion in Chemical Biology* **17**, 204–211.

Appendices

Figures

Tables

License Numbers

Figure 5: 4012090392864

Figure 7: 3957060869486

Acknowledgment

Dr. Martina Jahn möchte ich für die hervorragende Betreuung danken. Darüber hinaus für die Motivationsschübe und das “offene Ohr”. Schade, dass die Zeit so schnell verging.

Besonderer Dank gilt Prof. Dr. Dieter Jahn für die Möglichkeit diese Arbeit in seiner Arbeitsgruppe anzufertigen. Vielen Dank für die vielen konstruktiven Besprechungen und das entgegengebrachte Vertrauen.

Vielen Dank an Prof. Dr. Gunhild Layer für die Übernahme des Zweitgutachtens und die Unterstützung bezüglich meiner Arbeit und darüber hinaus.

Für die Übernahme der Prüfungskommission möchte ich Prof. Dr. Ralf-Rainer Mendel danken.

Danken möchte ich weiterhin den Kooperationspartnern für die produktive und unkomplizierte Zusammenarbeit. Zu nennen sind die Gruppen von Prof. Dr. Axel Magalon, Prof. Dr. Reinhard Köster und Prof. Dr. Martin Bröring, sowie Dr. Edward J. Reijerse und Dr. Eckhard Bill.

Natürlich möchte ich mich bei dem Labor 212 bedanken. Es war eine tolle Zeit mit euch. Besonders möchte ich Dagmar, Simone, Mareike, Melanie, Vanessa, Anna, Stefan, Toni und Ivana danken. Ich habe mich jeden Tag darauf gefreut euch zu sehen und natürlich mit euch zu arbeiten.

Weiterhin gab es viele Personen, die mich während meiner Zeit an diesem Institut begleitet haben. Da wären die komplette AG Layer und AG Moser. Danke für die Freitagsseminare und darüber hinaus. Natürlich danke ich Barbara und Dagmar. Ohne

euch hätte ich so manches Mal ohne Kolben oder Medium dagestanden. Dank Herrn Hoppe durfte ich die eine oder andere Dienstreise antreten. In diesem Zusammenhang danke an Daniela, Christina und Gunhild. Ihr habt mir immer geholfen wenn ich mal wieder nicht wusste wie ich etwas ausfüllen musste.

Dank der Zeit an diesem Institut habe ich viele Freunde gefunden. Dagmar, Jenny, Mareike, Mela, Steffi und Julia möchte ich gesondert erwähnen. Und vor allem danke an Mareike und Dagmar, die alles Korrektur gelesen haben.

Meiner Familie, vor allem Matthias und Malte, kann ich gar nicht genug für die Unterstützung, Aufmunterung und den “Rücken frei halten” danken. Was würde ich bloß ohne euch machen. Und danke an meine Eltern, dass sie mich überredet haben Französisch zu belegen…